GEOCHEMISTRY AND GEOLOGY OF THE PINAL SCHIST, COCHISE AND PIMA COUNTIES, ARIZONA

by

Peter Copeland

submitted in partial fulfillment
of the requirements for the degree of
Master of Science in Geology

New Mexico Institute of Mining and Technology
Socorro, New Mexico

January, 1986

The known is finite, the unknown infinite; intellectually we stand on an islet in the midst of an illimitable ocean of inexplicability. Our business in every generation is to reclaim a little more land.

T.H. Huxley, 1887

ABSTRACT

Early Proterozoic supracrustal rocks in southeastern Arizona are dominated by a large volume of meta-sandstones, with minor metavolcanic and subvolcanic rocks, both mafic and felsic. These rocks are collectively referred to as the Pinal Schist. Felsic metavolcanic rocks are an important part of the section only in the Dos Cabezas Mountains. Mafic metavolcanic rocks are a minor but widespread portion of the Pinal Schist in the study area. The mafic volcanic rocks of the Pinal Schist in the Dragoon, Dos Cabezas, and Chiricahua Mountains have incompatible element distributions characteristic of basalts erupted in modern metavolcanic arcs. In contrast, mafic metavolcanic rocks in the northeastern Little Dragoon Mountains have chemical traits similar to mid-ocean-ridge or within-plate basalts. Incompatible element distributions in felsic metavolcanic and subvolcanic rocks in the Dos Cabezas, Chiricahua, and Little Dragoon Mountains are similar to rhyolites from continental margin arcs and associated back-arc basins. Mafic rocks in the Dos Cabezas, Chiricahua, and Little Dragoon Mountains are tholeiitic while mafic metavolcanic rocks in the Dragoon Mountains have both tholeiitic and calc-alkaline characteristics. Felsic metavolcanic rocks throughout the area are calc-alkaline. The metasedimentary rocks of

the Pinal Schist are comprised of sandstones, pelites, and minor conglomerates. Metamorphism has obscured some of the original microscopic textures of these rocks, but it appears most of the meta-sandstones of the Pinal Schist may be classified as quartz-intermediate graywackes (Crook, 1974). These meta-sandstones have low concentrations of Fe, Mg, Ti, and Co, a feature characteristic of clastic sediments deposited on or near continental crust. Petrographic study and chemical compositions of the Pinal sandstones indicate a felsic plutonic-volcanic provenance with only a minor mafic component. Preserved sedimentary structures in these rocks suggest they were deposited in a series of submarine fans by turbidity or grain flow.

These data are consistent with an interpretation that the Pinal Schist was deposited in a continental margin back-arc basin. Continental detritus was rapidly fed into a tectonically active basin. This sediment was interbedded with and intruded by mafic volcanic and subvolcanic rocks. The mafic rocks of the Dragoon, Dos Cabezas, and Chiricahua Mountains were derived from a mantle source which had a significant subduction component while the mafic metavolcanic rocks in the northeastern Little Dragoon Mountains were derived from a within-plate mantle source.

ACKNOWLEDGMENTS

Many people are responsible for making this thesis possible. I would like to thank my major advisor, Kent C. Condie, for the opportunity to do this work. Thanks also to the other members of my committe, David Johnson and Andrew Campbell, for their constructive critisisms of my thesis. I appreciate the swift return of earlier versions of the thesis from all of my committee, especially KCC. G. Patrick Bowling was very helpful with many phases of the laboratory work. Discussions with Mike Knoper, Peter Swift and Sam Bowring helped clarify my thinking concerning the Precambrian of the southwest United States. This thesis was partially funded by National Science Foundation grant EAR-8313735 to K.C. Condie. Samples were irradiated at the nuclear reactor at Sandia National Labs, Albuquerque, NM. The reactor staff is gratefully acknowledged for their assistance.

TABLE OF CONTENTS

LIST OF FIGURES

LIST OF TABLES

INTRODUCTION

Early Proterozoic supracrustal rocks are exposed in most of the Basin and Range uplifts of southeastern Arizona (Plate 1, Fig. 1). These rocks which are collectively referred to as the Pinal Schist include a lithologically diverse suite of rocks dominated by quartz-rich metasediments with felsic and mafic metaigneous rocks. The metaigneous rocks occur both as subvolcanic intrusive dikes and sills and as extrusive flows and tuffs. Quartz-rich and quartz-intermediate metasediments are by far the dominant lithology and are found throughout the area (Erickson, 1969; Condie and others, 1985). Many of the metasediments have been interpreted to be deep-water turbidites deposited in a system of submarine fans (Silver, 1978; Condie and De Melas, 1985).

The purpose of this study is to characterize the geochemistry of the Pinal Schist in southeast Arizona and by comparison to modern environments, determine the tectonic setting in which the Pinal Schist formed. This objective has both local as well as regional importance. The tectonic history of the Proterozoic in the southwest United States will not be fully understood until each area is characterized by a variety of subdisciplines in the geosciences and all areas are integrated into a coherent regional framework.

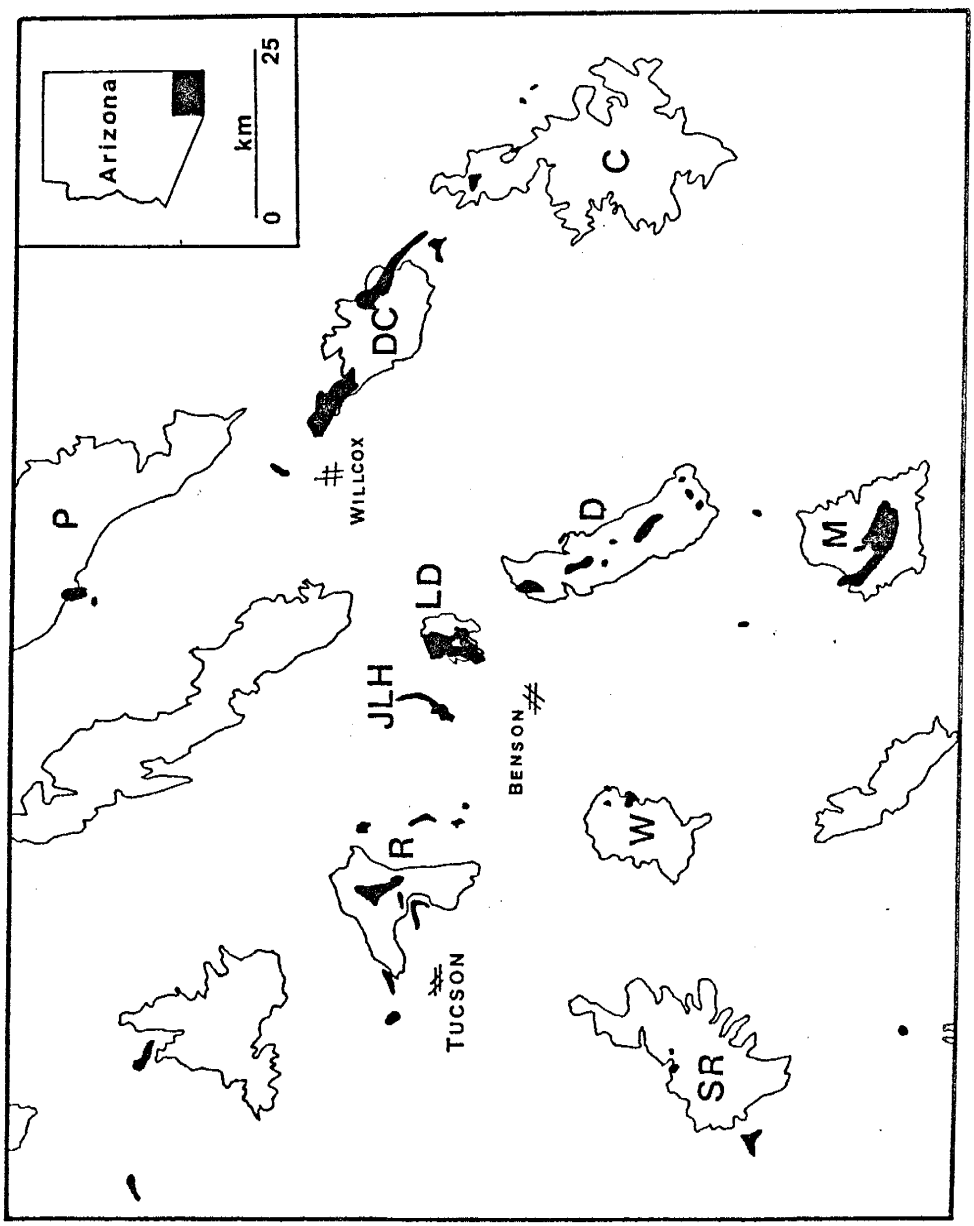

Figure 1. Map of southeastern Arizona showing major Precambrian exposures. P, Piñaleno Mountains; R, Rincon Mountains; JLH, Johnny Lyon Hills; LD, Little Dragoon Mountains; DC, Dos Cabezas Mountains; SR, Santa Rita Mountains; W, Whetstone Mountains; D, Dragoon Mountains; C, Chiricahua Mountains; M, Mule Mountains.

The Pinal Schist is the oldest known stratigraphic unit in southeastern Arizona. The basement to this supracrustal succession has yet to be recognized. The name Pinal Schist was first used by Ransome (1903) for quartz-sericite schists and quartzites in the Pinal Mountains. The term was subsequently extended to the Mule Mountains to describe quartz-rich metasediments near Bisbee (Ransome, 1904). Current usage refers to the schist in the Pinal Mountains as the type section although Ransome (1903) did not describe a section there. The term has been adopted by virtually all subsequent workers. Although the Pinal Schist is lithologically diverse, the whole succession appears to be genetically related. It has been included in the Pinal Supergroup by Conway and Silver (in press) which includes the Mazatzal, Alder, Haigler, and Hess Canyon Groups of central Arizona but no specific correlation is made between the central and southeastern parts of the state. In practical use the term "Pinal Schist" refers to foliated supracrustal rocks older than the ~1000 Ma Apache Group. It may be possible with the aid of detailed geochronology and detailed mapping to establish a more detailed stratigraphy, both within the Pinal Schist and relative to other supracrustal rocks in central Arizona. Until such data become readily available I do not favor an expansion of the

stratigraphic name "Pinal".

The coarsest grained metasediments of the Pinal Schist are found in the Dos Cabezas Mountains, where conglomerate and arkose are the dominant sedimentary rock types (Erickson, 1969; Condie and others, 1985). Throughout the remainder of Cochise and Pima Counties conglomerate is rare in the Pinal Schist. Metabasic rocks comprise a small (5-10 %) but widespread part of the succession, while felsic volcanic and subvolcanic rocks are important only in the Dos Cabezas Mountains. Scattered outcrops of felsic volcanic rocks are found in the Little Dragoon Mountains, Circle J Hills, the Piñaleno Mountains, and in the northern San Pedro Valley (Kreiger, 1968; 1974a; 1974b). One very minor carbonate unit has been described in the Dos Cabezas Mountains Mountains (Erickson, 1969; Condie and others, 1985).

Metamorphic grade in the Pinal Schist ranges from the greenschist to the lower amphibolite facies. Throughout the study area the Pinal Schist shows the effects of at least one Proterozoic metamorphic event. In the Rincon and Santa Rita Mountains, the Pinal Schist was subjected to a mid-Tertiary metamorphic-deformational event associated with the development of the many metamorphic core complexes of the North American Cordillera (Coney, 1980). Original textures are not

preserved in the Precambrian rocks of the Rincon or Santa Rita Mountains. Despite metamorphism, original sedimentary and igneous textures are present at many other localities. The lack of a significant metamorphic overprint allows a discussion of these rocks in terms of their protoliths. For convenience the prefix "meta" will be dropped from terms such as "metasandstone", "metabasalt", etc.

The age of the Pinal Schist is not well constrained but a U-Pb zircon date from a subvolcanic, predeformational felsic intrusion into the Pinal in the Dragoon quadrangle suggests an age of ~1690 Ma (Silver, 1963; 1978). All ages are calculated with the decay constants of Steiger and Jager (1977). The Madera quartz diorite, a syntectonic intrusion into the Pinal Schist near the type locality in the Pinal Mountains, yields a Rb-Sr isochron age of ~1690 Ma (Livingston, 1969). These ages are similar to those reported from felsic volcanics and granites from the Tonto Basin - Mazatzal Mountains area of central Arizona (Ludwig, 1974; Conway, 1976). These dates place only a lower limit on the age of the Pinal Schist. U-Pb zircon dates from volcanic rocks of the Pinal Schist are needed to more precisely constrain the age of the Pinal Schist.

The Pinal Schist has been subjected to at least two deformational events; at least one in the Proterozoic and

one during the Laramide orogeny. The Proterozoic deformation and metamorphism can be bracketed between ~1690 m.y., the age of predeformational intrusions in the Johnny Lyon Hills and Little Dragoon Mountains, and 1625 ± 10 m.y., the age of the post-deformational and unmetamorphosed Johnny Lyon Granodiorite which intrudes the Pinal Schist in the Johnny Lyon Hills (Silver and Duestch, 1961). Tertiary Basin and Range faulting is the chief control on the present outcrop pattern of the Pinal Schist today. Due to these several structural events, correlation of Precambrian units between mountain ranges is problematical. The rocks of the Pinal Schist in southeastern Arizona are herein treated in a regional context without attempting any detailed paleogeographic reconstructions.

Various tectonic settings have been suggested for the Pinal Schist. These include a classic eugeosynclinal setting (Cooper and Silver,1964; Silver, 1978), a continental rift setting (Condie and De Melas, 1985; Condie and others, 1985), and a continental margin (fore-arc) basin (De Melas, 1983; Conway and Silver, in press).

This thesis reports the results of a reconnaissance geochemical study of the Pinal Schist in Cochise and Pima Counties in southeastern Arizona. The study focuses on, in order of decreasing sample density, Proterozoic

supracrustal rocks from the Dragoon, Little Dragoon, Rincon, Whetstone, Mule, Chiricahua, Santa Rita and Dos Cabezas Mountains (Fig. 1, Plate 1). Sample locations and access to the study area are described in Appendix A. In addition to the new data presented here, the data of G.P. Bowling (in preparation) and R.K. Vance (1983) from the Dos Cabezas Mountains (which can be found in Condie and others, 1985) will be used to characterize the geochemistry of the Pinal Schist in southeastern Arizona.

From over 250 samples collected, 30 igneous (mostly volcanic) and 35 sedimentary rocks were selected for detailed chemical analysis. Analyses were performed by both X-ray fluorescence and instrumental neutron activation using well established methods (Gordon and others, 1968; Norrish and Hutton, 1969; Appendix B). Accuracy and precision of chemical data are discussed in Appendix C. Representative chemical compositions for the mafic, felsic, and sedimentary rocks are given in Tables 1, 2, and 6 respectively.

VOLCANIC ROCKS

Field Relationships

Mafic igneous rocks are a minor but widespread component of the Pinal Schist in the study area. Pillows and pillow breccias are present on the crest of the Dragoon Mountains between Cochise Stronghold East and Cochise Stronghold West (Drewes and Meyer, 1983; Plate 1). This is the most extensive outcrop area (2.5 km^2) of Pinal basalt yet described in southeastern Arizona. In the southern part of the area, the rocks are fine grained, massive, high MgO basalts with interbedded minor volcaniclastic units less than 0.5 m thick. Further north, the basalts contain amygdules filled with quartz and epidote. Abundant amygdules also occur in altered basalts on the eastern flank of the Dragoon Mountains, west of Sunsites (Drewes and Meyer, 1983; Plate 1). In the northernmost third of this outcrop area the basalts are extensively pillowed. The apparent thickness of the pillow basalt unit is ~400 m. The pillows, which appear to have been tectonically stretched, have a maximum dimension of 10 to 40 cm. Chilled margins on the pillows are preserved in some outcrops and can be seen in three dimensions. The basalts in the northern part of the area have more evolved compositions (Mg number of 35-48) than those in the south (Mg number 57-70). A similar

fragmental pillow breccia (maximum size of fragments ~ 10 cm) is present at the northwest tip of the Dos Cabezas Mountains. Cooper and Silver (1964) report evidence of a flow origin for the Pinal basalts in the Little Dragoon Mountains. Their evidence includes amygdules and possible pillow structures. The basalts in the Little Dragoon Mountains are concordant with the surrounding sedimentary rocks. The basaltic rocks in the Dos Cabezas Mountains have been interpreted by Erickson (1969) as flows and by Condie and others (1985) as sills. Mafic dikes crosscut metasediments in Jordan Canyon at the north end of the Dragoon Mountains (Plate 1). Metamorphism has obscured original textures in the Rincon and Santa Rita Mountains, but all basaltic rocks in these areas are concordant with the surrounding metasediments, suggesting they were originally flows or sills.

The felsic igneous rocks of the Dos Cabezas and Chiricahua Mountains are subaerial ash-flow tuffs and sills (Erickson 1969; Condie and others, 1985). The only other significant felsic igneous rocks of the Pinal Schist in the study area occur in the Johnny Lyon Hills and the Little Dragoon Mountains. Cooper and Silver (1964) mapped two felsic units in the Dragoon quadrangle. The most extensive of the two is a subvolcanic rhyodacite quartz porphyry. This unit occurs

as a large concordant mass in the northwest corner of the Little Dragoons and as several discordant dikes in the Johnny Lyon Hills. The other felsic unit mapped by Cooper and Silver occurs as a line of lensoidal outcrops which they interpreted as megaboudins. They cite evidence for a subaerial flow origin for this unit. Their evidence includes a chill zone at one contact with the surrounding sediments and a chilled flow-banded rhyolite breccia at the other contact. Cooper and Silver (1964) report the best evidence for flow origin of the rhyolite to be found at the largest of these lenses, southwest of the Seven Dash Ranch. It is the opinion of this author that field relations are equivocal between a flow and sill origin for this unit. This unit was not studied geochemically due to apparent alteration.

Petrography

Of the 14 mafic volcanic rocks studied in thin section, 11 have been metamorphosed to the grade of the biotite zone of the greenschist facies and the three rocks studied from the Rincon Mountains have been metamorphosed to the sillimanite-orthoclase zone of the amphibolite facies. The mineral assemblage of the Pinal basalts in the Little Dragoon and Dragoon Mountains is actinolite ± chlorite ± plagioclase ± epidote ± quartz ± magnetite ± calcite. Plagioclase content ranges from 5 to 40 percent with a maximum length of plagioclase

laths of ~1.5 mm. Calcite and most of the epidote and quartz appear in fractures, amygdules, or along the rinds of brecciated fragments. Actinolite and chlorite occur as fine grained (< 0.5 mm) radiating crystals.

The subvolcanic intrusive porphyry of the Little Dragoons and Johnny Lyon Hills is composed of ~25 % partially resorbed quartz phenocrysts (0.5-1.5 mm), ~ 15% sericitized subhedral plagioclase phenocrysts (0.3-0.7 mm), and 0-3 % subhedral hematite (0.1-0.4 mm). Plagioclase has indistinct boundaries with the surrounding matrix. The matrix is composed of fine grained (< 0.05 mm) quartz and sericite.

A more detailed petrographic description of individual samples can be found in Appendix D.

Geochemistry

Igneous rocks from the study area classified with the SiO_2 -Zr/ TiO_2 diagram of Winchester and Floyd (1976) include rhyolite, rhyodacite, andesite, subalkaline basalt (tholeiite), and alkali basalt (Fig. 2). The dominant igneous rock types are tholeiite and rhyodacite. For brevity, all the mafic volcanic and subvolcanic rocks will be referred to as basalts. The major element composition of these rocks displays characteristics intermediate between a tholeiitic series and a calc-alkaline series on both a Jensen cation plot (Jensen, 1976; Fig. 3) and a AFM plot (Irvine and

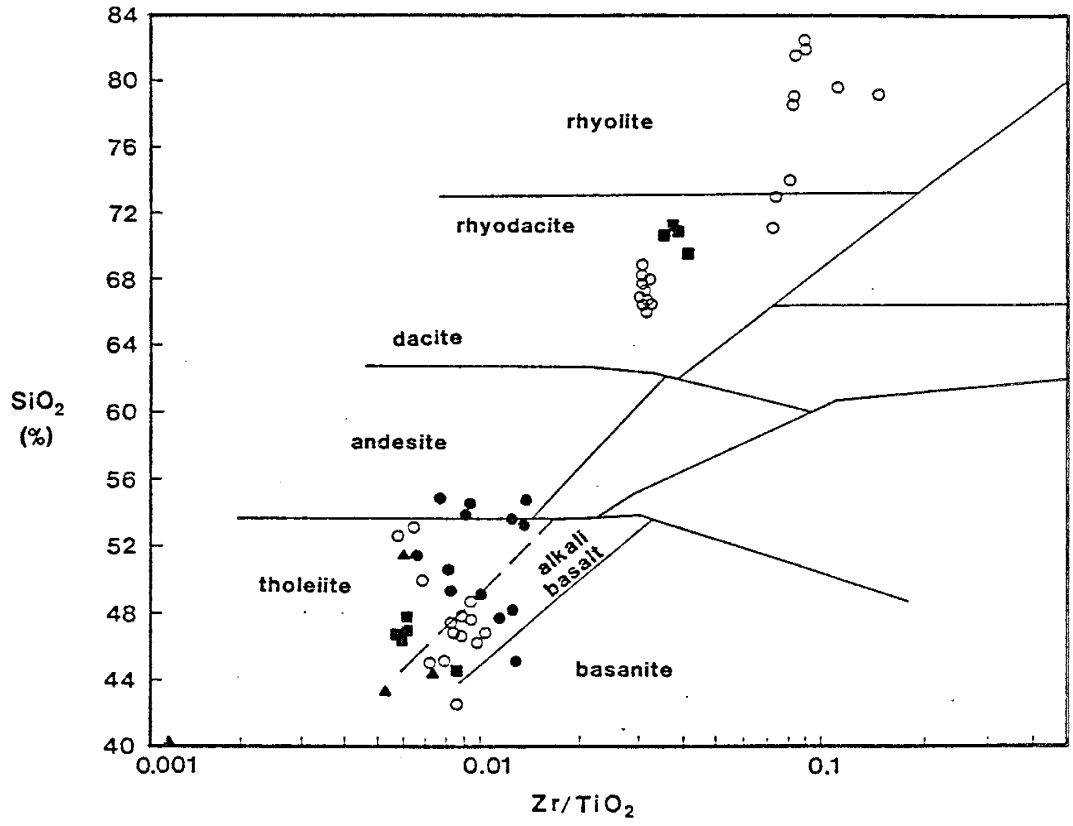

Figure 2. Classification of volcanic and subvolcanic rocks of the Pinal Schist in southeastern Arizona. Fields from Winchester and Floyd (1976). Filled circles, Dragoon Mountains; open circles, Dos Cabezas and Chiricahua Mountains; squares, Little Dragoon Mountains and Johnny Lyon Hills; triangles, Rincon and Santa Rita Mountains.

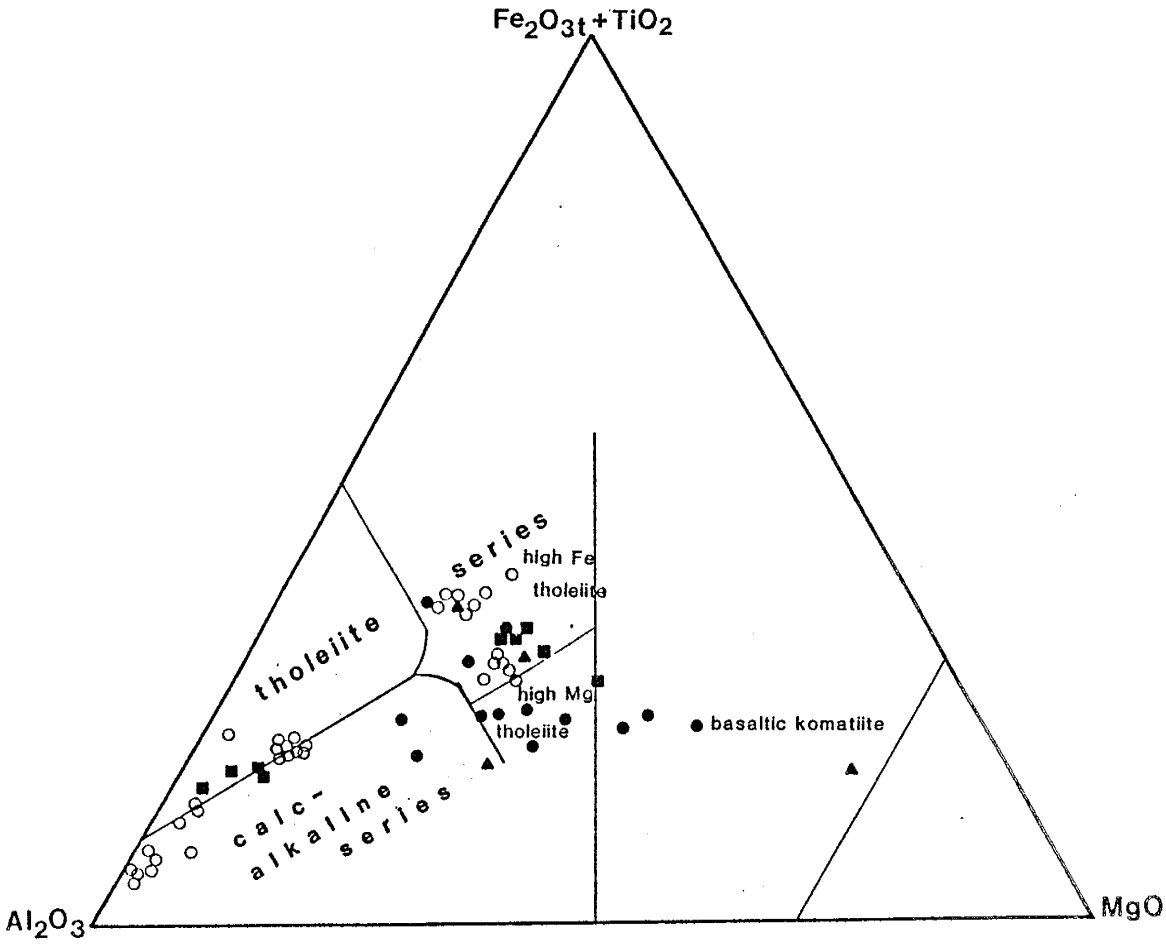

Figure 3. Jensen cation plot of volcanic and subvolcanic rocks of the Pinal Schist in southeastern Arizona. Filled circles, Dragoon Mountains; open circles, Dos Cabezas and Chiricahua Mountains; squares, Little Dragoon Mountains and Johnny Lyon Hills; triangles, Rincon and Santa Rita Mountains. Fields from Jensen (1976).

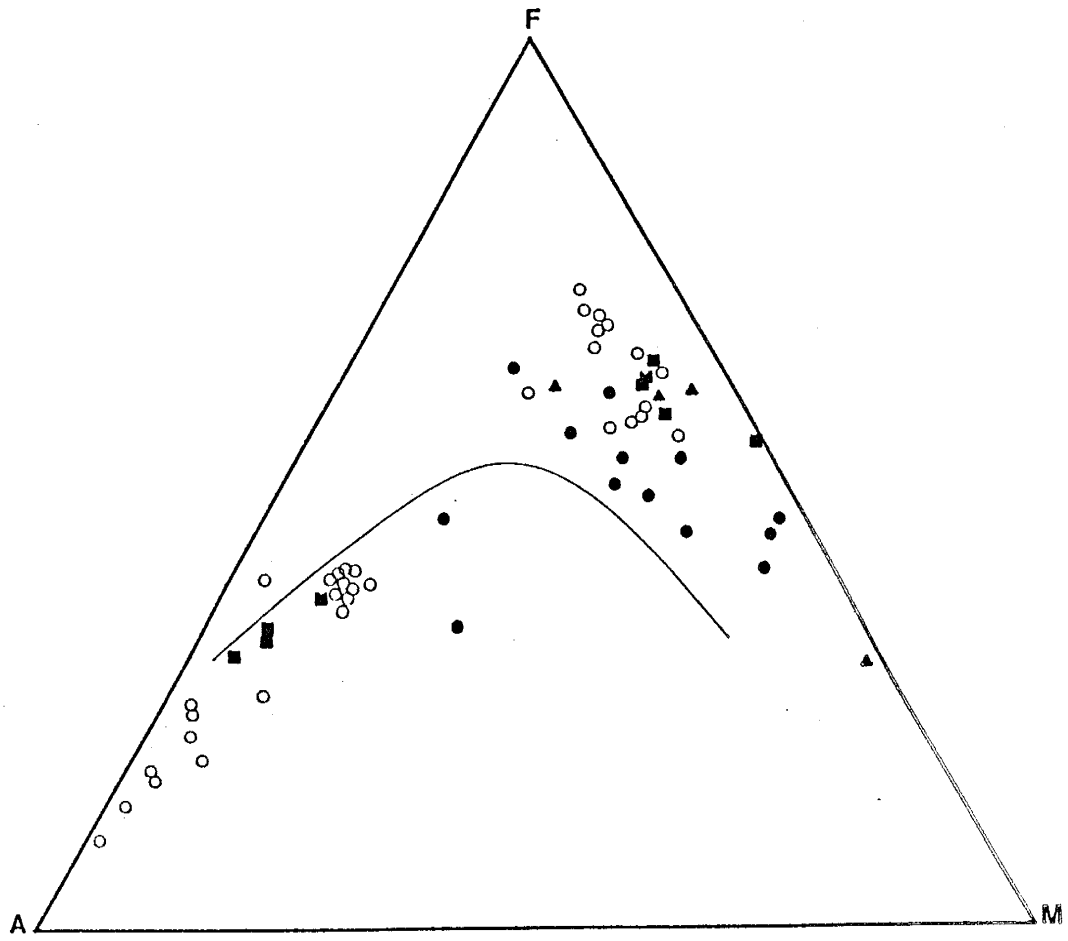

Figure 4. AFM plot (Irvine and Baragar, 1971) for volcanic and subvolcanic rocks of the Pinal Schist in southeastern Arizona. Filled circles, Dragoon Mountains; open circles, Dos Cabezas and Chiricahua Mountains; squares, Little Dragoon Mountains and Johnny Lyon Hills; triangles, Rincon and Santa Rita Mountains.

Baragar, 1971; Fig. 4). There is a compositional gap in this igneous series with rocks with SiO_2 contents between 55 and 65 % missing. This gap may be real or may be attributable to a sampling bias. The available chemical data have more characteristics of a continuous calc-alkaline series than many bimodal suites. The number and geographic distribution of samples analyzed may be inadequet to recognize all igneous rock types present in the Pinal Schist.

Mafic Rocks

The basalts in the study area have large ranges in MgO, TiO_2 , Cr, Ni, K, and Rb (Table 1). The chondrite normalized rare earth element (REE) patterns of the basalts are flat to slightly light REE enriched (Fig. 5). For the purpose of convenient comparison, averages of basalts from different geographic areas (Little Dragoon Mountains, Dragoon Mountains, Rincon Mountains, Dos Cabezas and Chiricahua Mountains) will be used (Table 1). This seems to be a reasonable approach as intra-group variations are less than inter-group variations. In averages of the basalts from the Little Dragoon Mountains sample AZ-15 has been excluded due to its high loss on ignition (> 8%).

The most primitive composition observed is from the one amphibolite analyzed from the Santa Rita Mountains (P.85.53, Table 1). This sample has 40% SiO_2 , 25.3%

Table 1. Chemical composition of mafic rocks

location	Drag	Drag	Drag	Drag	Drag
sample	P.84.128	P.84.132	P.84.133	P.84.135	P.85.20
SiO_2	47.90	53.43	50.99	50.56	54.50
TiO_2	0.97	0.92	0.96	0.85	1.52
Al_2O_3	11.58	11.72	15.61	15.09	13.98
Fe_2O_{3t}	12.46	10.31	10.99	11.02	14.88
MgO	12.43	10.77	6.60	7.14	3.49
CaO	12.68	10.88	10.62	12.25	6.97
Na_2O	0.49	0.78	3.10	1.60	4.01
K2O	0.19	0.21	0.12	0.20	0.44
MnO	0.37	0.40	0.23	0.20	0.25
P_2O_5	0.19	0.19	0.07	0.09	0.13
LOI	0.93	1.06	0.77	0.66	0.43
TOTAL	100.19	100.67	100.06	99.66	100.60
Rb	16	18	5.8	16	14
Ba	22	67	71	70	177
Cs	1.4	3.5	0.8	1.5	3.4
Sr	127	173	193	153	261
Pb	10	4.4	14	13	14
Th	1.8	2.5	1.4	1.1	3.9
U	0.76	1.0	0.38	2.6	1.2
Sc	36	38	51	24	40
Cr	1793	879	77	243	3.0
Co	59	52	50	47	44
Ni	472	197	51	79	26
Cu	48			108	
Zn	164	144	103	97	
Sb		1.5		0.82	0.50
Ga	18	14	16	16	
Y	26	27	25	23	40
Zr	111	125	74	69	140
Nb	10	9.4	5.7	6.0	6.1
Hf	2.7	3.9	2.4	1.8	4.0
Ta	0.36	0.39	0.15	0.15	0.38
La	9.3	13	5.0	5.2	15
Ce	22	33	13	12	36
Sm	3.5	4.2	2.8	2.2	5.1
Eu	0.75	0.95	0.90	0.89	1.4
Tb	0.89	0.91	0.70	0.51	0.96
Yb	2.4	2.6	2.7	2.4	3.8
Lu	0.33	0.43	0.47	0.38	0.61
Mg #	69	70	57	59	35

Table 1, continued

location	Drag	Drag	Drag	Drag	Drag
sample	P.85.21	P.85.40	P.85.45	P.85.22	P.84.162
SiO_2	53.88	48.12	54.71	49.47	45.12
TiO_2	1.17	0.88	0.94	1.71	0.69
Al_2O_3	14.42	12.66	15.56	13.67	9.73
Fe_2O_{3t}	13.18	10.56	7.03	15.44	11.44
MgO	5.32	8.57	4.46	6.24	13.17
CaO	8.60	11.84	4.89	9.93	10.21
Na_2O	3.48	1.45	4.86	2.54	0.88
K2O	0.73	1.27	2.64	0.45	0.80
MnO	0.23	0.66	0.09	0.25	0.27
P_2O_5	0.11	0.18	0.23	0.16	0.18
LOI	0.37	2.91	4.80	0.78	7.58
TOTAL	101.49	99.10	100.39	100.64	100.07
Rb	22	59	90	18	61
Ba				205	51
Cs	3.9	3.5	3.2	1.4	9.3
Sr	140	300	425	116	116
Pb	1.0	20	16	12	13
Th	2.5	4.5	2.2	1.5	2.3
U	0.43	1.2	0.63	0.67	0.73
Sc	42	32	15	43	32
Cr	12	685	138	123	1237
Co	44	33	21	44	67
Ni	16	196	57	72	518
Cu					
Zn	220	512	69		128
Sb	0.25	0.07	0.50	0.60	0.37
Ga					10
Y	36	23	18	45	21
Zr	107	112	131	140	89
Nb	5.3	7.6	6.3	6.3	7.7
Hf	3.1	2.7	3.3	3.1	2.5
Ta	0.24	0.36	0.29	0.26	0.33
La	10	19	15	8.6	10
Ce	25	43	42	23	25
Sm	4.0	4.4	3.5	4.8	3.7
Eu	1.2	1.0	1.2	1.3	0.98
Tb	0.84	0.58	0.47	1.0	0.50
Yb	3.5	1.7	1.1	3.8	2.0
Lu	0.53	0.41	0.45	0.60	0.31
Mg #	48	65	60	48	72

Table 1, continued

location	Drag	Drag	Drag		LD
sample	P.84.166	P.84.170	P.85.27	avgdrag	P.84.34
SiO_2	53.63	49.25	51.31	50.99	46.61
TiO_2	0.69	1.23	0.84	1.03	1.99
Al_2O_3	14.22	17.61	14.56	13.88	13.91
Fe_2O_{3t}	9.35	10.03	11.70	11.41	15.32
MgO	8.19	4.51	7.96	7.62	8.16
CaO	7.52	4.96	8.86	9.25	9.87
Na_2O	1.67	5.11	1.39	2.41	1.94
K2O	0.68	1.07	1.80	0.82	0.14
MnO	0.17	0.17	0.25	0.27	0.26
P_2O_5	0.09	0.35	0.06	0.16	0.20
LOI	4.35	6.25	2.01	2.53	1.60
TOTAL	100.56	100.54	100.74	100.36	100.00
Rb	46	54	168	45	4.7
Ba	218	168	1569	262	52
Cs	9.9	15	6.5	4.9	
Sr	360	268	293	255	233
Pb	31	16	20	14	15
Th	3.9	3.5	0.56	2.4	0.51
U	1.2	0.83	0.03	0.90	1.2
Sc	33	189	40	47	31
Cr	366	16	100	436	157
Co	47	32	40	45	57
Ni	131	18	73	147	88
Cu	71			76	65
Zn	88	167		169	133
Sb	1.2	0.88	0.41	0.65	2.6
Ga	14	16		15	20
Y	19	19	29	27	25
Zr	87	123	55	105	114
Nb	5.7	10	2.4	6.8	13
Hf	2.7	3.0	1.5	2.8	3.1
Ta	0.29	0.47	0.10	0.29	0.69
La	15	17	3.1	11	8.1
Ce	37	40	9.0	28	20
Sm	3.7	4.1	2.1	3.7	3.7
Eu	0.98	1.4	0.64	1.0	1.5
Tb	0.56	0.55	0.49	0.69	0.82
Yb	2.0	1.6	2.1	2.4	2.6
Lu	0.34	0.29	0.31	0.42	0.39
Mg #	66	50	60	60	54

Table 1, continued

location	LD	LD	LD	LD	
sample	P.84.36	AZ-7	AZ-8	AZ-15	avgLD
SiO_2	47.85	46.50	46.70	44.62	46.92
TiO_2	1.79	2.00	1.90	1.87	1.92
Al_2O_3	12.56	14.10	14.00	12.42	13.64
Fe_2O_{3t}	14.66	15.30	15.10	13.31	15.10
MgO	6.57	6.90	6.35	9.91	6.99
CaO	9.32	9.54	11.40	9.72	10.03
Na_2O	1.70	1.92	1.31	0.10	1.72
K20	0.02	0.004	0.04	0.01	0.05
MnO	0.24	0.21	0.21	0.23	0.23
P_2O_5	0.17	0.19	0.19	0.23	0.19
LOI	5.62	4.05	2.61	8.09	3.47
TOTAL	100.50	100.71	99.81	100.51	100.26
Rb	2.3	2.3	2.2	3.6	2.9
Ba	32	16	23	22	31
Cs		0.21	0.41	0.31	0.30
Sr	312	250	275	415	268
Pb	9.4		0.9	25	42
Th	0.53	0.65	0.61	2.9	0.58
U	0.04	0.19	0.19	0.56	0.40
Sc	41	46	43	34	40
Cr	94	112	88	598	113
Co	54	53	48	66	53
Ni	67	97	68	447	80
Cu	33			45	49
Zn	130	144	142	156	137
Sb	1.1		1.8	5.7	1.8
Ga	16			18	18
Y	27	29	30	18	28
Zr	109	115	115	160	113
Nb	13	8.5	9.1	19	11
Hf	3.2	2.9	2.8	4.6	3.0
Ta	0.59	0.67	0.57	1.1	0.63
La	7.8	8.5	7.6	23	8.0
Ce	21	22	19	54	21
Sm	4.0	4.7	4.3	6.0	4.2
Eu	1.3	1.5	1.5	1.6	1.5
Tb	0.77	0.92	0.94	0.68	0.86
Yb	2.6	2.6	2.4	1.5	2.6
Lu	0.45	0.41	0.45	0.26	0.43
Mg #	50	50	49	63	51

Table 1, continued

location	Rin	Rin	Rin		SR
sample	P.84.77	P.84.76	P.84.228	avgRin	P.85.53
SiO_2	51.36	43.31	44.40	46.36	39.96
TiO_2	1.22	1.45	3.28	1.98	0.19
Al_2O_3	13.65	18.57	15.57	15.93	7.74
Fe_2O_{3t}	14.36	16.04	15.93	15.44	12.39
MgO	7.10	8.62	5.13	6.95	25.25
CaO	9.73	10.48	8.24	9.48	3.86
Na_2O	1.26	0.92	2.75	1.64	0.43
K20	0.46	0.11	1.38	0.65	0.13
MnO	0.37	0.36	0.24	0.32	0.16
P_2O_5	0.09	0.13	1.12	0.45	0.05
LOI	0.93	0.27	1.23	0.81	8.55
TOTAL	100.53	100.26	99.27	100.02	98.71
Rb	35	10	59	35	7.5
Ba	56	25	511	197	
Cs	1.5	0.34	17	6.3	2.7
Sr	263	521	333	372	83
Pb	8.2	8.5	25	14	14
Th	0.38	6.1	1.9	2.8	0.55
U	0.29	5.7	0.44	2.1	0.29
Sc	41	38	28	36	12
Cr	81	139	45	88	2323
Co	55	60	58	58	135
Ni	83	111	62	85	1280
Cu			57		
Zn	180	150	189	173	106
Sb					2.5
Ga	19	32	26	26	
Y	25	32	49	35	6.4
Zr	73	79	239	130	23
Nb	7.9	8.5	15	10	4.7
Hf	2.1	1.7	7.1	3.6	0.68
Ta	0.25	0.55	0.88	0.56	0.06
La	4.7	4.3	26	12	3.0
Ce	12	12	68	31	9.0
Sm	2.6	3.0	11	5.5	0.74
Eu	0.93	1.5	3.5	2.0	0.22
Tb	0.55	0.84	1.5	1.0	0.10
Yb	2.3	3.4	4.5	3.4	0.52
Lu	0.34	0.56	0.73	0.54	0.07
Mg #	53	55	42	50	82

Table 1, continued

location	Chir	Chir	Chir
sample	P.85.6	P.85.7	P.85.8
SiO_2	47.09	47.55	46.67
TiO_2	2.31	2.56	2.31
Al_2O_3	15.48	14.41	15.42
Fe_2O_{3t}	16.85	17.58	17.13
MgO	5.21	5.44	5.60
CaO	10.88	9.92	10.37
Na_2O	1.69	1.92	2.49
K2O	0.36	0.40	0.29
MnO	0.24	0.25	0.29
P_2O_5	0.29	0.32	0.31
LOI	0.38	0.31	0.21
TOTAL	100.78	100.66	101.09
Rb	27	25	10
Ba	230	147	
Cs	1.9	3.2	0.31
Sr	293	201	278
Pb	16	14	14
Th	2.4	3.0	2.9
U	0.78	0.87	0.73
Sc	30	42	41
Cr	31	45	35
Co	51	70	69
Ni	83	87	92
Cu			
Zn	200		300
Sb	4.3	3.1	2.8
Ga			
Y	46	53	49
Zr	192	213	203
Nb	7.3	8.3	7.7
Hf	4.6	6.1	6.3
Ta	0.41	0.49	0.49
La	13	20	20
Ce	34	50	51
Sm	6.1	7.8	7.8
Eu	1.5	2.2	2.4
Tb	1.3	1.5	1.5
Yb	3.8	5.0	5.0
Lu	0.57	0.80	0.79
Mg #	41	41	42

Table 1, continued

EXPLANATION

Fe_2O_{3t}: total iron as Fe2O3
LOI: loss on ignition
Mg #: (MgO/(MgO+(0.79*Fe2O3t)))*100, molar proportions
major elements in percent
trace elements in ppm
Drag: Dragoon Mountains
LD: Little Dragoon Mountains
Rin: Rincon Mountains
SR: Santa Rita Mountains
Chir: Chiracahua Mountains
blank indicates not determined

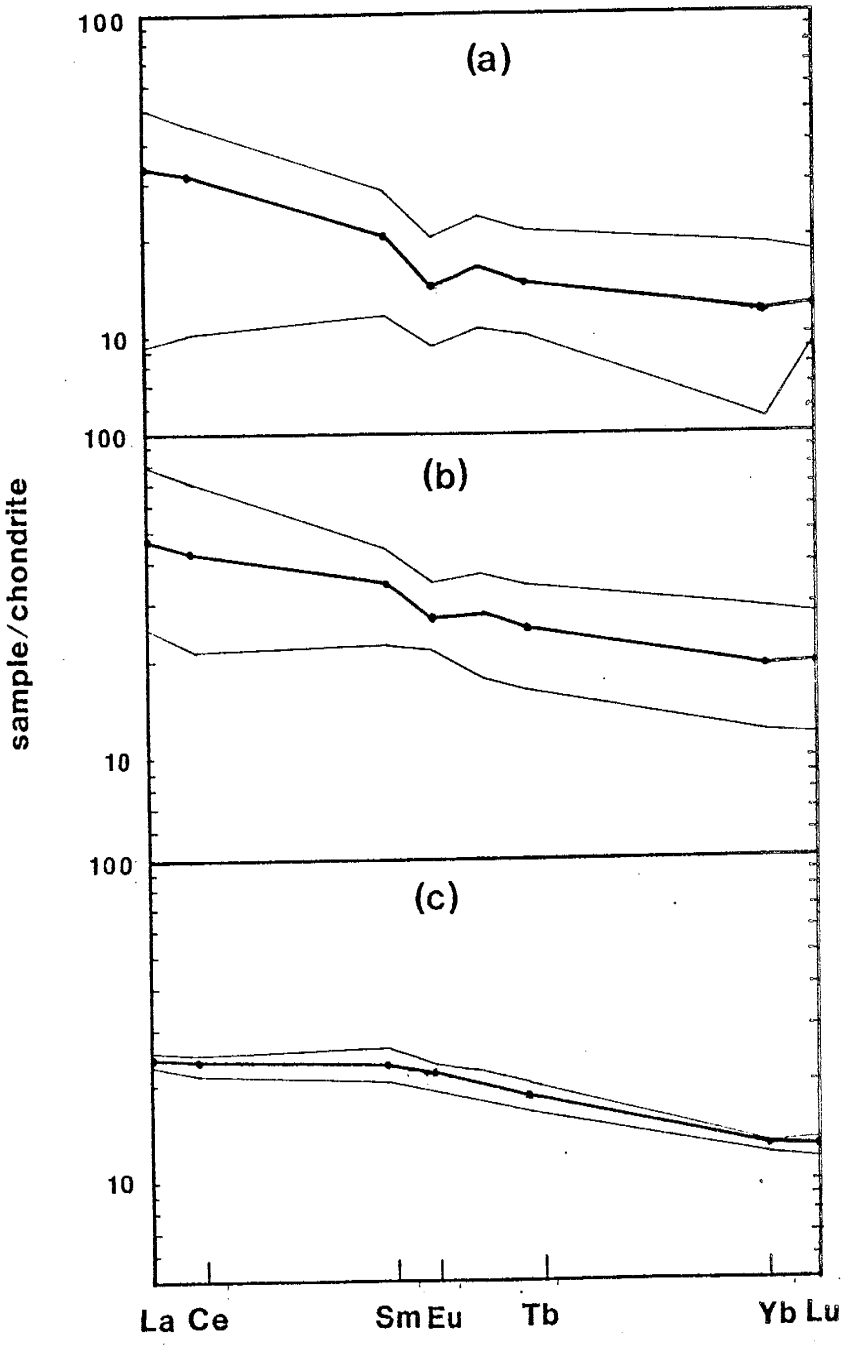

Figure 5. Chondrite normalized rare earth element distributions of Pinal basalts. Heavy line is average value, thin lines indicate range of samples (a) Dos Cabezas Mountains (n=14), (b) Dragoon Mountains (n=13), (c) Little Dragoon Mountains (n=4).

MgO, 2325 ppm Cr, 1280 ppm Ni, and a Mg number of 82. The unit from which the sample was collected is ~1.5 m thick with conformable contacts with the surrounding paragneisses. Original textures have been destroyed by metamorphism. The texture, field relationships, and chemical composition of this rock suggests it formed as an olivine cumulate in a sill intruded into sediments.

Geochemical modeling (Appendix E) indicates the large variation in the composition of Pinal basalts at Cochise Stronghold in the Dragoons may be related to fractional crystallization of clinopyroxene, plagioclase, olivine, and magnetite. This modeling scheme yields moderately satisfactory results for major elements but has a slightly poorer fit for trace elements. Small amounts of contamination of a primitive basalt with felsic volcanic rocks, quartz-rich sediments, or granitic rocks could sufficiently perturb this system to cause such a relationship. The smooth covariation of Mg number vs. Cr and Mg number vs. Ni (Fig. 6) suggests that fractional crystallization had a more significant effect on the geochemical trends in these rocks than contamination.

To further characterize the mafic rocks of the Pinal Schist, incompatible trace elements have been plotted on mid-ocean ridge basalt (MORB) normalized multi-element diagrams (Pearce, 1983). The shapes of patterns on such

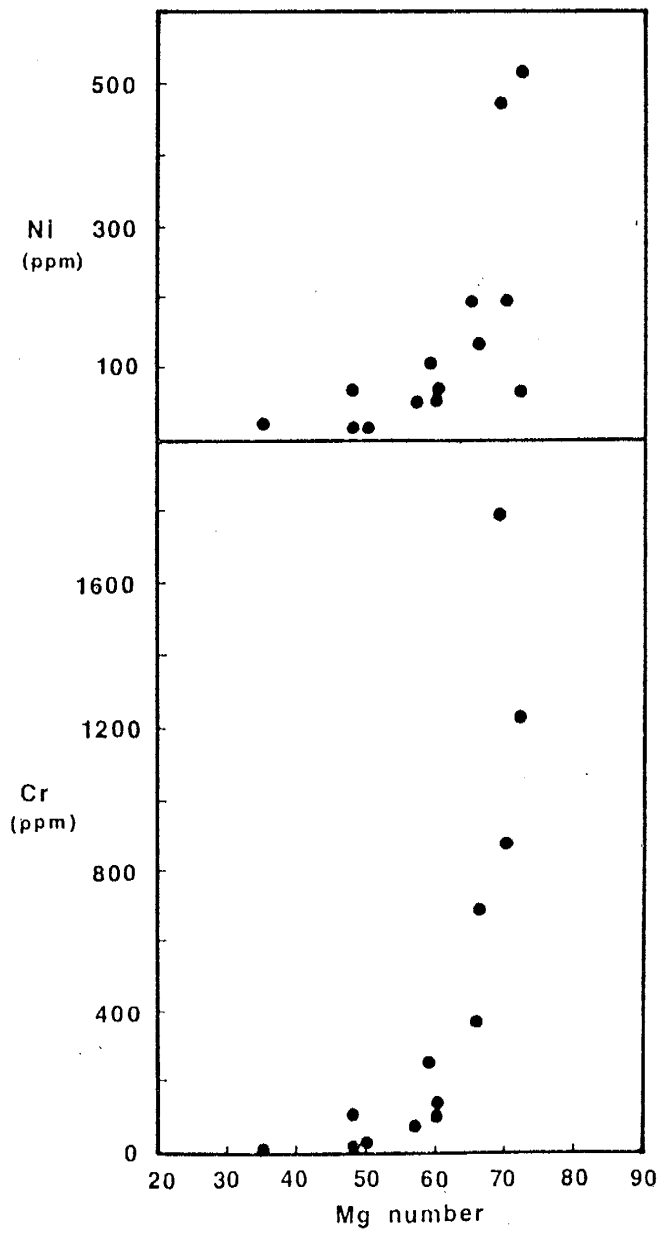

Figure 5. Chondrite normalized rare earth element distributions of Pinal basalts. Heavy line is average value, thin lines indicate range of samples (a) Dos Cabezas Mountains (n=14), (b) Dragoon Mountains (n=13), (c) Little Dragoon Mountains (n=4).

diagrams are influenced by the chemical composition of the source area of the samples in question and/or by contamination during their ascent through the crust, but are not greatly affected by fractional crystallization or partial melting (Pearce, 1983). Geochemical evolution of the upper mantle via fractional crystallization and partial melting is therefore likely to change the level but not the shape of these patterns. It is therefore reasonable to compare early Proterozoic basalt trace element patterns to patterns of younger rocks (Pharaoh and Pearce, 1984).

When plotted on MORB normalized diagrams, the mafic rocks of the Pinal Schist in the Dragoon, Dos Cabezas, and Rincon Mountains are enriched in large ion lithophile (LIL) elements such as Sr, K, Rb, Ba, and Th relative to high field strength (HFS) elements such as Ta, Nb, Ce, P, Zr, Hf, Sm, Ti, Y, and Yb (figures 7a, 7b). This enrichment of LIL elements relative to HFS elements is a feature characteristic of arc and back-arc magmas (Saunders and Tarney, 1984). This effect can be attributed to LIL element enrichment of the mantle beneath an arc which results from LIL elements being transferred with volatiles derived from a subducting, dehydrating slab. HFS elements, which are not greatly mobilized by aqueous fluids, are retained in the subducting slab in minerals such as zircon, rutile, and

magnetite and are returned to the deep mantle (for a more complete discussion of this process see Saunders and Tarney, 1984). Figure 7a compares average MORB normalized trace element compositions of the Rincon, Dragoon, and Dos Cabezas Mountains to average island arc tholeiite (IAT) of Pearce (1983). Figure 7b compares the same average compositions of rocks from the study area to the range of trace element compositions reported from the Sarmiento and Tortuga complexes of southern Chile (Saunders and others, 1979; Stern, 1980). These mafic complexes have been interpreted to be the remnants of a marginal basin which formed by ensialic back-arc spreading behind the Andean arc in the Cretaceous (Saunders and others, 1979; Stern, 1980; Dott and others, 1982). In figures 7a and 7b, the overall shape of the element patterns from Pinal basalts from the Rincon, Dragoon, and Dos Cabezas Mountains matches both the IAT and the back-arc basalts of southern Chile. The Pinal basalts also fall within the range of compositions seen in the Sarmiento and Tortuga complexes (Fig. 7b). The magnitude of the range seen for the south Chile rocks is strongly affected by a few anomalous samples. This is particularly true for the lower limit of Sr, K, and Ba and the upper limit of Ce, P, and Sm. The MORB normalized trace element patterns from the Pinal basalts of the Rincon, Dragoon, and Dos Cabezas Mountains are

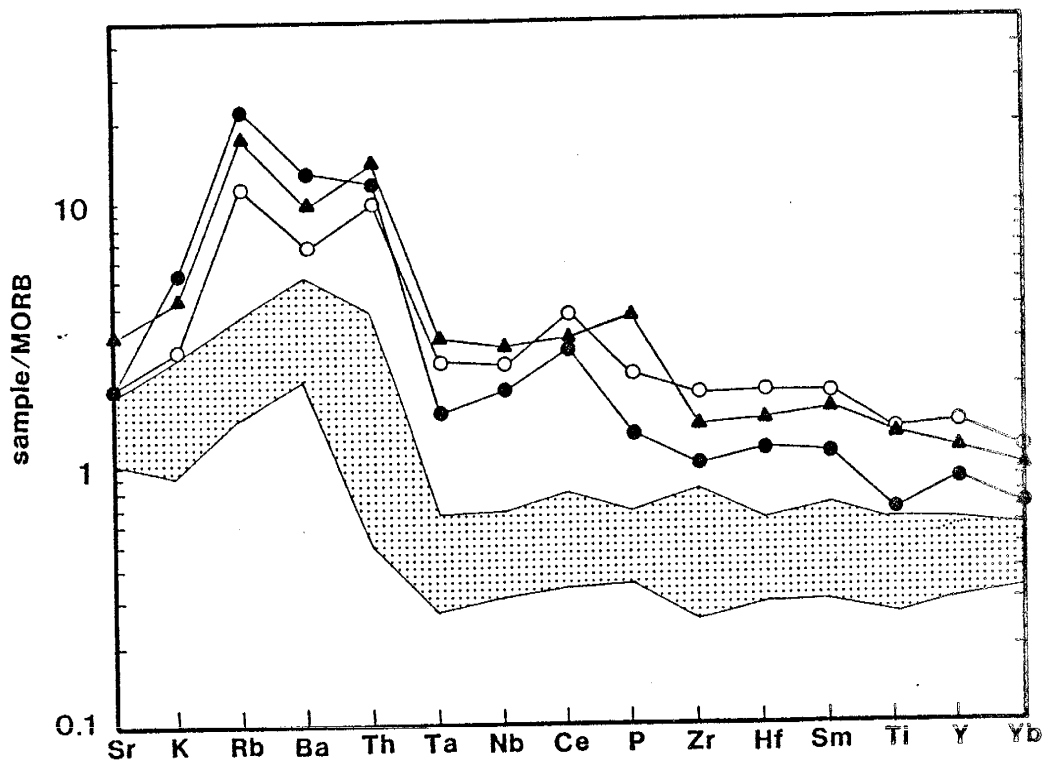

Figure 7a. Average MORB normalized trace element patterns of Pinal basalts compared to typical island arc tholeiite (Pearce, 1983). Open circles, Dos Cabezas Mountains (n=14); filled circles, Dragoon Mountains (n=13), triangles, Rincon Mountians (n=3).

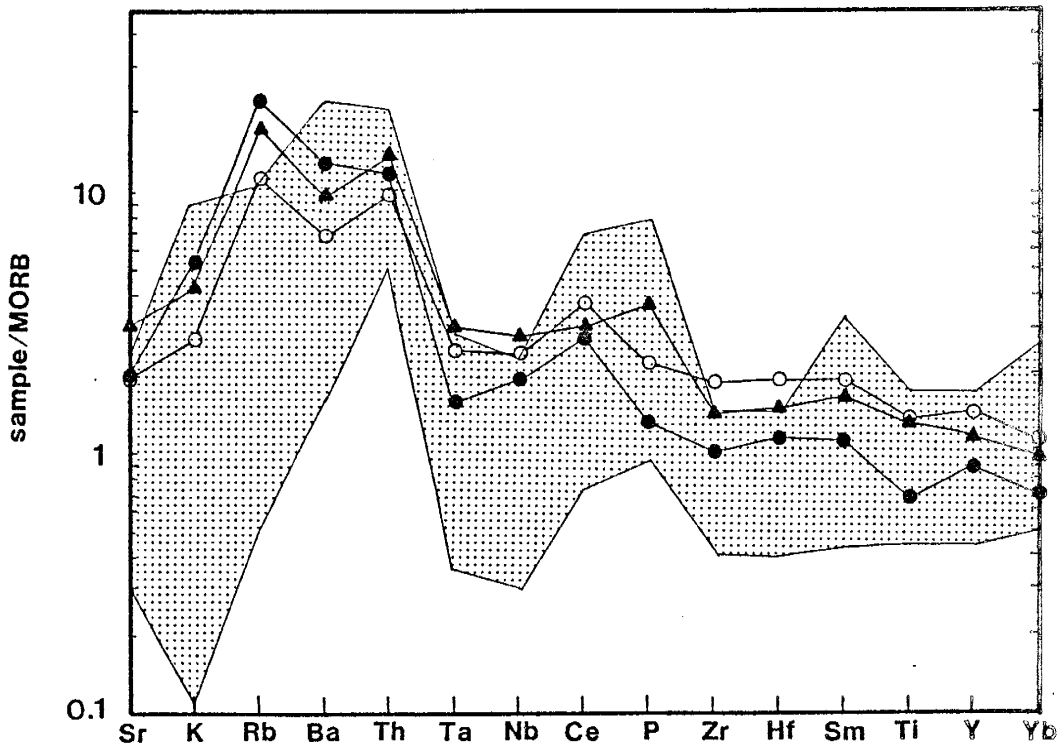

Figure 7b. Average MORB normalized trace element pattern of Pinal basalts compared to the range of compositions of the mafic rocks of the Sarmiento and Tortuga Complexes, southern Chile (Saunders and others, 1979; Stern, 1980). Symbols as in figure 7a.

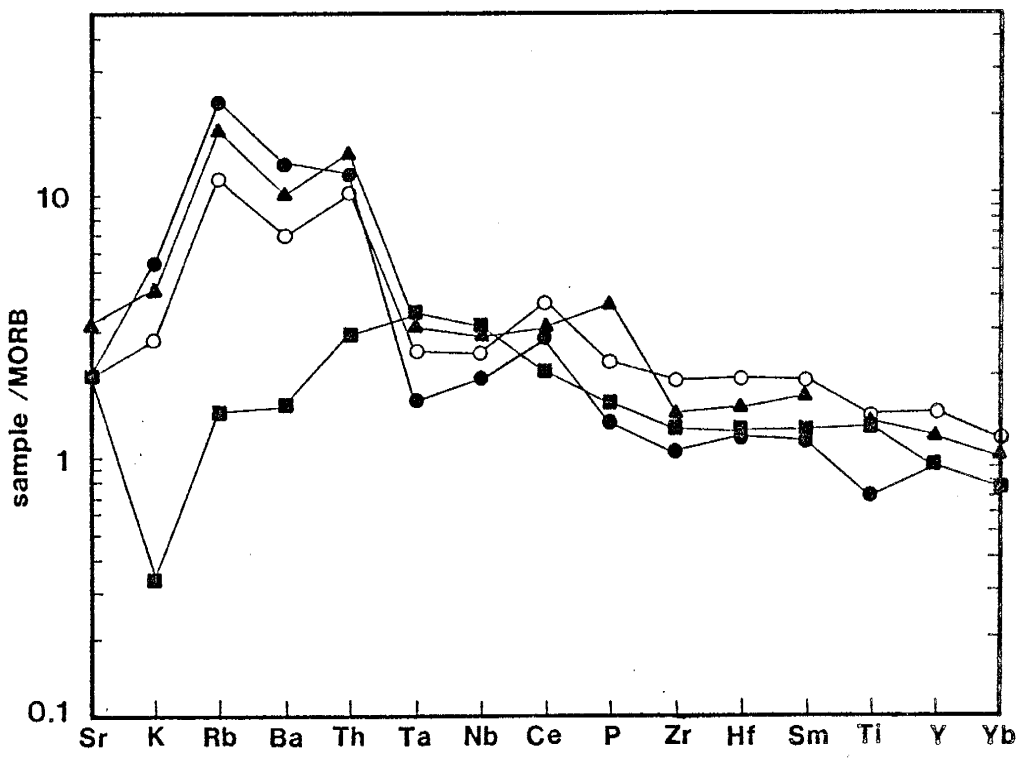

Figure 7c. Average MORB normalized trace element pattern of Pinal basalts from the study area. Open circles, Dos Cabezas (n=14); filled circles, Dragoons (n=13); triangles, Rincons (n=3); squares, Little Dragoons (n=4).

dissimilar to those from mid-ocean ridge basalts, oceanic island basalts, and continental flood basalts. These basalt types do not exhibit an enrichment of LIL elements relative to HFS elements.

As Figure 7c illustrates, basalts from the northeastern Little Dragoon Mountains near the abandoned Seven Dash Ranch are chemically distinct from other early Proterozoic basalts in the region. The Little Dragoon basalts do not show the LIL element vs. HFS element enrichment typical of arc and back-arc magmas (Fig. 7c). In fact, the Little Dragoon basalts are depleted in K relative to the HFS elements. It is possible that this feature is a result of alteration. When sample AZ-15 is included in the average, the Little Dragoon basalts appear depleted in Rb and Ba as well as K relative to the HFS elements. Despite this, Th, which is the least mobile of the LIL elements during metamorphism and alteration, is not enriched relative to and has a MORB normalized abundance similar to the HFS elements. Similar MORB normalized patterns have been observed from some oceanic back-arc basins (Marsh and others, 1980; Gill, 1976) and continental flood basalts such as the Snake River Plain basalts (Leeman and Vitalino, 1976).

To further characterize the chemical composition of the Pinal basalts and to constrain the tectonic setting in which they formed, geochemical data from the Pinal

basalts are plotted on a series of tectonomagmatic discrimination diagrams (Figs. 8, 9, 10, 11). A caution to the reader concerning the utility of comparing the geochemistry of early Proterozoic metavolcanic to modern volcanics is warranted here. Every plate tectonic environment that has existed in Earth's history may not be represented by those we see today. The mantle has also undergone a chemical evolution with time. These facts notwithstanding, the use of such discrimination diagrams provides a useful framework with which ancient and modern magmas can be compared (Pharaoh and Pearce, 1984). In applying this framework, certain tectonic and geochemical processes may be eliminated from consideration. Hypotheses may then be made based on similarities to modern examples. This is not to say that a geochemical match between two rock suites indicates that the two evolved under identical conditions but that such similarities do give us some insight into Precambrian processes.

When plotted on the Th-Hf-Ta discrimination diagram of Wood (1980), 27 of 28 volcanic rocks of the Dos Cabezas, Chiricahua and Dragoon Mountains fall in the destructive plate margin (DPM) field (Fig. 8a). All of the 13 samples from the Dragoon Mountains plot in the calc-alkaline subfield of the DPM field. Eight of the Dos Cabezas and Chiricahua samples fall within the calc-

alkaline subfield of the DPM field, five in the primitive arc subfield of the DPM field, and one in the field of enriched mid-ocean ridge basalt (EMORB) and tholeiitic within plate basalt. All of the felsic volcanic and subvolcanic rocks analyzed from the Dos Cabezas Mountains, Little Dragoon Mountains, and Johnny Lyon Hills fall in the calc-alkaline subfield of the DPM field (Fig. 8b). In Figure 8a the Little Dragoon basalts do not plot in the magmatic arc field but in the field of EMORB and tholeiitic within plate basalt. Figure 8c shows the distribution of basalts of the Chasma Group of central Peru (Atherton and others, 1985) is similar to that of the Pinal basalts (Fig. 8a). The Chasma Group was erupted in an ensialic back-arc basin in central Peru behind the Andean arc during the Cretaceous.

Figure 9 shows the Pinal basalts plotted on the Zr-Ti-Y tectonomagmatic discrimination diagram of Pearce and Cann (1973). This diagram is most effective in separating arc basalts, which plot in fields A, B, and C, from within plate basalts (WPB), which plot in field D. All of the Little Dragoon basalts fall within the WPB field or on the border of the WPB field and the IAT-MORB field while only three of the 30 samples from the Dos Cabezas, Chiricahua, Dragoon, and Rincon Mountains fall outside of the arc fields. Field B is also the field of mid-ocean ridge basalts. This origin can be ruled out

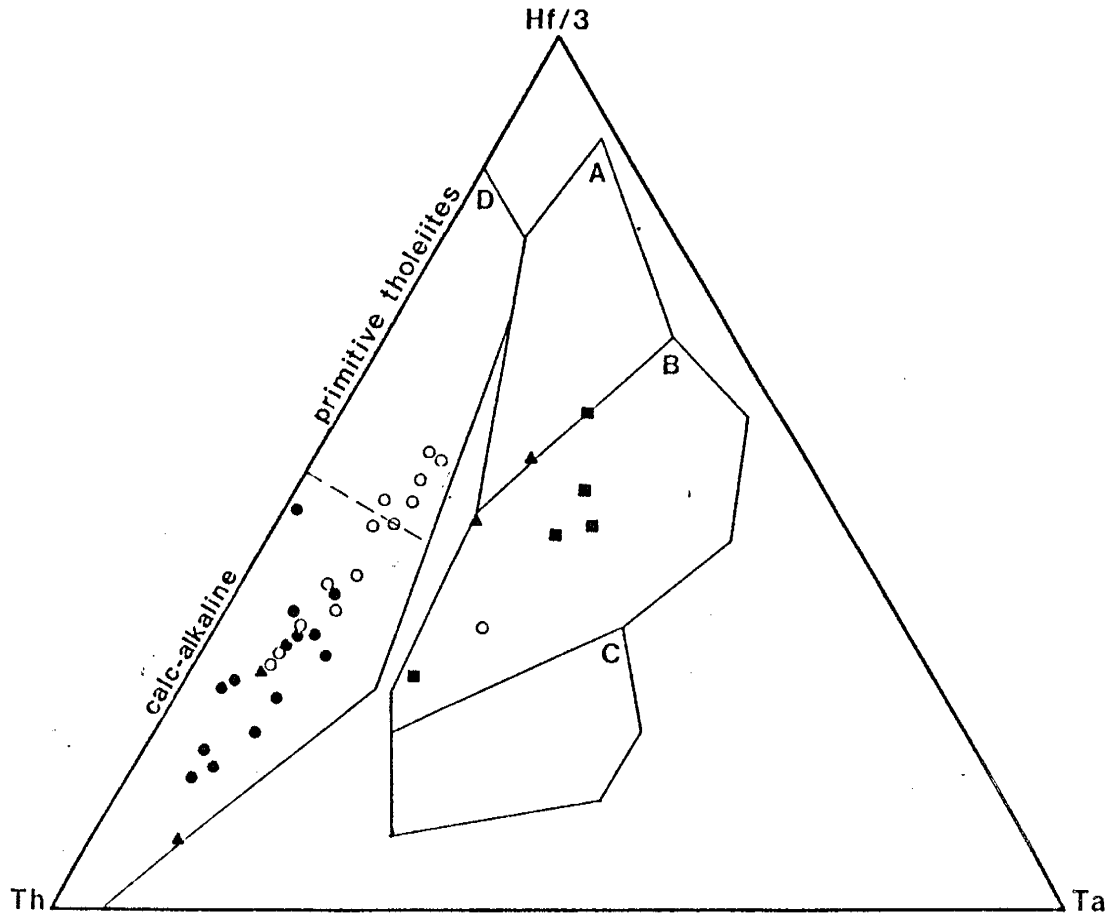

Figure 8a. Mafic rocks of the Pinal Schist in southeastern Arizona plotted on the Th-Hf-Ta tectonomagmatic discrimination diagram of Wood (1980). A: N-type MORB, B: E-type MORB and tholeiitic within plate basalt, C: alkaline within plate basalts, D: destructive plate margin magmas. Filled circles, Dragoon Mountains; open circles, Dos Cabezas and Chiricahua Mountains; squares, Little Dragoon Mountains and Johnny Lyon Hills; triangles, Rincon and Santa Rita Mountains.

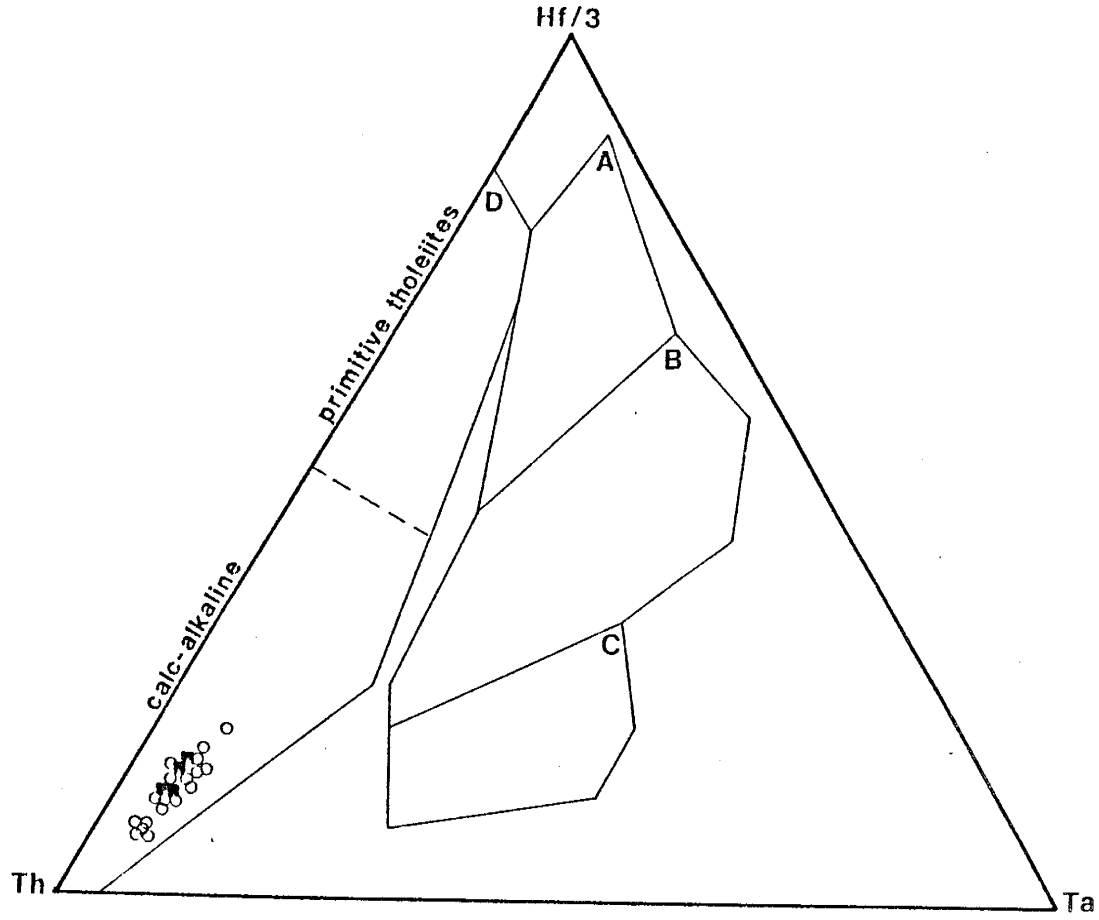

Figure 8b. Felsic rocks of the Pinal Schist in southeastern Arizona plotted on the Th-Hf-Ta tectonomagmatic discrimination diagram of Wood (1980). Fields and symbols as in figure 8a.

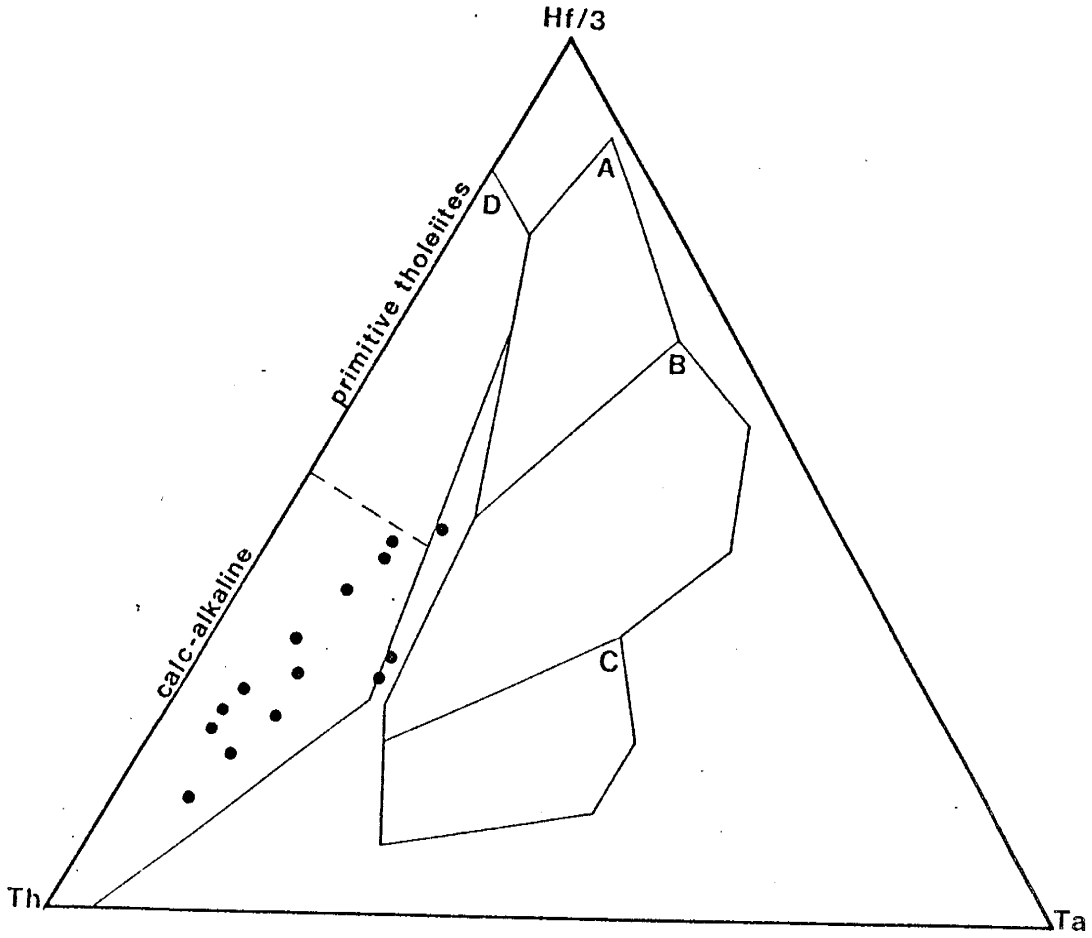

Figure 8c. Basalts of the Chasma Group, central Peru (Atherton and others, 1985) plotted on the Th-Hf-Ta tectonomagmatic discrimination diagram of Wood (1980). Fields as in figure 8a.

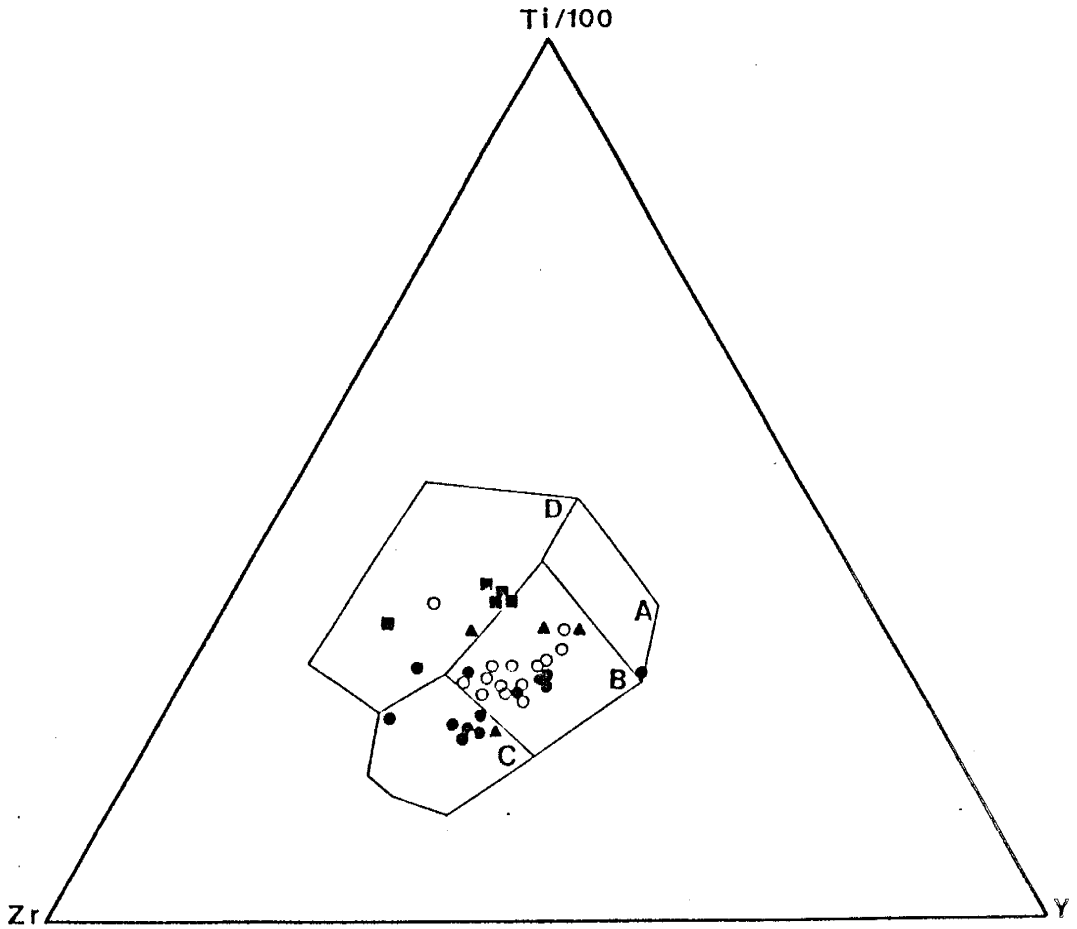

Figure 9. Pinal basalts plotted on the Zr-Ti-Y tectonomagmatic discrimination diagram of Pearce and Cann (1973). A: island arc tholeiites, B: island arc tholeiites and MORB, C: calk-alkaline basalts, D: within plate basalts. Filled circles, Dragoon Mountains; open circles, Dos Cabezas and Chiricahua Mountains; squares, Little Dragoon Mountains and Johnny Lyon Hills; triangles, Rincon and Santa Rita Mountains.

for the Dos Cabezas, Dragoon, and Rincon basalts by the use of the MORB normalized and Th-Hf-Ta diagrams (Figures 7, 8). Field C is the field of calc-alkaline basalts. Six of the 13 Dragoon Mountains basalts fall in this field while none of the Dos Cabezas basalts plot in this field.

For basalts of known arc affinity, Pearce (1983) has proposed the Zr/Y ratio as a discriminator between oceanic island arcs and continental margin arcs. Figure 10 shows the covariation of Zr/Y vs. Zr for the basalts from the Dragoon, Rincon, Dos Cabezas, and Chiricahua Mountains. All but three of these samples have Zr/Y ratios greater than 2.8, the proposed lower limit of continental arc basalts. It is unclear why the Dos Cabezas and Chiricahua basalts have high Zr concentrations but similar Zr/Y ratios relative to the Dragoon basalts.

The $MnO-TiO_2-P_2O_5$ tectonomagmatic discrimination diagram (Mullen, 1983) is shown in Figure 11. On this diagram, the Dragoon basalts fall entirely within the arc and back-arc basalt field. The Dos Cabezas and Chiricahua basalts fall in several fields but do not fall outside of the field of continental flood basalts. The Little Dragoon basalts fall in the MORB or flood basalt fields. This suggests for this minor element system that the Dos Cabezas basalts have affinities closer to the

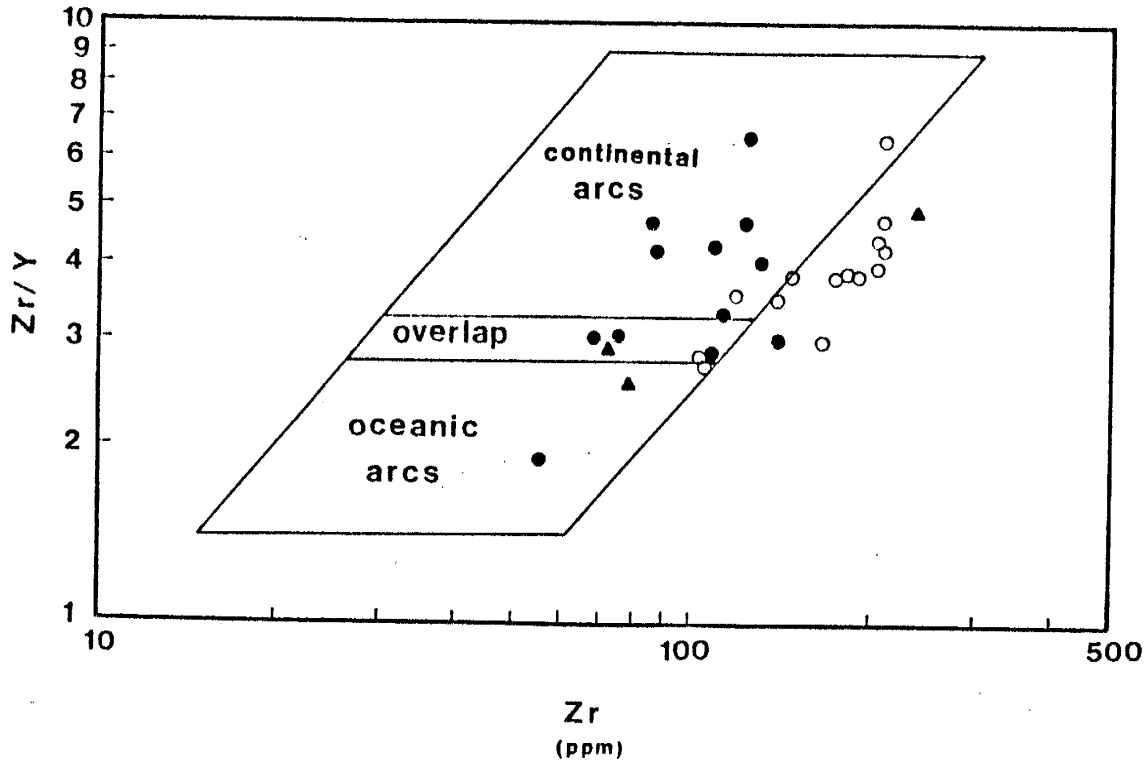

Figure 10. Zr/Y vs. Zr for Pinal basalts from the Rincon, Dragoon, and Dos Cabezas Mountains. Fields from Pearce (1983). Filled circles, Dragoon Mountains; open circles, Dos Cabezas and Chiricahua Mountains; squares, Little Dragoon Mountains and Johnny Lyon Hills; triangles, Rincon and Santa Rita Mountains.

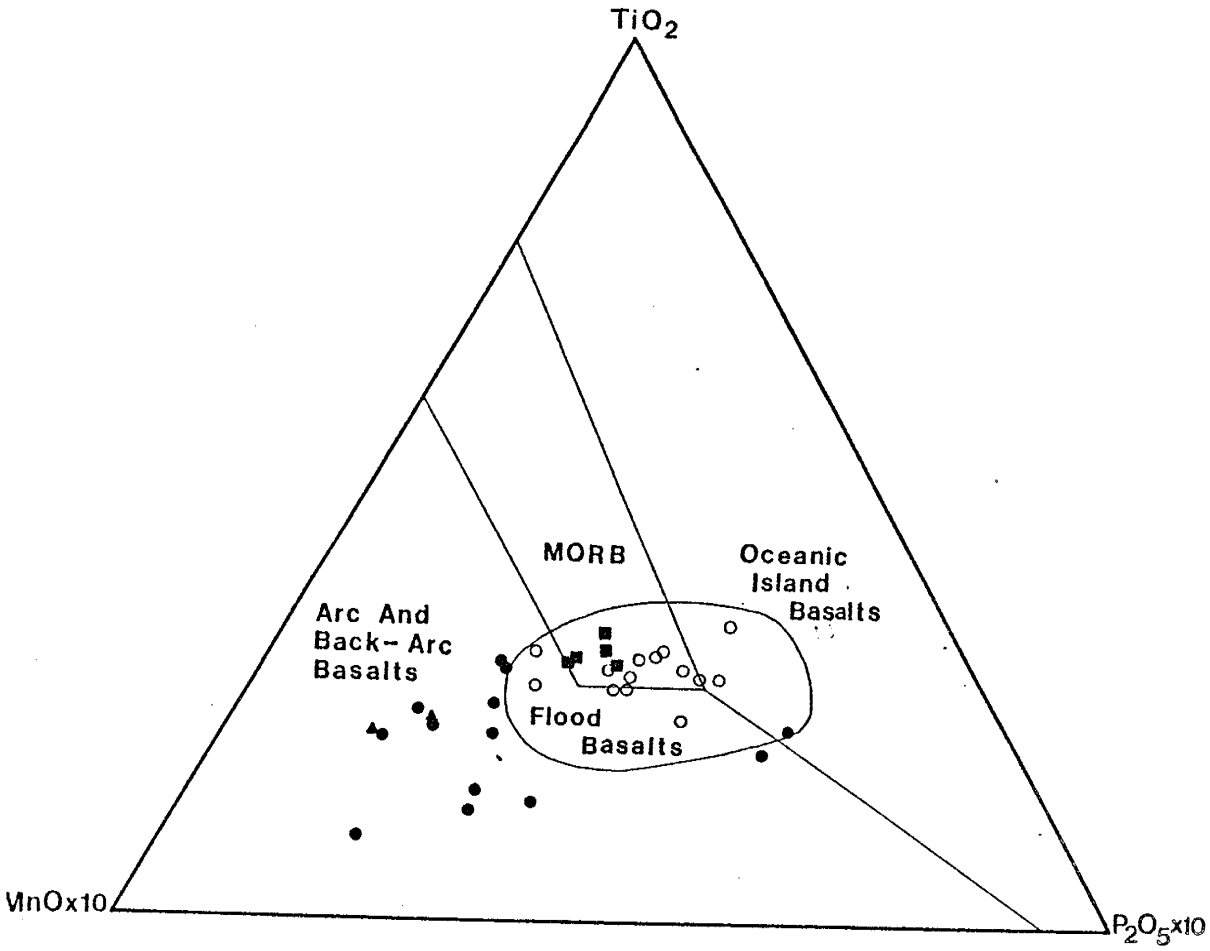

Figure 11. Mafic rocks of the Pinal Schist plotted on the MnO-TiO2-P2O5 tectonomagmatic discrimination diagram of Mullen (1983). Filled circles, Dragoon Mountains; open circles, Dos Cabezas and Chiricahua Mountains; squares, Little Dragoon Mountains and Johnny Lyon Hills; triangles, Rincon and Santa Rita Mountains.

Little Dragoon basalts than to the Dragoon basalts.

Felsic Rocks

The rhyodacite porphyries in the Little Dragoons and the Johnny Lyon Hills are chemically indistinguishable (Figs. 2, 3, 4, Table 2). These rocks exhibit moderate light REE enrichment and flat heavy REE patterns. Geochemical modeling (Appendix E) suggests that if major elements only are considered, the rhyodacite porphyry of the Little Dragoon Mountains could have been produced by fractional crystallization of of the basalts in the northeast corner of the Little Dragoons by removal of clinopyroxene, plagioclase, olivine, titanomagnetite and apatite . This model, however, does not fit the observed trace element concentrations and must be abandoned. In a manner similar to that employed by Condie and others (1985) on the felsic volcanic rocks of the Dos Cabezas Mountains, the rhyodacite porphyry of the Little Dragoon Mountains can be modelled to be a 20-25 % batch melt of a granulite source (Appendix E).

When plotted on a MORB normalized diagram (Fig. 12) along with averages of modern rhyolites from intracratonic rifts, continental margin arcs, and primitive oceanic arcs (Ewart, 1979; and references therein), the rhyodacite subvolcanic intrusive rocks of Little Dragoon Mountains, Johnny Lyon Hills, Dos Cabezas

Table 2. Chemical composition of felsic volcanic and subvolcanic rocks

location	LD	LD	LD	JLH	Chir
sample	P.84.19	P.84.28	P.84.32	P.85.32	P.85.1
SiO_2	71.10	70.90	69.57	70.47	68.87
TiO_2	0.63	0.60	0.68	0.67	0.91
Al_2O_3	13.60	13.65	14.35	14.13	14.59
Fe_2O_{3t}	4.25	3.66	4.59	4.65	5.77
MgO	0.67	0.42	0.75	1.12	0.41
CaO	1.67	1.64	1.39	1.09	1.60
Na_2O	3.52	3.73	4.07	3.13	3.74
K20	3.34	2.88	3.05	2.69	3.73
MnO	0.08	0.04	0.08	0.10	0.08
P_2O_5	0.13	0.13	0.14	0.15	0.20
LOI	1.10	2.23	1.44	1.69	0.97
TOTAL	100.09	99.88	100.11	99.98	100.87
Rb	129	118	134	125	188
Ba	670	579	742	526	
Cs	7.1		4.5	8.1	6.7
Sr	195	157	143	97	158
Pb	28	32	36	25	27
Th	16	14	14	15	13
U	5.3	4.7	3.7	3.8	3.2
Sc	17	13	10	13	13
Cr	30	17	18	19	25
Co	9.9	6.9	6.7	8.4	11
Y	53	50	60	57	58
Zr	238	214	274	250	281
Nb	14	13	13	13	13
Hf	8.8	6.9	6.1	6.8	7.5
Ta	1.3	1.2	1.0	1.1	1.1
La	45	38	33	37	40
Ce	99	82	77	86	93
Sm	9.0	8.1	8.2	8.2	9.3
Eu	1.8	1.4	1.1	1.2	1.6
Tb	1.5	1.3	1.4	1.4	1.4
Yb	5.7	5.0	4.3	4.7	4.7
Lu	0.96	0.71	0.60	0.68	0.66

LD: Little Dragoons, JLH: Johnny Lyon Hills, Chir: Chiracahua Mountains.

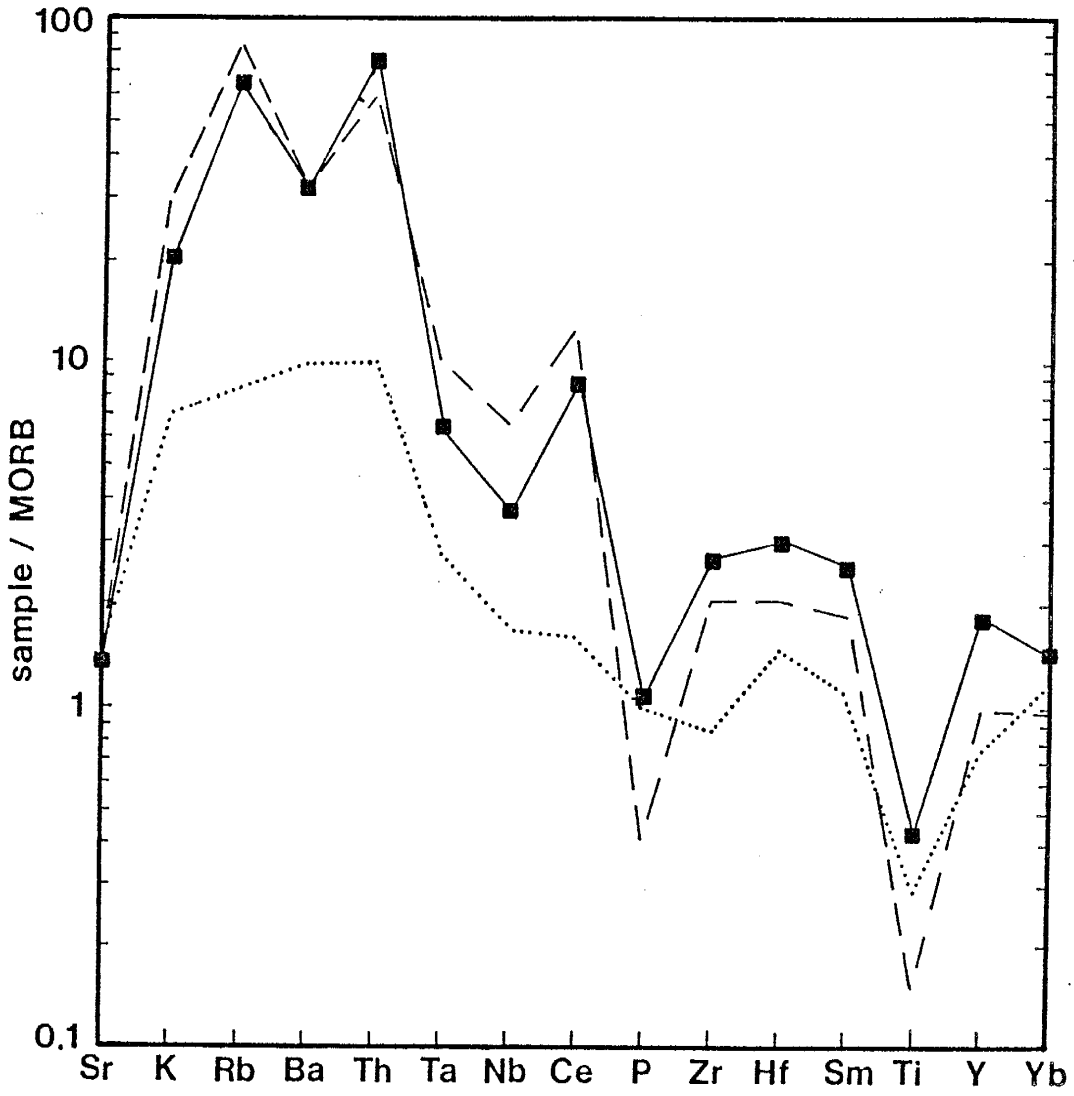

Figure 12. MORB normalized diagram of Little Dragoon Mountains and Johnny Lyon Hills subvolcanic rhyodacite porphyry and modern rhyolites. Squares, Little Dragoon and Johnny lyon Hills average; dotted line, average rhyolite from modern primitive island arc; dashed line, average rhyolite from modern continental margin arc.

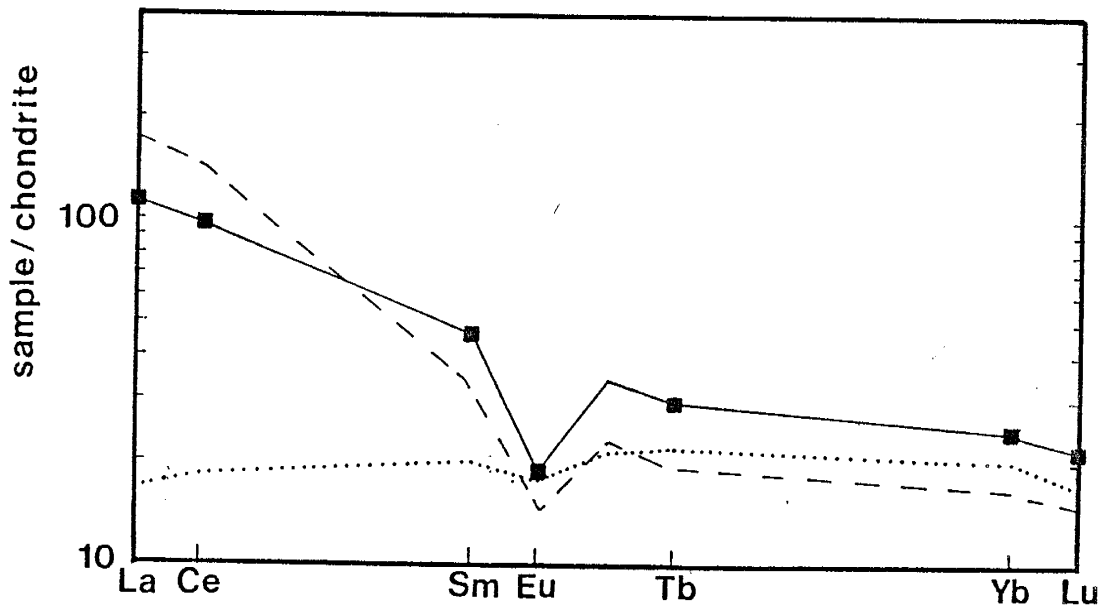

Figure 13. Chondrite normalized REE distribution for Little Dragoon Mountains and Johnny Lyon Hills rhyodacite porphyry and modern rhyolites. Symbols as in figure 12.

Mountains, and Chiricahua Mountains have a pattern most similar to that of continental margin arc rhyolites, similar to rhyolites from intracratonic continental rifts, and dissimilar to rhyolites from primitive oceanic island arcs. The felsic volcanic rocks of the Dos Cabezas and Chiricahua Mountains as well as the rhyodacite subvolcanic porphyry of the Little Dragoon Mountains and Johnny Lyon Hills are enriched in the light REE relative to the heavy REE, similar to modern rhyolites from continental margin volcanic arcs and intracratonic continental rifts but dissimilar to modern rhyolites from primitive oceanic island volcanic arcs (Fig. 13).

SEDIMENTARY ROCKS

Field Relations

The sedimentary rocks of the Pinal Schist in the study area are exclusively clastic rocks. They are by far the most abundant rock type in all the localities within the study area. Outside of the study area there is a minor carbonate unit included in the Pinal Schist in the northwestern Dos Cabezas Mountains (Condie and others, 1985). Lithologies vary from coarse conglomerate with clasts up to 15 cm long to fine grained units which were originally mud. Sedimentary rocks are also the dominant rock type in other areas of the Pinal Schist in southeastern Arizona except in the northwestern Dos Cabezas Mountains, where volcanic and subvolcanic rocks dominate.

The most common sedimentary rock in the study area is sandstone. The sedimentary sequence in the Dragoon, Little Dragoon, and Whetstone Mountains and the Johnny Lyon Hills can be generalized as a series of sandstones with interbedded shales with sandstones dominating. Individual sandstone bed thicknesses range from 1 cm to 2 m. The thickest, most massive, sandstones generally lack significant intervening fine layers. In the southern Johnny Lyon Hills, a sequence of sandstones occurs which contains seven distinct beds with thicknesses of 20 to 180 cm interbedded with fine

layers, each less than 1 cm thick. When the sand:shale ratio is close to one, the bed thickness of the sand layers is generally between 1 and 25 cm. In these sequences, pelitic layers are 0.5 to 15 cm thick. Grain size in the Pinal sandstones varies from very coarse to very fine sand but most of the grains in these rocks fall into the medium and fine sand categories. Graded bedding is the most commonly preserved sedimentary texture in these rocks. It is most common in beds which are 2-10 cm thick. Grading is most prominent in the lower one quarter of beds with little size change in the upper three quarters of beds.

In the Mule Mountains, the Pinal sediments are finer grained than their counterparts to the north. Thick massive sands without intervening fines are not observed. Coarse and very coarse sand grains are rare. Pelitic layers are abundant and heavy minerals are prominent in units from the Mule Mountains.

Sandstones from the Pinal Schist have many features characteristic of sediments deposited in submarine fans by turbidity flow and grain flow (Walker, 1978). Of the five subdivisions of the Bouma (1962) idealized turbidite sequence, T_a (massive and normally graded sand), T_b (plane parallel laminated sand), and T_e (pelitic mud) are preserved in these rocks. In the Dragoon, Mule, and Whetstone Mountains and in the Johnny Lyon Hills T_a ,

T_b , and T_{ab} sequences are most common and T_{abe} sequences are rare. It is important to note that T_c (rippled and cross-bedded sand and silt) is absent from these sequences. This may indicate that sedimentation was dominantly in the upper flow regime (Walker, 1965), or, less likely, that these structures did not survive deformation and metamorphism.

Conglomerate and arkose are the dominant sedimentary lithologies in the Dos Cabezas Mountains (Condie and others, 1985). The abundance of these lithologies in the Pinal Schist is unique to the section in the Dos Cabezas and may represent a distinct sedimentary environment. These rocks could also be the shallow water facies of a submarine fan or fans represented by the finer grained sediments to the west. Another indication of a shallow water environment includes the presence of minor carbonate (Erickson, 1969; Condie and others, 1985; G.P. Bowling, in prep.). In the Dos Cabezas Mountains, Pinal conglomerates are dominantly matrix supported with clasts ranging from 2 to 15 cm long. Rock types represented by the clasts are dominantly quartzite, felsic volcanics, and granite in order of decreasing abundance. Matrix in the conglomerate is composed of sand grains of quartz and K-feldspar (Condie and others, 1985). In sandy beds within the conglomerate, cross bedding with prominent heavy mineral banding is present. The bed thickness of

units with cross bedding is approximately 10 cm.

Within the rest of the study area, conglomerate is rare. Silver (1978) reports minor volcanic pebble conglomerate in the Little Dragoon Mountains. In Jordan Canyon, in the northern Dragoon Mountains, there is a single unit of pebble conglomerate approximately 2 m thick. Clasts in this unit are 1 to 5 cm in diameter, subrounded to angular, both clast and matrix supported, and are composed of subequal amounts of granite and quartzite. Matrix is composed mostly of quartz sand grains with minor feldspar grains. Within 2 km of this outcrop, Drewes (1981) and Drewes and Meyer (1983) have mapped a conglomerate unit of Pinal Schist near 4F Peak (Fig. A-5). This unit is composed of angular granitoid clasts up to 1 m in diameter and sedimentary clasts 1 to 5 cm long. The sedimentary clasts appear to have been subjected to a greater degree of metamorphism than the surrounding matrix and the granitic clasts in this unit and have lithologic similarities to units within the Pinal Schist. Contacts of this unit with surrounding rocks are not well exposed but appear to be faults as mapped by Drewes and Meyer (1983). To the east this unit is in contact with a middle Proterozoic granitic pluton. To the west the unit is in contact with medium grained sandstones of the Pinal Schist similar to rocks of the Pinal Schist in Jordan Canyon and in the southern

Dragoons near South Pass. The northern Dragoon Mountains, and the area around 4F Peak in particular, is an area of intense Laramide brittle deformation. I feel this unit may be a fault breccia containing clasts of Pinal Schist and a nearby granitic pluton. However, the mineralogy and grain size in the granitic clasts in this unit are more varied than would be expected from a single planar zone in one pluton. Isotopic analysis of zircons separated from one of the larger granitic clasts from this unit may help resolve this problem. If this unit is indeed a conglomerate deposited during Pinal time, it represents an environment of deposition similar to that of the rocks in the Happy Camp Canyon area of the Dos Cabezas Mountains, possibly an alluvial fan. This would also unequivocally confirm the presence of granitic plutons exposed to erosion in the source area of the Pinal Schist.

Deformation is most severe in the fine grained units where boundinage, transposition, and disruption of beds can be intense. Thick, structureless sands may appear relatively undeformed on an outcrop scale.

Petrography

The sedimentary rocks of the Pinal Schist in the study area exhibit significant effects of metamorphism. A detailed discussion of petrographic features of individual samples can be found in Appendix D. The

metamorphic overprint is least intense in the Little Dragoon and Dragoon Mountains and in the Johnny Lyon Hills. Even in these areas the percentage of matrix is considerable (45 to 65%) and transitions occur from slightly altered plagioclase and lithic fragments to completely recrystallized grains which now comprise the matrix. Matrix in these rocks is defined as grains less than 0.1 mm long. Quartz, which occurs both as framework supported and matrix supported grains, is generally 0.5 to 2.0 mm long. In the least metamorphosed examples, quartz grains are subrounded with sharp boundaries. Where the effects of metamorphism and deformation are greater, such as in the Rincon, Whetstone, Chiricahua, and the Dos Cabezas Mountains, quartz grains have sutured boundaries, pressure shadows, and may be completely recrystallized. The sandstones of the Pinal Schist are chiefly quartz and matrix. Much (most?) of the matrix appears to have developed at the expense of rock fragments and feldspars during metamorphic recrystallization. Variable subordinant proportions of plagioclase and rock fragments are present in all but a few samples. Staining of thin sections indicates K-feldspar is rare.

Identifiable rock fragments are 0.5 to 2 mm long and are often elongated in the plane of the foliation of the rock. Indistinct boundaries between matrix and both rock

fragments and feldspars are common. Rock fragments in fine grained rocks appear to be dominantly felsic volcanic rock fragments, but it is difficult to distinguish between fine-grained felsic volcanic and sedimentary rock fragments at this grade of metamorphism. In thin section, the rock fragments are of three general types. One type is composed of recrystallized quartz and feldspar crystals (< 0.05 mm long). A second type is comprised of dominantly fine grained sericite (< 0.05 mm long) with minor quartz approximately 0.05 mm in diameter. A third and rarest type is granitic rock fragments. These consist of intergrown quartz and feldspar crystals up 1.0 mm long. Myrmykitic texture was observed in one granitic rock fragment.

The proportion of quartz, feldspar, and rock fragments in arenaceous sediments has been shown to be a sensitive indicator of the interrelationships between provenance and tectonic setting (e.g. Dickinson and others, 1983). In any sedimentary rock that has been metamorphosed or deformed, the proportion of quartz in the quartz, feldspar, lithic fragments (QFL) system will increase due to the recrystallization of feldspar and lithic fragments. For metasediments, McLennnan (1984) has proposed a relation between the original proportion of Q in the QFL system (Q_o), the apparent value of Q

today (Q_a) and the amount of matrix in the rock (m) given by the equation $Q_o = Q_a (1-m)$. This method (M method) assumes that all the matrix in the rock is of secondary origin and derived from the recrystallization of rock fragments and feldspar. This is probably not the case for most sediments, but is a reasonable first approximation for rocks with a significant amount of matrix. Original modes, QFL values, and recalculated Q values by the M method are listed in Table 3 for 12 samples.

A second method of estimating the original position of some Pinal metasediments on the QFL diagram is to make use of the major element concentrations to constrain the original mineralogical makeup of the matrix. This is done two ways. The first (R method) way is to assume that all the excess Al_2O_3 in the rock was originally in felsic volcanic rock fragments which are assumed to contain 14% Al_2O_3 Al_2O_3 is determined by subtracting the amount of Al_2O_3 calculated to be in plagioclase present in the modal analysis from the Al_2O_3 in the whole rock. In this calculation Al_2O_3 in the plagioclase is assumed to be 30%. Excess Al_2O_3 is then divided by 14 to give a maximum allowable proportion of rock fragments with 14% Al_2O_3 Results of the R method recalculation on the QFL system on several metasediments are listed in Table 4. A similar method (K method) was used to calculate the

Table 3. Effect of matrix recalculation on Q values (M method).

	MATRIX	QTZ	FELD	RF	Q	F	L	QS1os0
P.84.66	50.2	38.9	9.7	1.1	78.3	19.5	2.2	39.0
P.84.90	57.2	41.1	0.1	1.6	96.0	0.2	3.7	41.0
P.85.28	67.4	22.6	7.1	2.9	69.2	21.8	8.9	23.0
P.84.35	47.4	30.8	20.5	1.3	58.5	39.0	2.5	30.8
P.84.164	69.6	27.9	2.5	0.0	91.8	8.2	0.0	27.9
P.84.70	60.2	26.1	5.8	7.8	65.7	14.5	19.7	26.1
P.84.191	52.9	31.4	4.9	10.9	66.6	10.3	23.1	31.4
P.84.210	43.3	34.7	11.6	10.4	61.2	20.4	18.4	34.7
P.84.92	54.3	33.2	1.0	11.5	72.7	2.2	25.1	33.3
P.85.30	62.1	26.8	6.1	5.0	70.7	16.0	13.3	26.8
P.84.85	49.3	48.1	2.4	0.1	94.8	4.8	0.4	48.0
P.85.3	65.0	33.0	2.0	0.0	94.3	5.7	0.0	33.0

QTZ: modal quartz
FELD: modal fedspar
RF: modal rock fragments
Q: (QTZ/QTZ+FELD+RF)*100
F: (FELD/QTZ+FELD+RF)*100
L: (RF/QTZ+FELD+RF)*100
QS1oS0: Q*(1-(MATRIX/100))

Table 4. Effect of matrix recalculation on QFL system

(R method)

	observed			recalculated		
	Q	F	L	Q	F	L
P.84.66	78.3	19.5	2.2	42.9	10.7	46.3
P.84.90	96.0	0.2	3.7	43.1	0.1	56.8
P.85.28	69.2	21.8	8.9	22.5	7.1	70.4
P.84.35	58.5	39.0	2.5	34.5	22.9	42.5
P.84.164	91.8	8.2	0.0	26.9	2.4	69.6
P.84.70	65.7	14.5	19.7	25.3	5.6	69.1
P.84.191	66.6	10.3	23.1	34.2	5.3	60.5
P.84.210	61.2	20.4	18.4	32.9	11.0	53.2
P.84.92	72.7	2.2	25.1	40.9	1.2	57.8

symbols defined in table 3

Table 5. Effect of matrix recalculation on QFL system (K method).

	observed			recalculated		
	Q	F	L	Q	F	L
P.84.66	78.3	19.5	2.2	63.5	32.9	1.8
P.84.90	96.0	0.2	3.7	54.8	43.0	2.1
P.85.28	69.2	21.8	8.9	40.7	54.1	5.2
P.84.35	58.5	39.0	2.5	44.5	53.3	1.9
P.84.164	91.8	8.2	0.0	41.1	58.9	0.0
P.84.70	65.7	14.5	19.7	40.4	47.4	12.2
P.84.191	66.6	10.3	23.1	45.6	38.6	15.8
P.84.210	61.2	20.4	18.4	39.7	48.4	11.9
P.84.92	72.7	2.2	25.1	50.1	32.6	17.3

symbols defined in table 3

maximum allowable component of K-feldspar in the matrix. For this calculation, rock fragments are assumed to be 3.8 % K_2O and plagioclase is assumed to be 0.5 % K_2O Excess K_2O is determined by subtracting calculated K_2O in plagioclase and rock fragments from K_2O in the whole rock. Recalculated QFL values by the K method are listed in Table 5.

Crook (1974) subdivided graywackes into quartz-rich, quartz-intermediate, and quartz-poor types. He placed the boundary between the quartz-rich and the quartz-intermediate types at ~65% Q in the QFL system. As Tables 3, 4, 5, and figure 14 show, recalculation of Q moves the Pinal sediments from the quartz-rich category to the quartz-intermediate category. Figure 14 graphically displays the effects of recalculation of matrix has on the QFL system on 12 sedimentary rocks of the Pinal Schist. Since the M method does not recalculate F or L, the recalculated Q value is plotted with the same F/L ratio that is observed in the rock. As figure 14 shows, recalculation of the matrix by the three methods discussed yields significantly different results. These three methods all assume only one detrital component in the matrix, while the true composition of the original matrix falls intermediate between the three points on each diagram. One feature common to all three methods is the reduction of the value

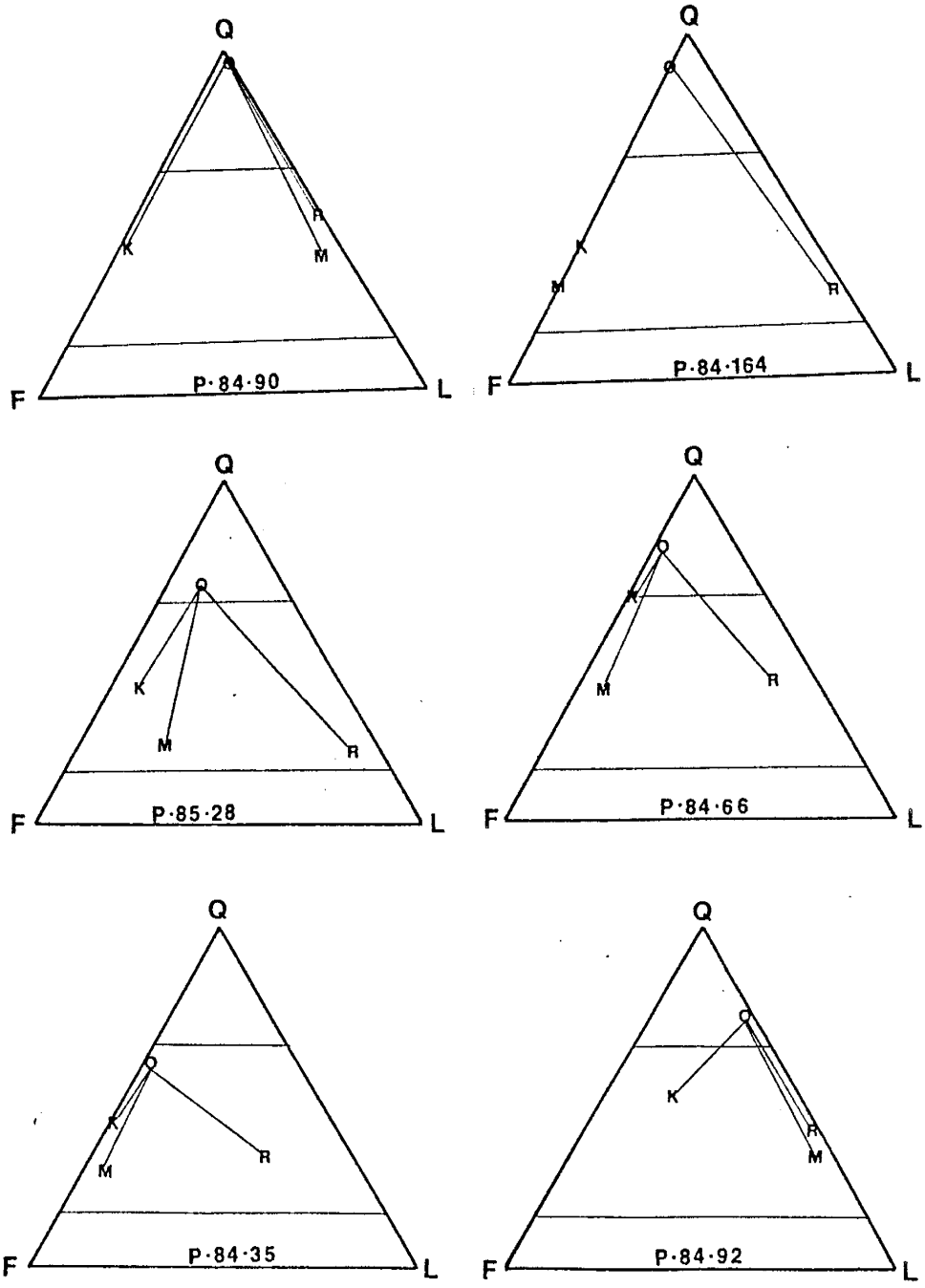

Figure 14. QFL diagrams for Pinal Schist metasediments showing effects of matrix calculation by M, R, and K methods (see text). symbols: O, observed composition; K, composition calculated by K method; M, composition calculated by M method; R, composition calculated by R method.

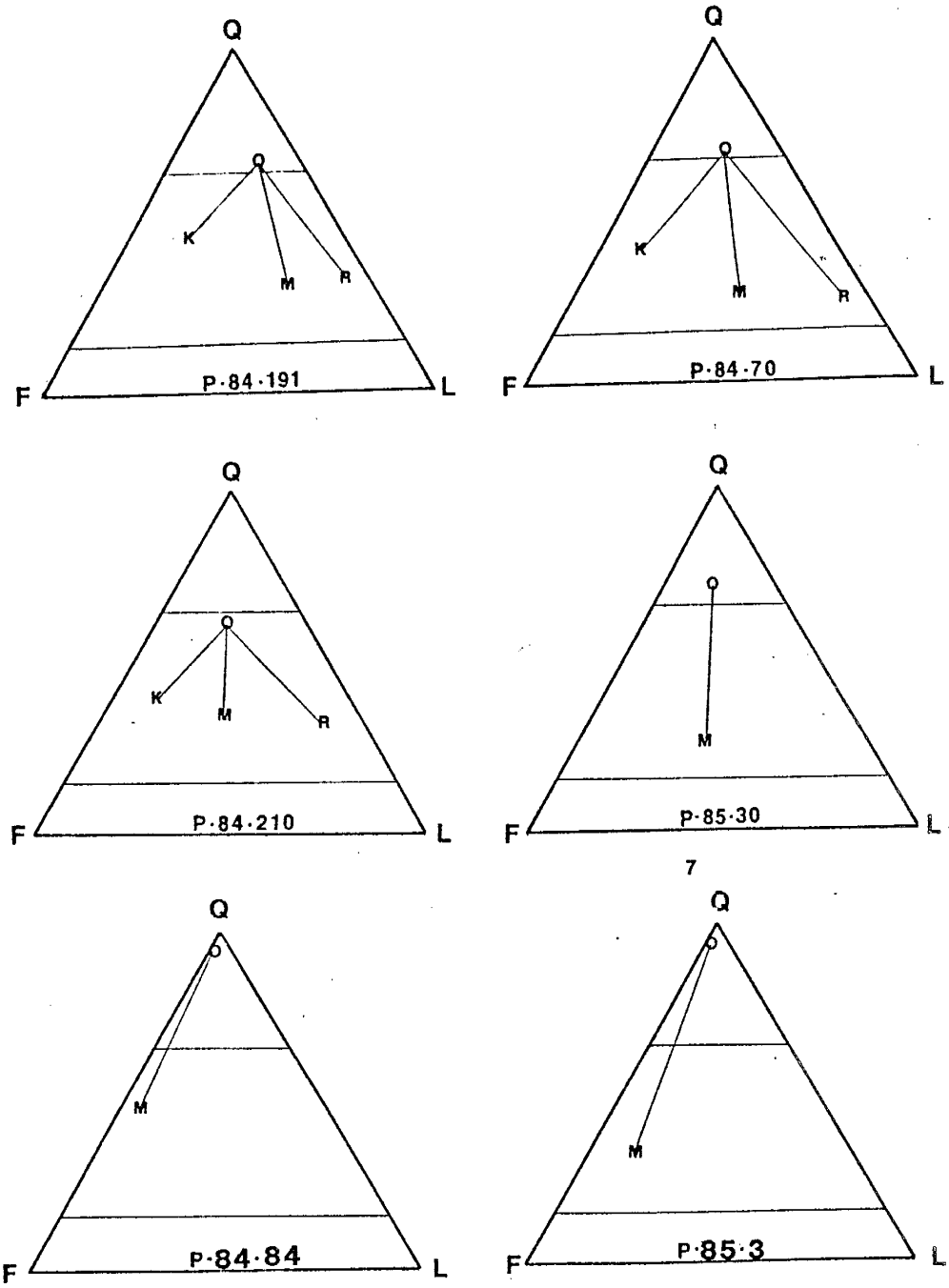

Figure 14, continued.

of Q by approximately 50 %. While the exact position on the QFL diagram cannot be determined, it is very likely that the original framework composition of the Pinal sediments lies within the quartz-intermediate field of Crook (1974).

Because of the high degree of recrystallization of lithic fragments and feldspars in most of the Pinal sandstones, it is not possible to use QFL-type tectonic discrimination diagrams developed by Dickinson and coworkers (e.g. Dickinson and others, 1983) for the sediments of the Pinal Schist. These rocks have greater than 20 % matrix and should therefore be excluded from diagrams of this type for tectonic discrimination (Ingersoll, 1978). Moreover, there are inherent shortcomings in the QFL approach particularily during transitions between tectonic regimes and modifications of sandstone composition by weathering processes (Mack, 1984; Potter, 1984; Velbel, 1985). As discussed below, a transition between tectonic regimes may have had an influence on the sedimentation of the Pinal Schist. Furthermore, recent work indicates considerable overlap on the QFL diagram for modern marine sands from different tectonic environments (Valloni, 1985), in particular turbidites (Valloni and Mezzadri, 1984).

Geochemistry

Major Elements

Because the petrographic studies of the Pinal sandstones cannot be interpreted unambiguously, these rocks were analyzed to determine their chemical composition (Table 6) in an effort to evaluate their tectonic seting and provenance. In Table 6, the Pinal metasediments have been assigned to four subgroups. These groupings are made based on essentially three parameters: SiO_2 / Al_2O_3 (S/A), K_2O /(Na_2O +CaO) (K/NC), and Fe_2O_3 +MgO+ TiO_2 (FMT). These groups are selected by plotting the values of S/A, K/NC, and FMT on a ternary diagram (Fig. 15). By comparing these three parameters simultaneously differences become more apparent. For example, groups B and C have similar ranges in S/A values (Table 7) but become separated on Figure 15. Table 7 summarizes the variations of these parameters in the Pinal sandstones. Groups A, B, and C have relatively small ranges for all three parameters. Group D has large ranges for S/A and K/NC but are grouped together because of their high SiO_2 values and low FMT values. Table 8 lists the geographic distribution of the four groups. Group A has chemical and textural characteristics of Fe-poor feldspathic wackes. Groups B,

Table 6. Chemical composition of metasediments.

group	A	A	A	A	A
location	Rin	Rin	JLH	Mule	Mule
sample	P.84.81	P.84.84	P.85.28	P.84.191	P.84.194
SiO_2	72.04	76.71	70.90	81.35	79.14
TiO_2	0.22	0.55	0.60	0.47	0.41
Al_2O_3	15.30	11.77	13.65	9.09	10.40
Fe_2O_{3t}	1.35	4.12	3.66	2.96	2.92
MgO	0.30	0.69	0.42	0.35	0.35
CaO	1.98	0.18	1.64	0.10	0.17
Na_2O	4.26	1.99	3.73	1.62	1.56
K2O	3.75	2.04	2.88	3.00	3.28
MnO	0.03	0.05	0.04	0.02	0.03
P_2O_5	0.07	0.08	0.13	0.04	0.03
LOI	0.38	1.49	2.23	1.08	1.27
TOTAL	99.68	99.67	99.88	100.08	100.16
Rb	129	108	131	129	145
Ba	838	390	531	649	625
Cs	3.8	6.5	7.1	4.6	8.5
Sr	326	59	49	42	40
Pb	23	22	19	25	20
Th	12	12	11	9.9	11
U	2.6	2.6	2.2	3.0	3.1
Sc	1.9	9.5	11	5.9	7.6
Cr	4.6	59	56	25	37
Co	21	9.2	13	3.8	4.8
Y	6.5	26	30	30	20
Zr	134	242	204	236	218
Nb	5.4	11	7.2	9.4	10
Hf	3.2	6.5	6.5	7.5	6.2
Ta	0.70	1.2	0.71	0.75	0.93
La	19	18	26	18	18
Ce	31	34	65	39	25
Sm	1.8	3.3	4.8	3.6	3.4
Eu	0.55	0.67	1.0	0.69	0.68
Tb	0.18	0.63	0.67	0.61	0.47
Yb	0.39	3.0	2.4	2.7	2.6
Lu	0.07	0.45	0.40	0.47	0.37
S/A	4.7	6.5	5.2	8.9	7.6
K/NC	0.6	0.9	0.5	1.7	1.9
FMT	1.9	5.4	4.7	3.8	3.7
CIA	51.2	67.1	52.9	60.1	67.1

Table 6, continued

group	A	A	A	A	A
location	LR	LR	LD	LD	JLH
sample	P.84.14	P.84.17	P.84.21	P.84.27	P.84.66
SiO_2	77.62	76.37	74.34	77.23	80.02
TiO_2	0.17	0.54	0.92	0.60	0.54
Al_2O_3	12.61	10.67	11.27	11.18	8.77
Fe_2O_{3t}	1.49	3.48	5.13	4.01	4.60
MgO	0.17	0.41	0.40	0.57	0.68
CaO	2.10	1.37	1.29	0.37	0.94
Na_2O	4.28	2.23	2.92	2.10	2.54
K20	1.04	3.44	1.81	2.82	1.28
MnO	0.03	0.08	0.08	0.04	0.06
P_2O_5	0.07	0.25	0.12	0.06	0.04
LOI	0.38	1.03	1.79	1.42	1.18
TOTAL	99.96	99.87	100.07	100.40	100.65
Rb	36	180	105	145	46
Ba	141	792	194	390	244
Cs	2.0	8.3	10	13	3.0
Sr	230	28	90	46	110
Pb	14	13	33	21	25
Th	7.3	15	23	13	13
U	3.4	2.9	5.3	3.7	2.3
Sc	1.0	12	4.9	11	6.9
Cr	14	14	102	70	91
Co	2.3	6.5	8.9	10	8.3
Y	48	34	59	38	21
Zr	214	247	600	303	251
Nb	7.2	7.2	18	11	9.6
Hf	6.5	6.7	18	9.9	8.9
Ta	0.98	1.1	1.9	1.1	0.80
La	24	40	51	35	31
Ce	53	88	109	79	68
Sm	6.0	8.5	9.8	5.8	5.1
Eu	1.2	2.0	1.6	1.4	1.1
Tb	1.3	0.96	1.6	0.98	0.67
Yb	6.1	3.3	6.5	4.1	2.6
Lu	0.91	0.45	0.95	0.65	0.49
S/A	6.2	7.2	6.6	6.9	9.1
K/NC	0.2	1.0	0.4	1.1	0.4
FMT	1.8	4.4	6.5	5.2	5.8
CIA	51.3	52.1	55.4	61.1	54.8

Table 6, continued

group	A	B	B	B	B
location	LD	Rin	JLH	JLH	Whet
sample	P.84.35	P.84.117	P.84.70	JL-5	P.84.102
SiO_2	77.86	77.19	70.01	69.82	77.36
TiO_2	0.43	0.52	0.63	0.69	0.79
Al_2O_3	11.35	11.21	15.46	14.22	11.83
Fe_2O_{3t}	3.33	4.15	4.53	4.36	5.04
MgO	0.63	0.38	1.19	0.83	0.72
CaO	0.20	0.40	0.52	0.78	0.20
Na_2O	2.47	0.75	2.34	3.19	0.97
K2O	2.12	2.94	3.20	3.42	2.13
MnO	0.06	0.04	0.08	0.05	0.05
P_2O_5	0.07	0.11	0.09	0.14	0.12
LOI	1.64	2.22	2.27	1.97	1.50
TOTAL	100.16	99.21	100.32	99.47	100.71
Rb	99	156	152	161	132
Ba	426	10	603	669	
Cs	7.8	14	13	8.8	9.6
Sr	48	178	14	8.3	56
Pb	19	30	18	27	15
Th	10	8.7	10	17	19
U	1.7	1.4	3.4	4.6	4.3
Sc	6.1	7.8	12	17	11
Cr	19	18	65	34	113
Co	8.3	4.2	13	11	11
Y	29	37	35	57	52
Zr	171	226	212	248	476
Nb	9.8	11	12	14	14
Hf	4.8	7.6	5.9	7.7	13
Ta	0.81	0.90	0.96	1.4	1.2
La	28	25	32	45	42
Ce	58	52	68	99	90
Sm	4.9	4.2	6.4	9.2	8.4
Eu	0.93	1.0	1.4	1.8	1.6
Tb	0.67	0.76	0.95	1.5	1.4
Yb	2.3	3.7	3.7	5.8	5.2
Lu	0.30	0.58	0.58	0.87	0.82
S/A	6.9	6.9	4.5	4.9	6.5
K/NC	0.8	2.6	1.1	0.9	1.8
FMT	4.4	5.1	6.4	5.9	6.6
CIA	63.0	73.3	65.4	58.0	73.7

Table 6, continued

group	B	B	B	B	C
location	Drag	Drag	DC	Drag	LR
sample	P.84.154	P.84.158	P.84.210	P.84.171	P.84.2
SiO_2	75.00	69.36	71.82	74.14	65.52
TiO_2	0.69	0.71	1.39	0.56	0.64
Al_2O_3	12.67	15.20	11.65	12.57	16.77
Fe_2O_{3t}	4.78	5.56	7.95	4.42	5.07
MgO	1.01	1.37	0.07	0.91	1.54
CaO	1.26	0.65	0.57	0.23	3.39
Na_2O	0.13	1.37	1.36	2.00	3.78
K2O	1.34	3.41	3.93	3.67	2.02
MnO	0.10	0.07	0.11	0.03	0.07
P_2O_5	0.08	0.09	0.08	0.07	0.09
LOI	2.52	2.10	1.53	1.72	0.80
TOTAL	99.58	99.89	100.46	100.32	99.69
Rb	84	191	217	153	106
Ba	1159	15	738	480	868
Cs	12	15	134	12	9.3
Sr	88	65	66	88	117
Pb	13	11	33	19	26
Th	10	12	11	11	13
U	2.6	3.3	9.7	3.5	2.9
Sc	11	16	10	11	13
Cr	52	76	78	62	47
Co	11	14	11	8.9	11
Y	28	49	37	32	35
Zr	302	207	199	212	223
Nb	14	13	26	9.8	13
Hf	8.8	6.2	5.5	6.2	5.9
Ta	1.2	1.3	1.7	1.0	0.99
La	20	33	30	29	35
Ce	40	73	66	61	74
Sm	4.3	6.9	5.4	5.7	6.5
Eu	1.1	1.4	1.0	1.2	1.3
Tb	0.80	1.3	0.94	0.92	0.96
Yb	3.1	4.4	3.8	3.4	3.3
Lu	0.49	0.67	0.61	0.54	0.45
S/A	5.9	4.6	6.2	5.9	3.9
K/NC	1.0	1.7	2.0	1.6	0.3
FMT	6.5	7.6	9.4	5.9	7.3
CIA	76.3	68.3	61.0	62.3	64.6

Table 6, continued

group	C	C	C	C	C
location	Drag	Drag	JLH	Drag	Drag
sample	P.84.127	P.84.134	P.84.67	P.85.34	P.85.36
SiO_2	61.96	62.88	63.52	58.89	66.22
TiO_2	0.64	0.67	0.70	0.67	0.77
Al_2O_3	19.17	19.31	18.47	21.65	12.27
Fe_2O_{3t}	6.47	5.82	6.29	7.05	4.42
MgO	1.41	1.50	1.73	1.63	0.62
CaO	0.47	0.48	0.21	0.15	0.64
Na_2O	1.81	0.82	1.19	0.53	0.90
K2O	5.47	5.26	4.87	6.83	3.12
MnO	0.09	0.17	0.08	0.09	0.03
P_2O_5	0.10	0.11	0.10	0.07	0.73
LOI	2.95	3.42	2.94	3.41	3.00
TOTAL	100.54	100.44	100.10	100.96	99.79
Rb	287	306	226	281	
Ba	731	704	729		
Cs	16		21	15	
Sr	79	53	78	37	
Pb	19	18	23	24	
Th	13		14	13	
U	3.0		2.9	1.7	
Sc	16		21	14	
Cr	40		82	40	
Co	16		18	11	
Y	43	48	43	60	
Zr	167	189	172	165	
Nb	15	16	15	14	
Hf	4.8		5.5	3.9	
Ta	1.0		1.2	1.0	
La	43		39	29	
Ce	91		84	71	
Sm	7.9		7.0	7.5	
Eu	1.4		1.6	1.2	
Tb	1.2		1.1	1.2	
Yb	3.9		4.5	3.9	
Lu	0.60		0.63	0.55	
S/A	3.2	3.3	3.4	2.7	3.4
K/NC	2.4	4.0	3.5	10.0	2.0
FMT	8.5	8.0	8.7	9.3	5.9
CIA	66.5	71.2	71.1	72.0	76.4

Table 6, continued

group	C	C	C	D	D
location	Whet	Drag	LR	Drag	LR
sample	P.84.99	P.84.152	P.84.107	P.84.164	P.84.3
SiO_2	61.34	62.54	64.67	76.81	80.56
TiO_2	0.62	0.81	0.73	0.41	0.13
Al_2O_3	20.27	20.52	17.94	12.94	12.34
Fe_2O_{3t}	6.55	6.26	6.46	2.63	1.01
MgO	0.93	0.67	1.48	0.55	0.07
CaO	0.01	0.37	0.66	0.07	0.44
Na_2O	1.18	0.24	1.65	0.05	1.21
K2O	5.01	4.61	3.76	4.35	2.97
MnO	0.05	0.02	0.10	0.01	0.04
P_2O_5	0.11	0.06	0.10	0.06	0.04
LOI	3.54	3.40	2.09	2.02	1.18
TOTAL	99.61	99.50	99.64	99.90	99.99
Rb	324	242	192	160	81
Ba	9.0	1369	608	408	
Cs	25	9.8	9.3	14	1.5
Sr	56	115	117	5.6	167
Pb	15	5.1	26	13	16
Th	13	16	13	10	15
U	3.3	4.0	2.9	2.6	2.0
Sc	22	15	23	0.80	5.8
Cr	78	71	84	41	
Co	17	4.4	17	4.2	0.92
Y	51	30	35	31	54
Zr	171	194	161	150	114
Nb	15	17	14		11
Hf	5.2	4.9	5.1	4.4	4.4
Ta	1.3	1.4	1.3	0.80	0.70
La	48	17	39	21	37
Ce	101	40	88	50	80
Sm	8.4	3.4	7.3	4.7	6.4
Eu	1.9	0.75	1.6	1.0	1.5
Tb	1.3	0.51	1.1	0.75	1.5
Yb	4.9	3.0	4.4	3.2	0.83
Lu	0.66	0.54	0.72	0.46	0.83
S/A	3.0	3.0	3.6	5.9	6.5
K/NC	4.2	7.6	1.6	36.3	1.8
FMT	8.1	7.7	8.7	3.6	1.2
CIA	73.6	77.5	69.4	74.3	67.5

Table 6, continued

group	D	D	D	D	D
location	Whet	Whet	Whet	Drag	Drag
sample	P.84.88	P.84.90	P.84.92	P.84.148	P.84.151
SiO_2	82.60	84.56	82.14	94.15	87.82
TiO_2	0.47	0.46	0.65	0.17	0.43
Al_2O_3	8.57	7.59	8.23	3.70	8.18
Fe_2O_{3t}	3.80	3.09	4.07	0.12	0.07
MgO	0.56	0.35	0.47	0.001	0.002
CaO	0.09	0.27	0.04	0.01	0.68
Na_2O	0.11	0.01	0.01	0.45	0.11
K20	2.54	2.72	2.90	0.85	1.34
MnO	0.03	0.01	0.01	0.01	0.01
P_2O_5	0.07	0.03	0.05	0.01	0.01
LOI	1.87	0.96	1.19	0.79	1.47
TOTAL	100.71	100.05	99.76	100.35	100..12
Rb	110	122	130	41	70
Ba	456	413	482	129	398
Cs	8.1	12	15	2.1	3.5
Sr	15	4.7	6.7	24	55
Pb	14	8.0	16	20	12
Th	11	12	20	3.6	7.6
U	2.4	3.0	4.8	1.4	2.4
Sc	8.1	6.8	8.6	2.0	6.3
Cr	123	56	93	10	30
Co	8.3	4.0	4.6	0.33	0.28
Y	28	15	21	14	13
Zr	248	260	428	149	258
Nb	10		12	2.5	6.7
Hf	7.7	7.5	13	5.0	8.7
Ta	0.99	1.1	1.5	0.51	0.79
La	26	2.6	6.2	11	19
Ce	56	7.7	19	23	43
Sm	4.7	1.9	2.8	1.6	3.1
Eu	1.1	0.41	0.62	0.42	0.77
Tb	0.74	0.34	0.49	0.40	0.32
Yb	3.1	2.0	3.0	1.5	2.1
Lu	0.49	0.32	0.44	0.24	0.33
S/A	9.6	11.1	10.0	25.4	10.7
K/NC	12.7	9.7	58.0	0.6	1.7
FMT	4.8	3.9	5.2	0.3	0.5
CIA	73.8	69.1	72.2	67.0	74.2

table 6, continued

sample	aAVG	S.D.	bAVG	S.D.	cAVG	S.D.	dAVG	S.D.
SiO_2	70.61	3.1	73.09	3.1	63.06	2.1	85.31	4.6
TiO_2	0.46	0.2	0.75	0.3	0.69	0.06	0.39	0.2
Al_2O_3	10.83	1.7	13.10	1.5	19.26	1.4	8.10	2.5
Fe_2O_{3t}	3.18	1.1	5.10	1.2	6.05	0.8	2.03	1.7
MgO	0.49	0.2	0.81	0.4	1.28	0.4	0.24	0.2
CaO	0.84	0.7	0.58	0.3	0.71	1.0	0.27	0.2
Na_2O	2.36	1.1	1.51	0.9	1.34	1.0	0.32	0.4
K2O	2.39	0.9	3.01	0.8	4.55	1.3	2.22	0.8
MnO	0.08	0.02	0.07	0.03	0.08	0.04	0.02	0.01
P_2O_5	0.12	0.05	0.10	0.02	0.16	0.2	0.04	0.02
LOI	1.28	0.5	1.98	0.3	2.84	0.8	1.24	0.4
TOTAL	100.04	0.3	100.08	0.4	100.03	0.5	100.16	0.3
Rb	108	39	156	36	246	67	92	31
Ba	432	206	525	379	718	371	376	127
Cs	6.9	3.5	54	53	16	5.3	7.0	5.1
Sr	83	87	70	49	118	114	45	57
Pb	19	5.3	21	7.7	20	7.0	14	3.7
Th	11	3.6	12	3.4	14	1.1	12	5.2
U	2.8	0.8	4.1	2.3	3.0	0.6	2.7	1.1
Sc	6.1	3.6	12	2.9	18	3.6	6.3	2.1
Cr	41	29	63	27	63	19	62	41
Co	7.8	4.6	11	2.9	13	4.6	3.1	2.9
Y	29	12	41	9.7	43	9.2	24	14
Zr	229	110	260	87	180	19	243	100
Nb	8.9	3.0	14	4.7	15	1.2	8.4	3.5
Hf	6.9	3.5	7.6	2.3	5.0	0.6	7.7	2.8
Ta	0.94	0.31	1.2	0.3	1.2	0.2	0.93	0.32
La	25	9.5	32	7.7	36	9.4	17	12
Ce	54	23	69	18	78	18	38	25
Sm	4.8	2.1	6.3	1.7	6.9	1.5	3.4	1.7
Eu	1.0	0.4	1.3	0.3	1.4	0.3	0.80	0.38
Tb	0.77	0.35	1.1	0.3	1.1	0.2	0.63	0.41
Yb	3.1	1.5	4.1	0.9	4.0	0.6	2.1	0.8
Lu	0.49	0.22	0.65	0.13	0.59	0.08	0.44	0.19
S/A	6.2	1.2	5.7	0.8	3.3	0.3	12.3	6.1
K/NC	3.5	9.4	1.6	0.5	4.0	2.9	14.2	20.5
FMT	4.1	1.3	6.7	1.3	8.0	1.0	2.7	2.0
CIA	59.1	7.3	66.7	6.3	70.1	7.1	70.6	3.2

Table 6, continued

sample	AVG	S.D.	EXPLANATION
SiO_2	73.77	8.04	Fe_2O_{3t}, total iron as Fe_2O_3
TiO_2	0.59	0.23	
Al_2O_3	13.35	4.22	LOI, loss on ignition
Fe_2O_{3t}	4.24	1.86	major elements in %
MgO	0.72	0.48	trace elements in ppm
CaO	0.66	0.71	
Na_2O	1.61	1.22	Rin, Rincon Mtns
K2O	3.11	1.35	LR, Little Rincon Mtns
MnO	0.05	0.03	LD, Little Dragoon Mtns
P_2O_5	0.10	0.12	JLH, Johnny Lyon Hills
LOI	1.86	0.86	Whet, Whetstone Mtns
TOTAL	100.05	0.38	Drag, Dragoon Mtns
			Mule, Mule Mtns
Rb	152	72	DC, Dos Cabezas Mtns
Ba	523	311	$CIA, \frac{Al_2O_3}{Al_2O_3+K_2O+CaO+Na_2O}$
Cs			
Sr	84	88	(molar proportions)
Pb	19	6.6	
Th	12	3.7	
U	3.2	1.5	
Sc	10	5.6	S/A, SiO_2/Al_2O_3
Cr	56	31	K/NC, $K_2O/(Na_2O+CaO)$
Co	9.0	5.2	FMT, $Fe2O3+MgO+TiO_2$
Y	35	14	
Zr	234	96	
Nb	12	4.3	
Hf	7.0	2.9	
Ta	1.1	0.3	
La	28	12	
Ce	61	25	
Sm	5.5	2.2	
Eu	1.1	0.4	
Tb	0.89	0.37	
Yb	3.4	1.4	
Lu	0.54	0.19	

Table 7. Summary of chemical subgroups from table 6 of Pinal metasediments based on S/A, K/NC, and FMT parameters.

Group	S/A	K/NC	FMT	CAI
A	5.2-9.1	0.2-1.7	1.8-6.4	51.2-72.8
B	3.4-6.9	0.3-2.6	3.1-7.6	58.0-76.3
C	3.0-6.2	2.0-10.0	8.0-9.4	53.6-77.5
D	5.9-25.4	1.8-58.0	0.3-5.2	67.0-74.2

Group	SiO_2	Na_2O	Fe_2O_3	Al_2O_3
A	72.0-81.4	4.3-0.1	1.4-5.1	8.8-15.3
B	69.4-77.4	3.2-0.1	4.2-8.0	11.7-15.2
C	58.9-66.2	1.8-0.2	4.4-7.1	12.3-21.7
D	80.6-94.2	1.2-0.1	0.1-4.1	3.7-12.3

Table 8. Geographic distribution of chemical subgroups of metasediments. Numbers indicate the number of samples from each group by geographic locality.

	A	B	C	D
Rincon Mtns.	2	1		
Little Rincon Mtns.	2	1	1	1
Johnny Lyon Hills	2	2	1	
Little Dragoon Mtns.	3			
Dragoon Mtns.		4	4	3
Whetstone Mtns.		1	1	3
Mule Mtns.	2			
Dos Cabezas Mtns.			1	

Table 9. Average modal composition of chemical subgroups of table 6.

GROUP	MATRIX	QTZ	FELD	RF	n
A	54.5	30.9	9.4	4.1	4
B+C	57.3	30.4	8.7	9.1	2
D	60.4	34.1	1.2	4.4	3

symbols defined in table 3

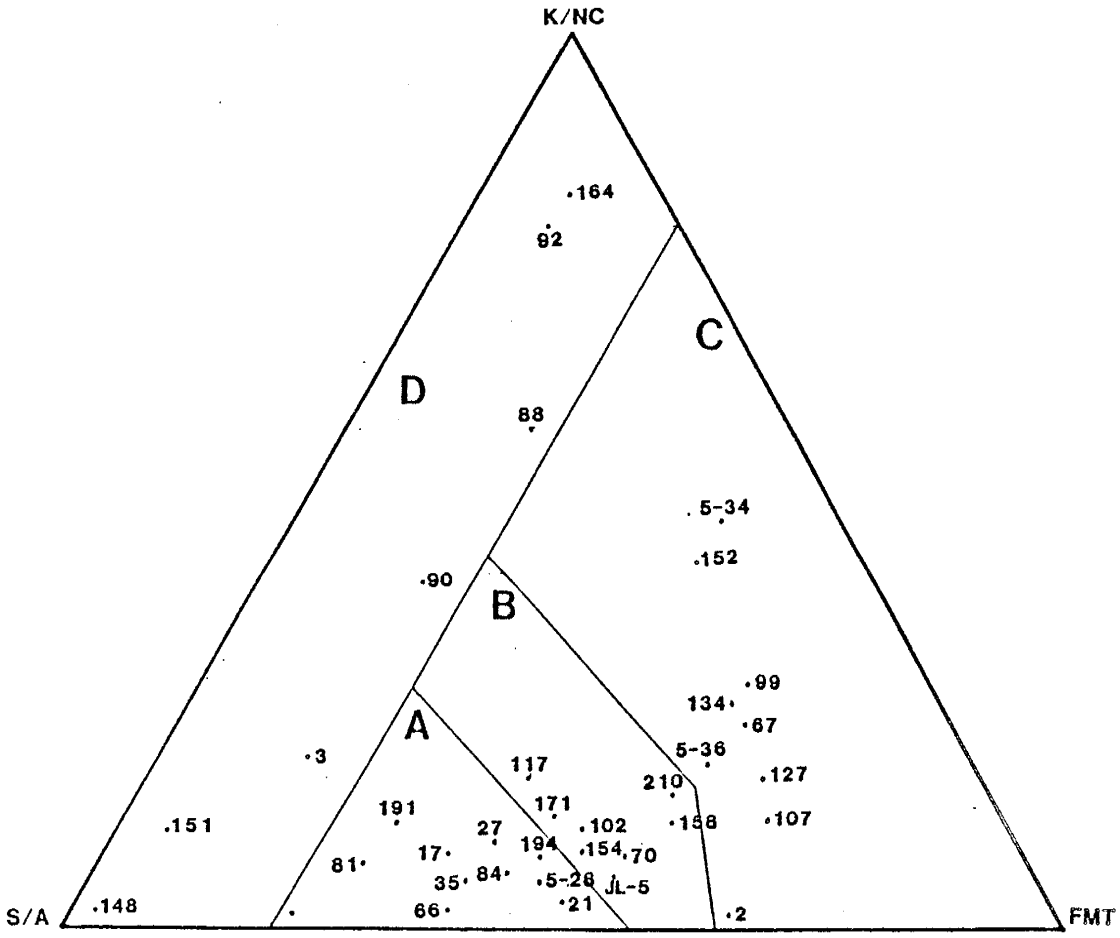

Figure 15. Covariation of S/A, K/NC, and FMT values of Pinal metasediments.

C, and D have characteristics of Fe-rich feldspathic wackes, Fe, Al-rich wackes, and quartz wackes respectively.

These groups are not restricted to any particular locality (Figs. 16a, 20a) but rather are found interbedded. For example, samples P.84.158 (group B), P.84.148 (group D), P.84.151 (group D), P.84.152 (group C), and P.84.154 (group B) occur within 0.4 km of each other. Stratigraphic relationships are complicated by faulting in this area but these samples appear to be part of the same stratigraphic package.

There are fewer thin section analyses than chemical analyses available for these rocks but available data suggest that in a progression A, B, C, D there is an increase in matrix and a decrease in feldspar (Table 9). Since these rocks have all experienced the same grade of metamorphism, a greater proportion of matrix probably reflects a greater proportion of clay minerals in the original detrital composition of the rock.

Table 6 lists the chemical alteration index (CIA, Nesbitt and Young, 1982) for the Pinal metasediments. The CIA is defined as the molecular ratio Al_2O_3 /(Al_2O_3 + Na_2O +CaO+ K_2O). As igneous rocks are weathered ultimately to become clay and silt the composition of the detritus becomes more aluminous relative to lime, soda, and potash than the original rock. High CIA values

indicate a greater degree of chemical alteration of an original igneous composition during weathering and deposition. CIA values in sedimentary rocks range from about 50 to about 85. For the Pinal sediments, group A has the lowest CIA values (Table 7). This along with the presence or indication of greater feldspar in group A relative to groups B, C, and D suggests that group A experienced less mechanical as well as chemical weathering than the other groups. Group A may have been more rapidly deposited than groups B, C, and D thus shortening the period of mechanical erosion. The CIA values of groups B and C have large ranges which are roughly coincident (Table 7). The range of CIA in group D (67.0-74.2) is completely within the range of groups B and C (53.6-77.5) but is restricted to only the upper part of this range. CIA values along with the high S/A values and low feldspar and rock fragment contents of group D suggest that of the four sediment groups, these rocks have experienced the greatest amount of reworking.

In figure 16, arenaceous sedimentary rocks with Al_2O_3 greater than 5 % (these conditions exclude 2 of the 35 samples analyzed) are plotted on the ternary diagram Na_2O -(Fe_2O_3 +MgO)-K_2O been proposed that these parameters provide an effective discrimination between graywackes, arkoses, and lithic sandstones (Blatt and others, 1980). In figure 16 most of the Pinal sandstones

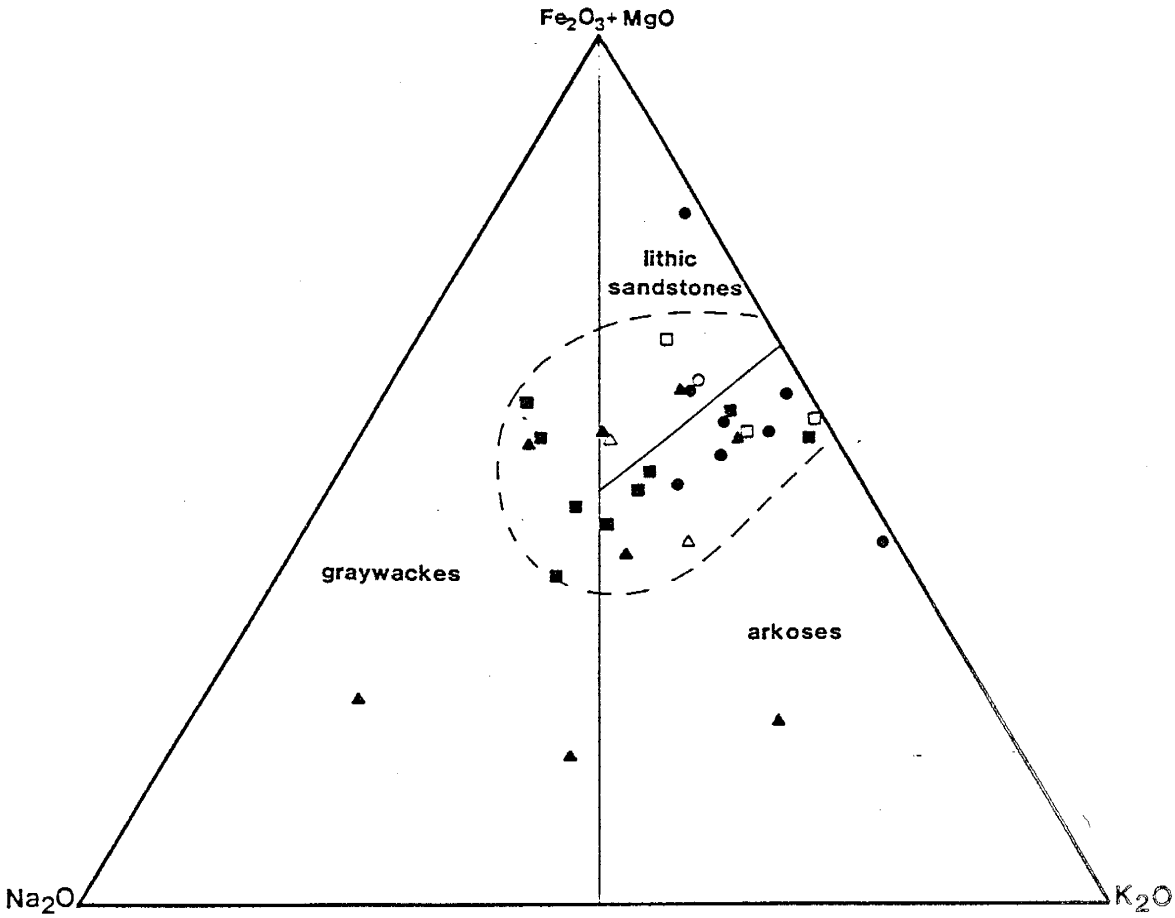

Figure 16a. Na2O-(Fe2O3+MgO)-K2O diagram for arenaceous Pinal metasediments from the study area with > 5% Al2O3. Open circle, Dos Cabezas Mountains; filled circles, Dragoon Mountains; filled squares, Little Dragoon Mountains and Johnny Lyon Hills; open squares, Whetstones Mountains; filled triangles, Rincon Mountains; open triangles, Mule Mountains. Fields from Blatt and others (1980).

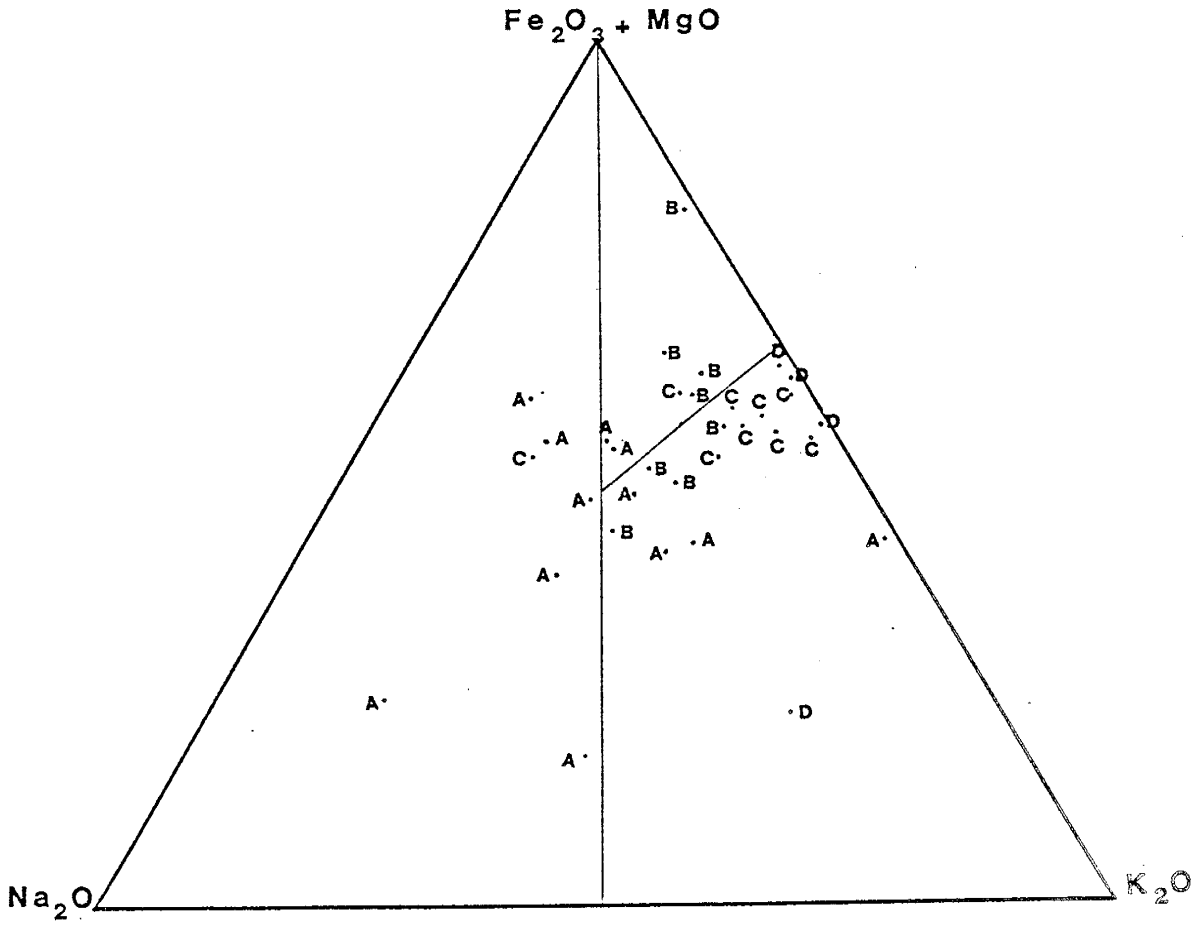

Figure 16b. Na2O-(Fe2O3+MgO)-K2O diagram. Symbols correspond to groups chemical groups in table 6.

Table 10. Comparison of Pinal Schist metasediments to other rock types

	1	2	3	4	5	6	7	8	9
SiO_2	61.5	69.5	72.9	70.1	66.7	77.1	72.1	73.8	77.8
TiO_2			0.5	0.5	0.6	0.3	0.7	0.6	0.5
Al_2O_3	15.2	14.1	14.5	14.0	13.5	8.7	13.9	13.4	10.6
Fe_2O_3	7.7	3.9	4.7	4.6	5.5	2.3	4.9	4.2	3.7
MgO	3.8	1.9	1.8	2.3	2.1	0.5	0.8	0.7	0.8
CaO	6.7	4.4	1.1	2.5	2.5	2.7	0.6	0.7	0.7
Na_2O	1.4	3.6	2.9	3.7	2.9	1.5	1.6	1.6	1.9
K_2O	3.8	2.6	1.5	1.8	2.0	2.8	3.3	3.1	2.5

	A	B	C	D
SiO_2	70.6	73.1	63.1	85.3
TiO_2	0.5	0.8	0.7	0.4
Al_2O_3	10.8	13.1	19.3	8.1
Fe_2O_3	3.2	5.1	6.1	2.0
MgO	0.5	0.8	1.3	0.2
CaO	0.8	0.6	0.7	0.3
Na_2O	2.4	1.5	1.3	0.3
K_2O	2.4	3.0	4.6	2.2

1: Island arc fore-arc sand (Maynard et al., 1982)
2: Continental margin arc sand (Maynard et al., 1982)
3: Harz Mountain graywacke (Huckenholz, 1963)
4: Franciscan graywacke (Crook, 1974)
5: Avearge graywacke (Pettijohn, 1963)
6: Average arkose (Pettijohn, 1963)
7: "Typical" Pinal metasediment (this study)
8: Average Pinal metasediment (this study)
9: Average Pinal metasediment (De Melas, 1983)
A: Average of group A (this study)
B: Average of group B (this study)
C: Average of group C (this study)
D: Average of group D (this study)

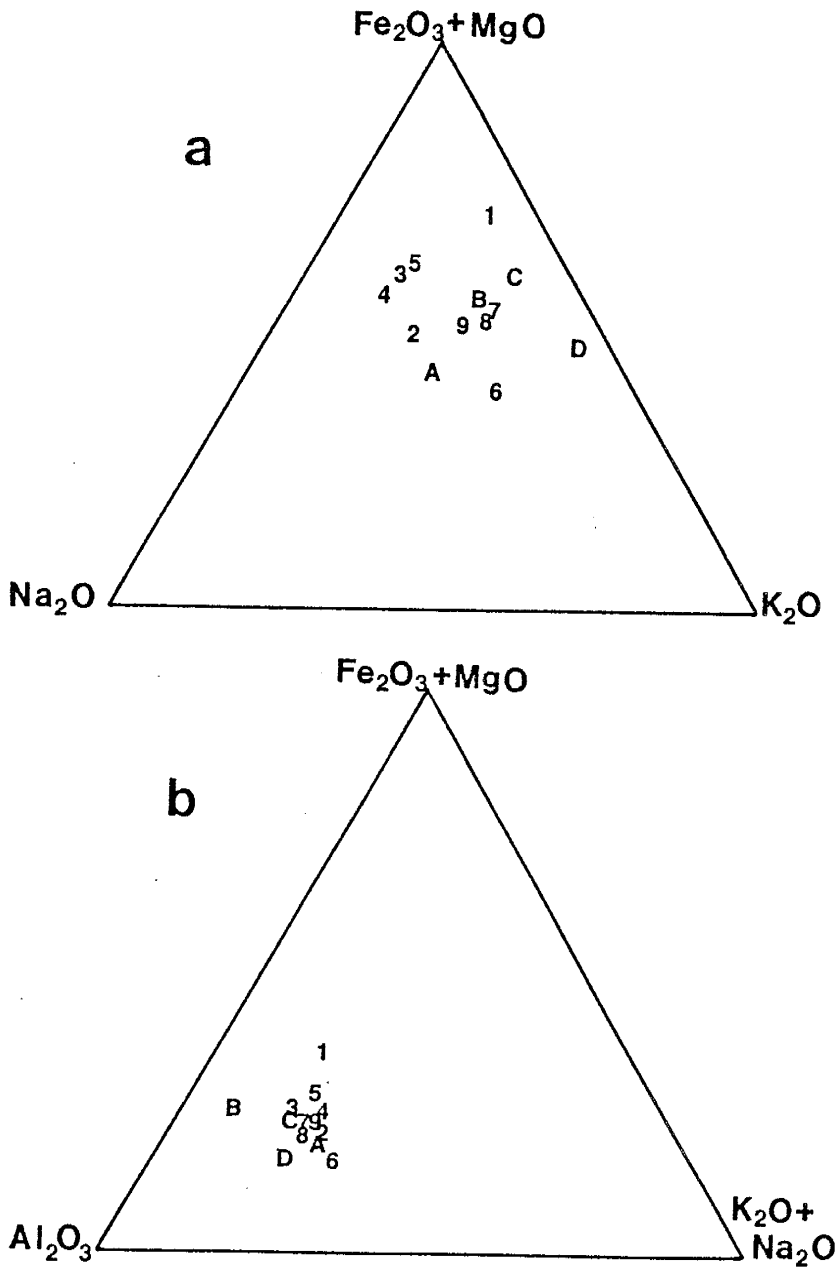

Figure 17. Average Pinal Schist metasediments compared to average composition of various rock types. Symbols correspond to columns in Table 9.

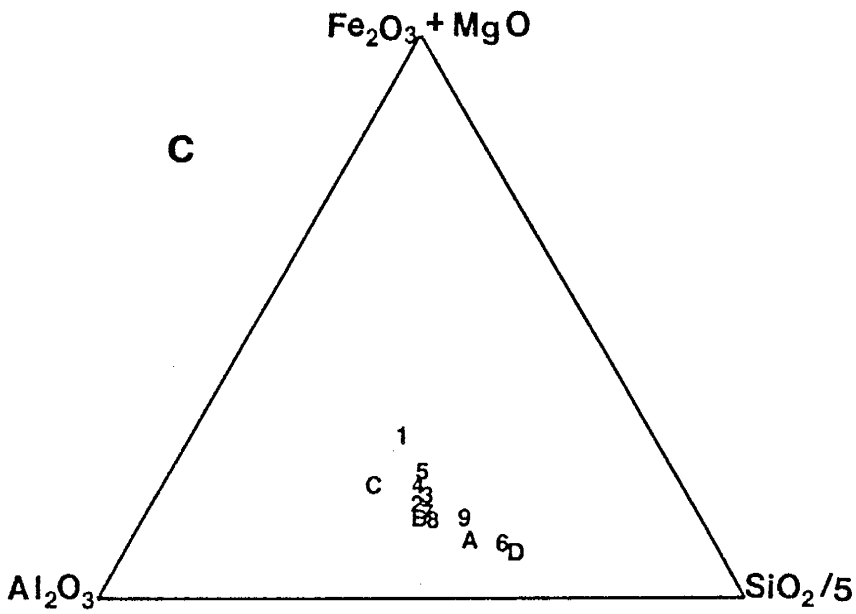

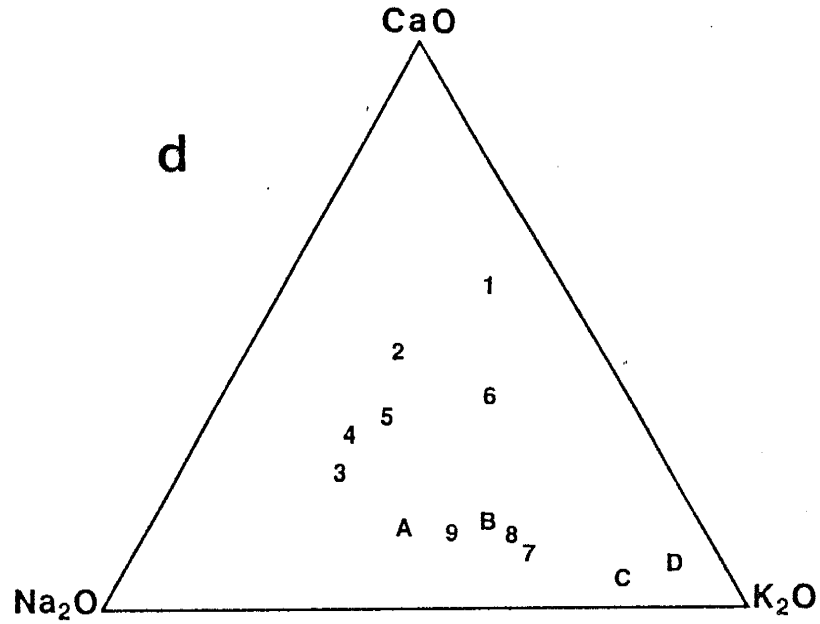

Figure 17, continued

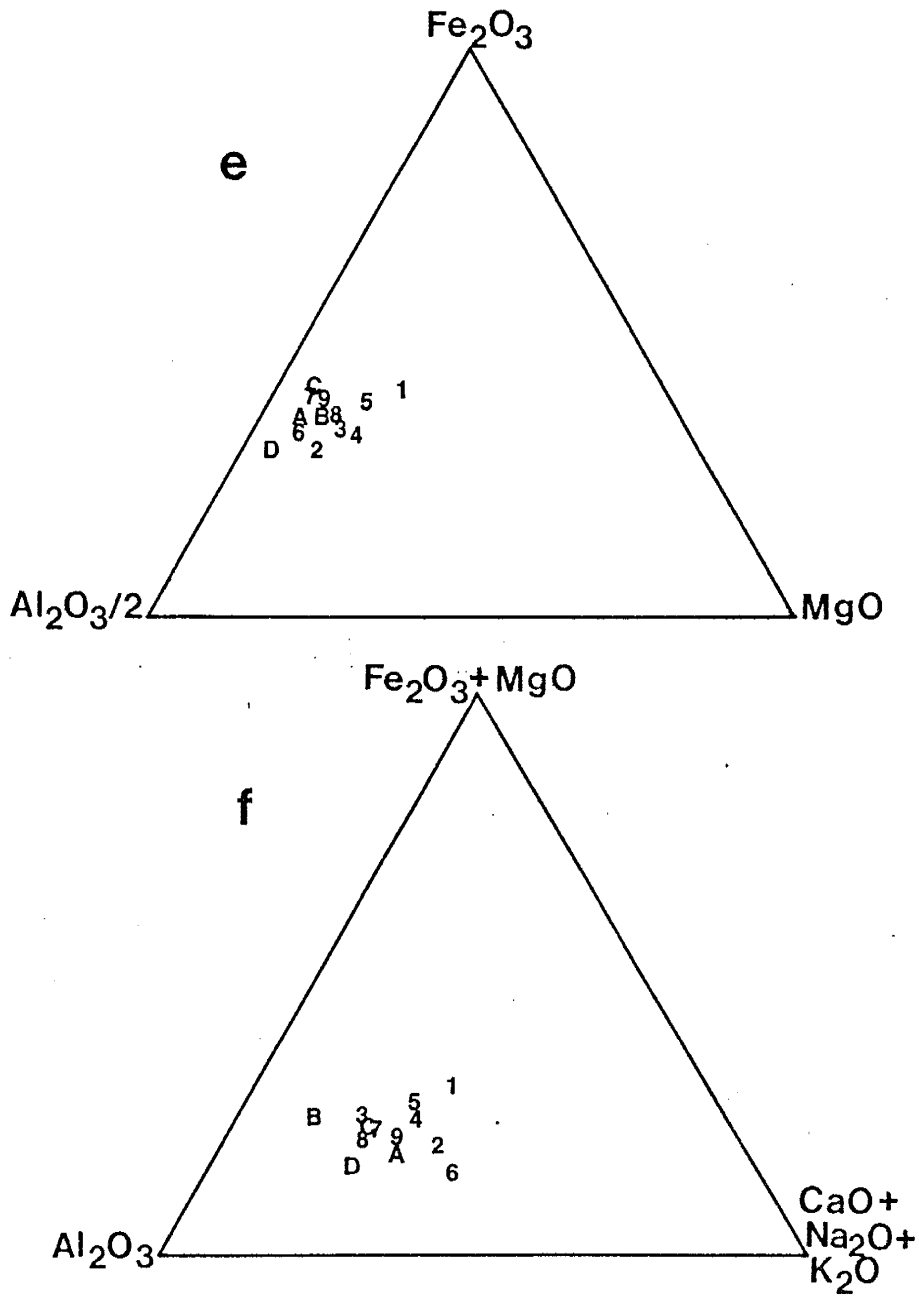

Figure 17, continued

plot near the proposed boundaries between these three rock types. The 27 samples which are enclosed by the dotted line in figure 16a are considered the "typical" Pinal sandstone in the study area. Figure 16b shows the distribution of the four chemical subgroups on the Na_2O - (Fe_2O_3 +MgO)-K_2O diagram. The greatest variation is seen in Na_2O , with group A having the highest Na_2O , groups B and C having intermediate values of Na_2O and group D having little or no Na_2O diagram, Na_2O is probably a measure of feldspar content. This suggests that group A has a high feldspar content and group D a low feldspar content and thus confirms the petrographic data (Table 9).

Table 10 compares the mean chemical composition of the "typical" Pinal sandstone, the average of all Pinal metasediments analyzed from the study area, the average sandstone of the Pinal Schist in the Pinal Mountains (De Melas, 1983), and the four chemical subgroups from Table 6 to various average rock types from the literature. Figure 17 graphically compares the data in Table 10 on a series of ternary diagrams. When comparing averages such as those in Table 10 and figure 17 one must keep in mind that averages distill large amounts of data with potentially large ranges into a single data point. This is clear when comparing points 7 and 8 on figure 17a with the range of data they represent on figure 16. This

problem notwithstanding, I feel the data in Table 10 and their graphical representation in figure 17 indicate that the sediments of the Pinal Schist are chemically distinct from sediments in modern island arc fore-arc basins. The most clear-cut distinction between the Pinal sediments and island arc sediments can be seen in the Fe and Mg content of these rocks. The Pinal rocks also have low concentrations of Co, Cr, and Sc (Fig. 20).

The Pinal sediment averages bear some similarities to the graywackes and continental margin arc sands. As mentioned, averages may represent a large range of compositions but it is worth note that the Pinal averages plot close to points 2, 3, 4, and 5 in figures 16 b,c,e, and f. In figures 16a and 16d the Pinal averages do not fall near points 2, 3, 4, and 5. Figures 16a and 16d each have K_2O as one of their verticies and each shows the enrichment of the Pinal metasediments in K relative to the other rocks in Table 10. Figure 17d, the Na_2O -CaO-K_2O ternary diagram, is strongly affected by the feldspar composition in these rocks. On the basis of this diagram, one might conclude that K-feldspar was a significant proportion of the feldspar population in the Pinal sediments. Moreover, this would tend to indicate a cratonic provenance for the Pinal Schist as K-feldspar dominates the feldspar suite of sandstones formed in continental settings (Ehlers and Blatt, 1982).

Petrographic analysis of the Pinal sandstones in the study area, however, does not bear out this hypothesis of abundant K-feldspar in these rocks. It therefore must be assumed that most of the K-feldspar was destroyed during metamorphism or that K in these rocks is found in some other mineral or in rock fragments. Condie and others (1985) indicate K-feldspar to be the dominant feldspar in the metasediments of the Dos Cabezas Mountains. This and the K content of the Pinal sandstones to the west suggest K-feldspar may have been present before metamorphism. Maynard (1984) suggests that high-K plagioclase is less resistant to weathering than low-K plagioclase. Some of the group D rocks with high K/NC and low S/A values may have had appreciable amounts of high K, high Al clays in their original detrital composition. While it appears that K may have been removed by secondary processes from the Pinal basalts in the northeast Little Dragoon Mountains, it is not possible to assess to what extent K has been mobilized in the Pinal metasediments.

Trace Elements

The REE distributions for an average of 33 Pinal sedimentary rocks from throughout the study area are shown in figure 18a. The REE distributions of the individual chemical subgroups are shown in figure 18b. The shape of the REE patterns of the four subgroups in figure 18b are essentially the same with the only

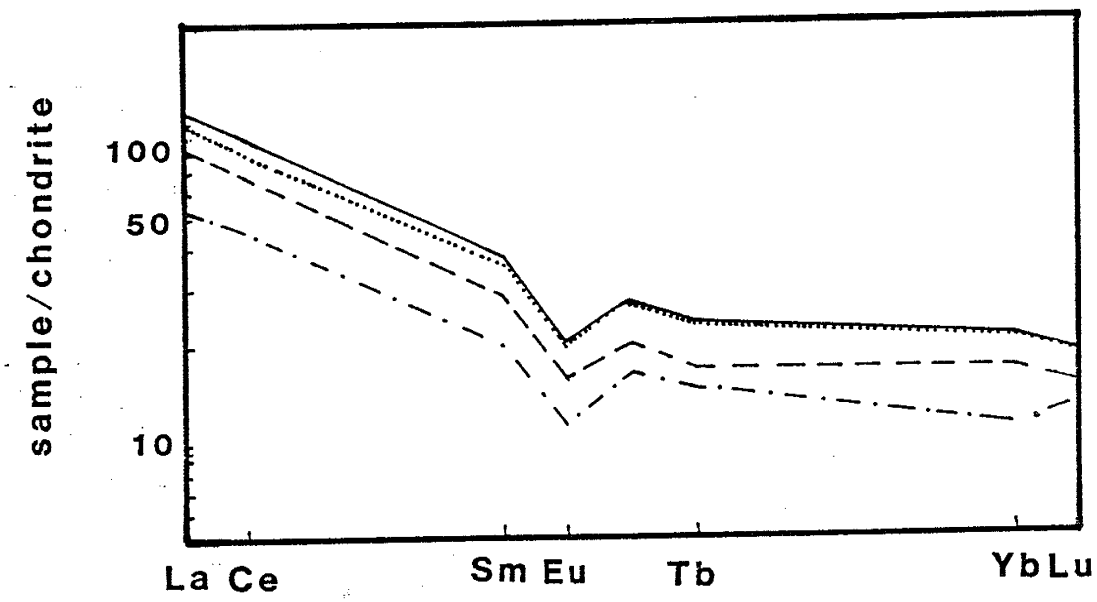

Figure 18b. REE distribution of chemical subgroups from table 6. Solid line, group C; dotted line, group A; dashed line, group B; dots and dashes, group D.

difference being the concentration level of each group. This appears to be a quartz dilution effect as there is a negative correlation between the REE concentration and SiO_2 concentration. Eu is depleted in all of the Pinal sediments relative to the other REE. The only important Phanerozoic sedimentary rock types which do not exhibit Eu depletion are some first cycle volcanogenic sediments deposited in fore-arc basins of island-arcs (Taylor and McLennan, 1985). There is a remarkable similarity between the REE patterns of the Pinal sediments and the North American Shale Composite (NASC; Gromet and others, 1984; Fig. 18). The sediments of the Pinal Schist in the type locality in the Pinal Mountains (Condie and De Melas, 1985) and in the Slate Mountains in southern Pinal County (M. Sunderland, unpub. data) also have REE distributions similar to the NASC. The NASC is thought to be representative of the continental crust exposed to erosion (Gromet and others, 1984). REE patterns of sedimentary rocks can be strongly effected by the presence of minor minerals such as allanite, monazite, and zircon (Gromet and others, 1984; Appendix A) and the sediments of the Pinal Schist are generally coarser grained than the NASC. Nevertheless, the strong similarity of these two sedimentary REE distributions suggests a similar type of provenance. This precludes a significant input of detritus derived from an oceanic

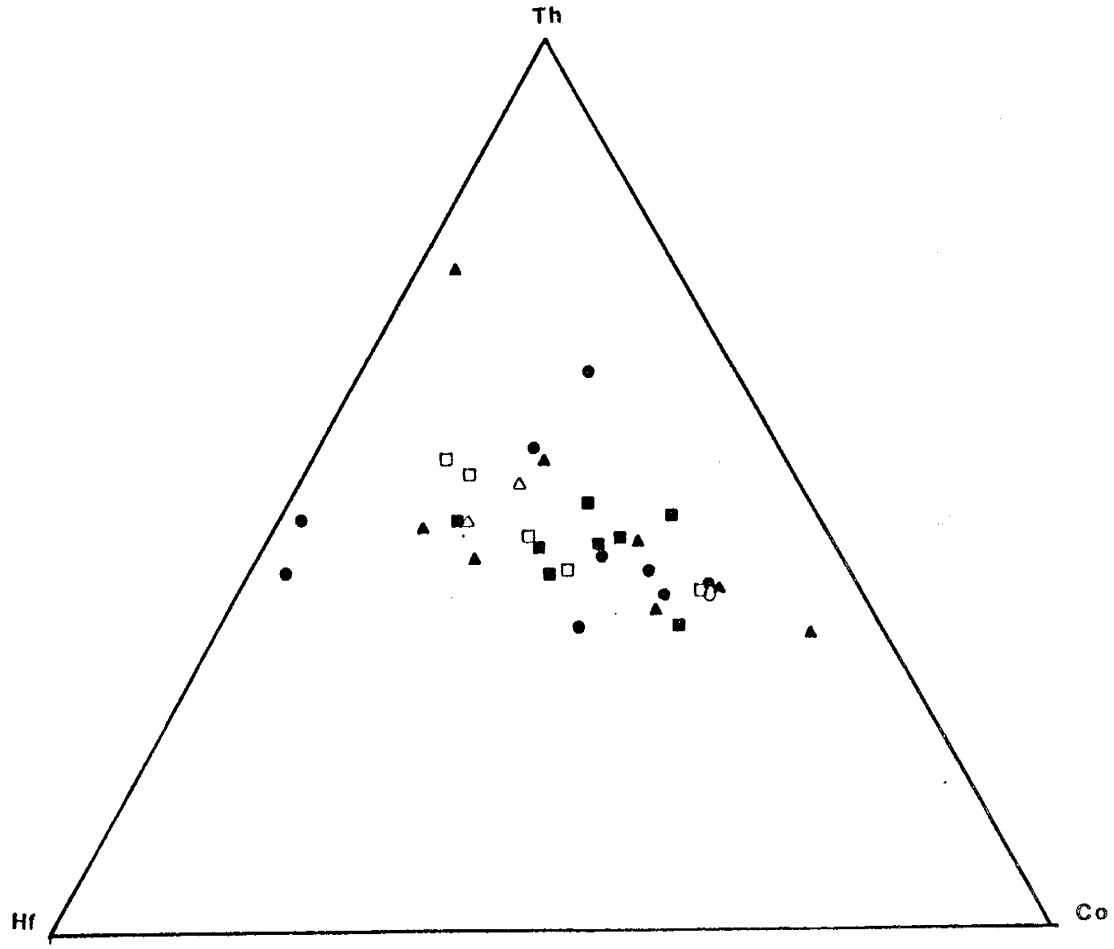

Figure 19a. TiO_2 -(Fe_2O_3 +MgO) covariation of Pinal metasediments. Fields from Bhatia (1983). Open circle, Dos Cabezas Mountains; filled circles, Dragoon Mountains; filled squares, Little Dragoon Mountains and Johnny Lyon Hills; open squares, Whetstones Mountains; filled triangles, Rincon Mountains; open triangles, Mule Mountains.

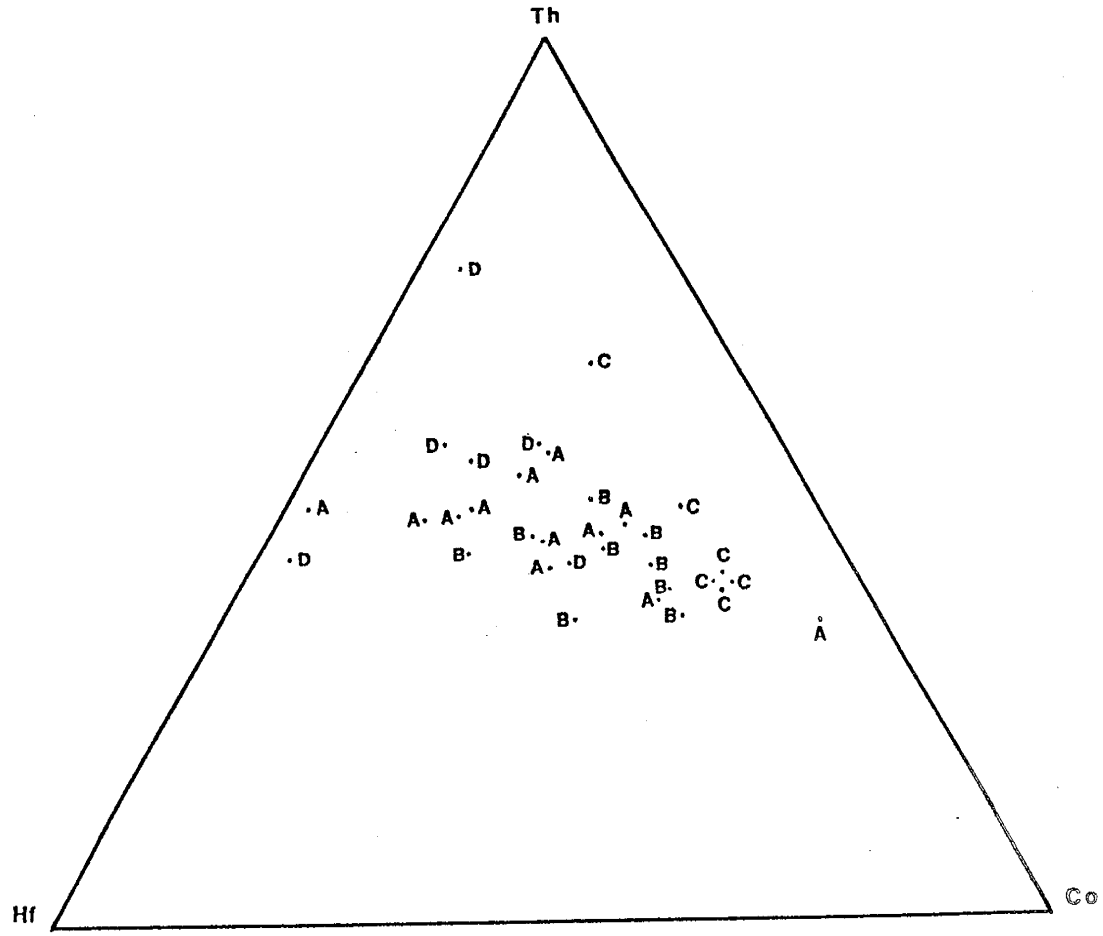

Figure 19b. TiO_2 vs. Fe_2O_3 +MgO. Symbols correspond to groups in table 6.

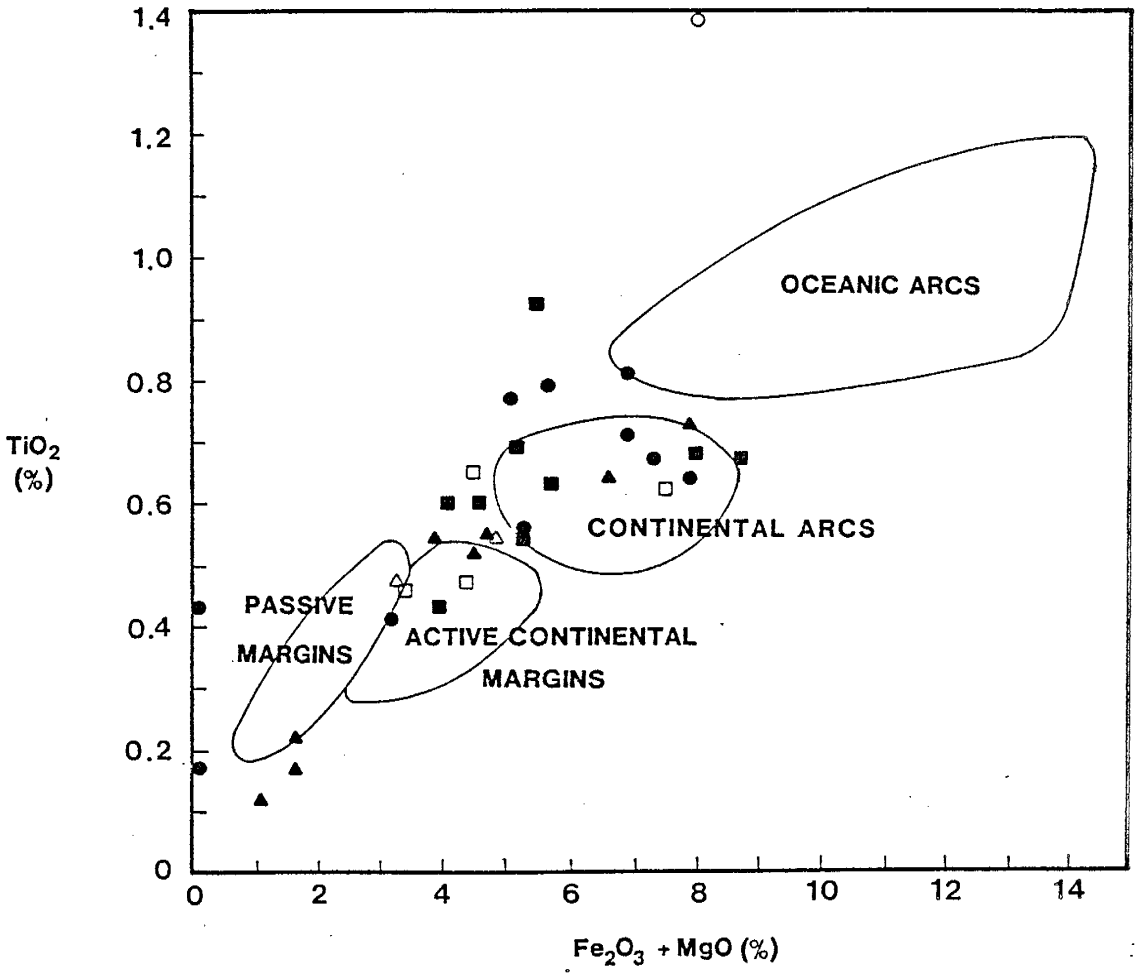

Figure 20a. Hf-Th-Co variation of Pinal metasediments. Open circle, Dos Cabezas Mountains; filled circles, Dragoon Mountains; filled squares, Little Dragoon Mountains and Johnny Lyon Hills; open squares, Whetstones Mountains; filled triangles, Rincon Mountains; open triangles, Mule Mountains.

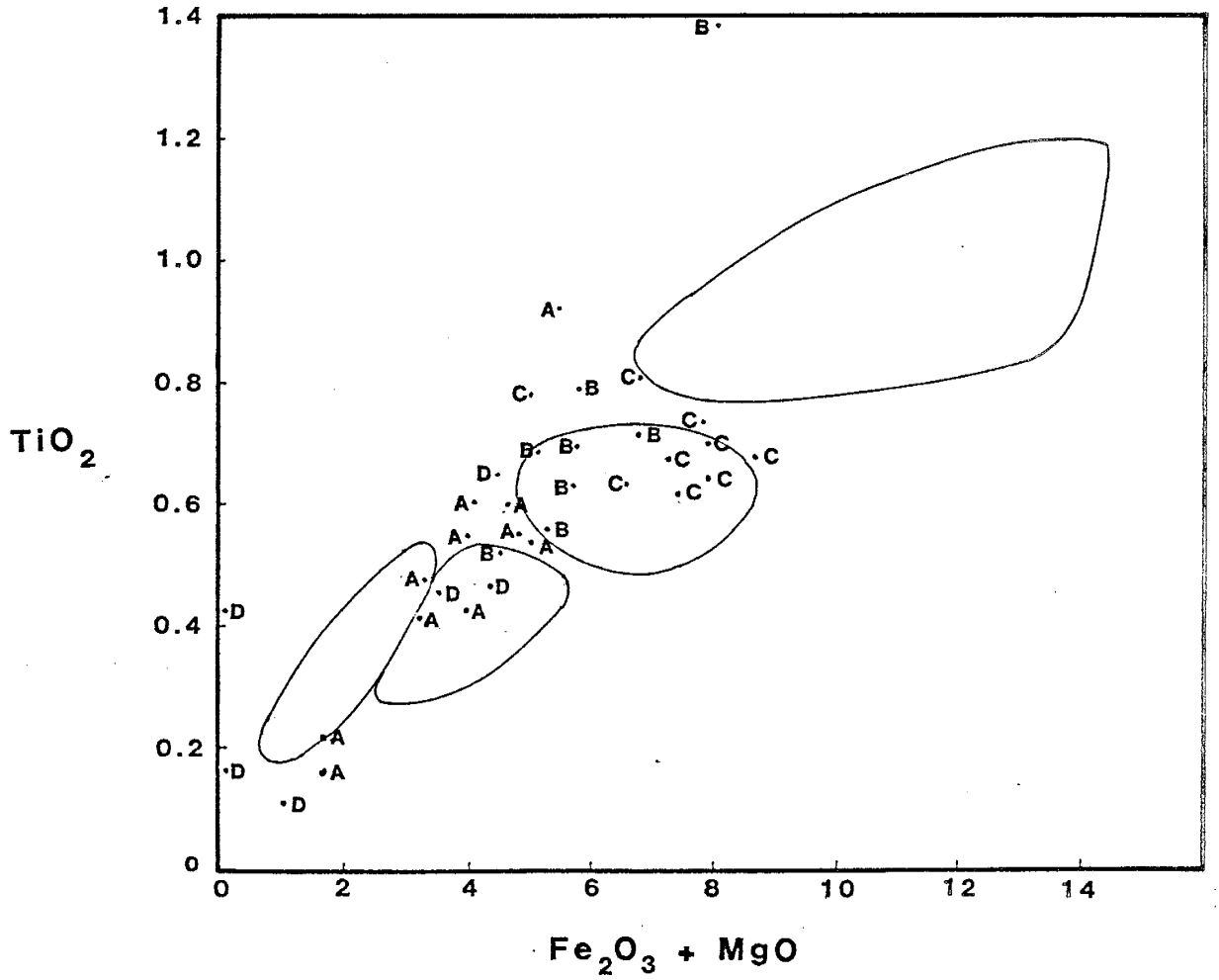

Figure 20b. Hf-Th-Co variations of Pinal metasediments. Symbols correspond to groups in table 6.

island arc.

The lack of an island arc component in the Pinal sediments also can be seen in figure 19, a tectonic discrimination diagram of Bhatia (1983). These fields may not be unique and should not be used as tectonic indicators alone, however, of the 33 Pinal metasediments analysed, only one comes close to the field of island arcs on figure 19. The dominant portion of the Pinal sediments fall in or near fields of continental provenance on figure 19. Groups B and C appear to have a greater concentration of mafic minerals than groups A and D. This is, however, expected as Fe_2O_3 , MgO and TiO_2 are parameters used in the definition of these groups.

Taylor and McLennan (1984) proposed a Hf-Th-Co diagram as a measure of the contribution of continental and oceanic crustal sources to sediments. In this diagram Co is a monitor of mafic contributions. When the Pinal sediments are plotted in this diagram (Fig. 20), group C shows the greatest input of a mafic component. Group D show the least input of a mafic component. As in figures 16a and 18a, figure 20a does not show any geographic trends.

Possible post-depositional tectonic transport of these mountain ranges (Drewes, 1981) makes interpretation of the chemical variations in sandstones from area to area problematical. The rocks of French Joe Canyon

(group D) in the Whetstone Mountains appear to be the most mature sediments in the area. These rocks have high SiO_2 , low FMT, and lack a significant proportion of rock fragments. Perhaps these rocks were deposited in a zone of intense reworking. The lower SiO_2 , and high FMT values of the group C rocks relative to the other groups may suggest a greater contribution of mafic and intermediate volcanic detritus to these rocks. The widespread distribution of group C rocks, however, indicates that this possible bias towards a mafic component did not occur at any particular location.

The geographic variability of all four chemical subgroups of the Pinal sandstones in the study area suggests a depositional environment which did not effectively sort this detritus. The presence of any grouping at all, however, indicates that some sorting was taking place on a local scale. One possible mechanism that would produce local variations rather than regional variations is sedimentation by turbidity flow into a small basin. Turbidity currents produce a gross separation of coarse grains and heavy grains from fine grains and light grains. Successive turbidite accumulation from a heterogeneous source area could produce many small scale variations in a sedimentary sequence.

A second possible explanation for the chemical

variation seen in the Pinal sandstones is variation in the source materials. Coalescing submarine fans with different provenances could produce a distribution of sandstones with chemical characteristics such as those seen in the Pinal Schist.

DISCUSSION

The data presented in this study are consistent with an interpretation that the rocks of the Pinal Schist in southeastern Arizona evolved in or near a magmatic arc environment (Figs. 7, 8, 9, 11, 12, 13). This arc had geochemical characteristics transitional between the tholeiite and calc-alkaline series (Figs. 3, 4, 8, 9). Although no Sm-Nd, Lu-Hf, or Pb-Pb isotopic data are available for the basaltic rocks of the area, chemical analyses of both igneous and sedimentary rocks of the Pinal Schist appear to preclude the possibility that the arc formed in an oceanic setting (Figs. 8, 10, 12, 13, 16, 17, 18). Given that the rocks of the Pinal Schist are products of a continental margin magmatic arc, it becomes necessary to determine what portion of the arc is represented by the relatively small area of Pinal Schist in southeastern Arizona.

Mafic Volcanic Rocks

There is a geochemical transition from the basalts in the Dragoon Mountains to the basalts in the Dos Cabezas and Chiricahua Mountains to the basalts in the Little Dragoon Mountains which is strongly reflected in figures 9 and 11 and less strongly so in figures 3, 4, and 8a. The basalts in the Dragoons have a significant subduction component on MORB normalized diagrams. Many of these rocks have major and trace element

characteristics of calc-alkaline basalts. The Dos Cabezas basalts also exhibit a subduction component on MORB normalized diagrams. The magnitude of this subduction component is not as prominent as that reflected in the Dragoon basalts, although the difference is small. The Dos Cabezas and Rincon basalts have a more tholeiitic character than the Dragoon basalts and have some characteristics of within plate basalts (Fig. 11). The Little Dragoon basalts do not exhibit a subduction component on MORB normalized diagrams and are tholeiitic. Weaver and others (1979) observed a similar geochemical variation in the basalts of the Bransfield Strait, a narrow ensialic back-arc basin separating the South Shetland Islands from the Antarctic Peninsula. The Bransfield Strait basalts have characteristics of both calc-alkaline arc-type lavas and MORB. Weaver and others (1979) suggested that these variations are due to different mantle sources which have been affected by a previous subduction event. Given the presently available data, a similar origin for the Pinal basalts cannot be ruled out.

The variation in composition of the Pinal basalts may be summarized by equating the Dragoon and the Dos Cabezas basalts with a calc-alkaline arc environment, and the Little Dragoon basalts with a back-arc or within plate environment. Such variations could be caused by

inhomogeneities in the source area, as discussed above, or be the signature of a distance-to-the-trench relationship. Such a relationship could be satisfied in a back-arc basin behind a continental margin arc where the Little Dragoon basalts represent the most distant rocks from the trench and the Dragoon basalts represent rocks closer to the arc.

Felsic Volcanic Rocks

Geochemical modelling relationships (Appendix E; Condie and others, 1985) suggest that the felsic volcanic and subvolcanic rock of the study area are not differentiates of the local mafic rocks but rather have characteristics of partial melts of a material with the composition of continental crust. An interpretation consistent with these data is that mafic magma rising from a subducting slab provided sufficient heat to melt portions of previously existing sialic material. These melts rose buoyantly and were then erupted as ignimbrites and emplaced as shallow, subvolcanic sills and dikes.

Sedimentary Rocks

The sedimentology and chemical composition of the Pinal sediments have some similarities with flysh-type graywackes from orogenic belts (Maynard and others, 1982; Crook, 1974). Such a sediment type is consistent with deposition in a basin near a continental margin magmatic

arc. Figures 17, 18, 19, and 20 as well as the low Sc and Co content of the metasediments indicate the provenance of the Pinal Schist sandstones did not include a significant proportion of mafic or intermediate igneous rocks. This geochemical evidence is consistent with petrographic study of the Pinal metasediments which indicates rock fragments in the Pinal sandstones were dominantly if not exclusively of felsic volcanic, sedimentary, and granitic origin. Sand-rich submarine fans have been observed in Mesozoic continental margin arc environments in California (Busby-Spera, 1984; 1985) and southern Chile (Dott and others, 1982; Tanner, 1982).

Proposed Model

One model which is consistent with the available data from the Pinal Schist is formation of the Pinal Schist in a continental margin back-arc basin. This is shown schematically in Figure 21. This arc and its related subduction zone were probably located to the southeast or south of the study area. Subduction would have been directed to the northwest or north striking northeast-southwest. This orientation between the proposed arc and back-arc has the same strike of major Proterozoic structures and terrane boundaries in central Arizona (Conway and Silver, in press).

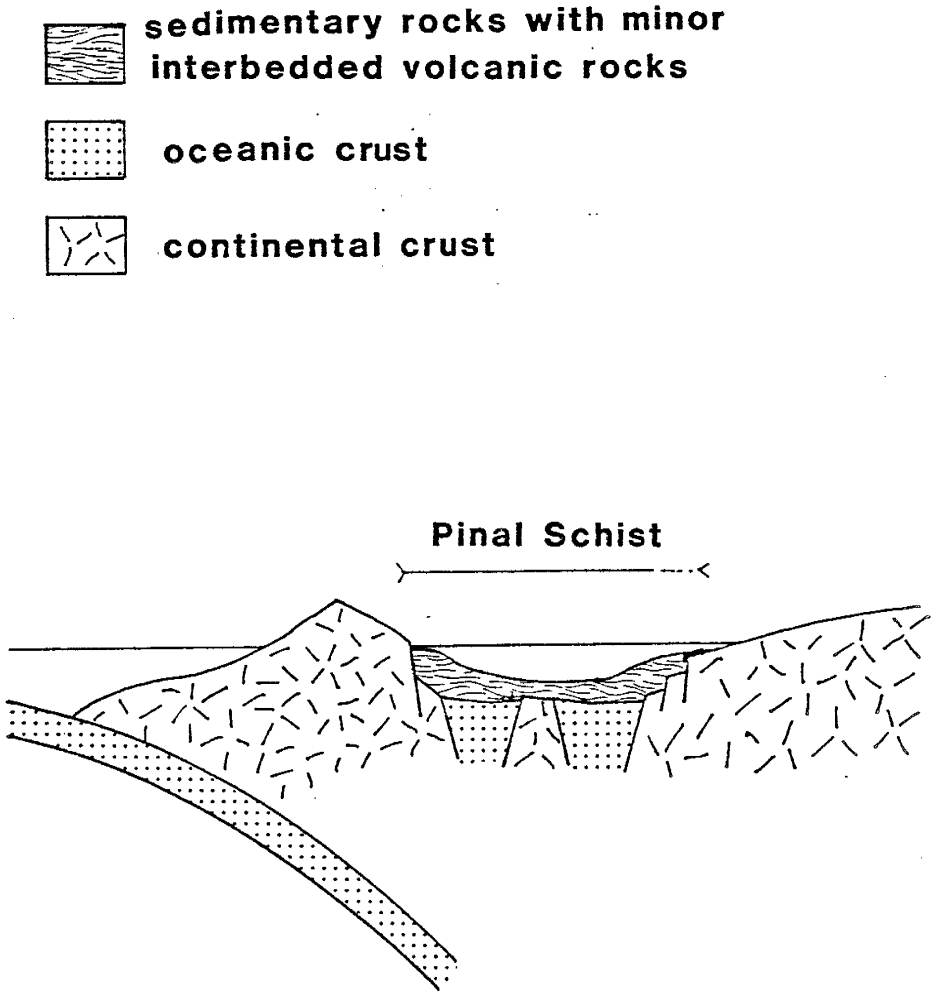

Figure 21. Schematic geologic cartoon of proposed model for the environment of formation of the Pinal Schist.

The basalts from the Chasma Group of central Peru (Fig. 8c) have been interpreted by Atherton and others (1985) to have formed in a back-arc basin opening wide enough to take on an oceanic geochemical signature in some places. Given the available data, the same interpretaion is applicable to the basalts from the Pinal Schist in southeastern Arizona. In this model the rocks of the Little Dragoon Mountains represent an environment near the center of this basin. Bonatii (1985) has shown that the transition from a continental to an oceanic rift may occur in localized hot areas rather than in an linear zone of spreading. The Little Dragoon basalts could possibly be the product of such a localized transition. Alternatively, the Little Dragoon basalts could represent an early stage in arc development (pre-arc of Pearce and others, 1984) before the source of arc magmas was significantly enriched in LIL elements by fluids rising from a subducting slab. As there is some overlap in the geochemical characteristics of MORB and within plate basalts, such initial spreading could have occurred in either a continental or oceanic setting. An oceanic setting is preferred based on the sedimentary structures of the sediments of the Pinal Schist in the Little Dragoons and surrounding mountain ranges. These rocks appear to have been deposited below wave base.

One potential problem with a back-arc model for the

formation of the Pinal Schist is the small volume of basaltic rocks. The Mesozoic continental marginal basin of central Chile is dominated by clastic sedimentary rocks with a small component of basaltic rock and minor fresh water limestone (Levi and Aguirre, 1981). In marginal basins with high sedimentation rates, Layer 2 of the oceanic crust may be emplaced as sills rather than flows (Saunders and Tarney, 1984), possibly obscuring a basaltic component in the upper part of the section. Such a basin need not have been of great width (<150 km). A narrow basin would not necessarily be floored by new oceanic crust. The volume of basaltic rock is not inconsistent with an origin in a back-arc basin with high sedimentation rates. A narrow, tectonically active basin would also receive abundant sediments from both the arc and the craton side of the basin. An ensialic marginal basin could develop rocks such as those seen in the Pinal Schist without the creation of new ocean floor (Levi and Aguirre, 1981; Atherton and others, 1985) or this ocean floor could have continuously covered by sediment fed into the basin.

An ensialic back-arc basin represents both a transition between tectonic regimes and a superpositon of one tectonic regime on another. Such relationships present special problems in evaluating the processes which formed rocks during such a transition (Mack, 1984;

Weaver and others, 1979). It is important to note that while the lithotectonic assemblage represented by the Pinal Schist in outheastern Arizona has features of a rift environment as recognized by Condie and others (1985), this rifting seems to have been superimposed on a previous arc environment. It is the point of view of this report that any extension associated with the evolution of the Pinal Schist was a small part of a larger regime which was dominated by compressional tectonics. There are numerous examples of such zones of extension within continental arcs throughout geologic history (Hildebrand and Bowring, 1984; Busby-Spera, 1984; Levi and Aqurie, 1981).

Detailed structural studies of a regional extent are needed to place the Pinal Schist in a regional tectonic framework for the Southwest Precambrian. Structural studies of rocks of similar age to the Pinal Schist in the Tonto Basin-Mazatzal Mountains area in central Arizona underway by Karl Karlstrom and students are revealing a structural style similar to many foreland fold and thrust belts (Karlstrom and Puls, 1984). The tectonic events which deformed the rocks in the Mazatzal Mountains also could have affected the rocks of the Pinal Schist to the south. Mesoscale structures in sediments in the Brady Butte area in central Arizona are similar to some in the Johnny Lyon Hills, Little Dragoon Mountains,

and the Mule Mountains. During the closing of Phanerozoic ensialic back-arc basins similar structures have developed (Mercier, 1981). I would therefore tentatively suggest that at least some of the Proterozoic structures in the Pinal Schist in southeastern Arizona are the result of a closing of a back-arc basin.

Regional Implications

If the hypothesis that the Pinal Schist accumulated in a continental back-arc marginal basin is accepted, the question of where is the arc or root zone of the arc today must be addressed. Little is known about the Proterozoic geology of Sonora. Study of this area could provide a test of this hypothesis. This model predicts rocks of continental arc affinity, particularily felsic volcanic and plutonic rocks, to be present to the south or southeast of the outcrop area of the Pinal Schist. As noted, minor to trace amounts of felsic igneous rocks are scattered throughout the Early Proterozoic of southeastern Arizona but not in the great volume one would associate with a continental margin arc. One possibility that cannot be ruled out by the presently available data is that the Pinal Schist in the Dos Cabezas and Chiricahua Mountains may represent part of a rifted remnant arc. This is the only place in the study area where felsic volcanic rocks and coarse grained arkosic rocks are an important part of the section.

To the east and west of the study area there are few outcrops of Proterozoic supracrustal rocks that might be related to the Pinal Schist. To the east the closest area of Proterozoic supracrustals is in the Burro Mountains in Grant County, southwestern New Mexico. These rocks contain two supracrustal sequences. The older series is a series of paragneisses, the younger a thick sequence of carbonates and clastic sedimentary rocks (Hewitt, 1959). Few details are known about the lithologies, structure, and most importantly, the geochronology of these rocks. To the west of the Slate Mountains in southern Pinal County (Plate 1), Proterozoic rocks are either covered by younger strata or metamorphosed to such a degree that recognition of the protolith is difficult. Extension of the proposed tectonic regime along strike is therefore problematic.

The Early Proterozoic of the southwestern United States can be generalized as a series of magmatic arcs which were accreted to the Archean nucleus of North America between 1800 and 1600 Ma ago (Condie, 1982). These several arc successions have been interpreted within a framework of Phanerozoic-style buoyancy driven plate tectonics. While the style of Proterozoic tectonics was probably substantially similar to that we observe in the Phanerozoic, it is quite likely that the rate of tectonism was substantially higher in the Early

Proterozoic than in the Phanerozoic (Karlstrom and Houston, 1984; Hoffman and Bowring, 1984). In the 1.9 Ga Wopmay Orogen, an ocean basin wider than the one proposed in this report opened and closed in less than 20 m.y. (Hoffman and Bowring, 1984). More detailed structural, geochronologic, and geochemical work is needed to test the back-arc hypothesis for the origin of the Pinal Schist (Appendix G).

CONCLUSIONS

Volcanic Rocks

The mafic volcanic and subvolcanic rocks of the Pinal Schist were deposited as submarine flows and emplaced as shallow dikes and sills. These melts were derived from a subducting slab and provided heat to melt previously existing sialic material. These felsic magmas were erupted as ignimbrites and emplaced as shallow, subvolcanic sills.

Sedimentary Rocks

The sedimentary rocks of the Pinal Schist were deposited in a tectonically active basin. The detritus fed into this basin was predominantly of a granitic provenance with some minor mafic components (perhaps intrabasinal). These sediments were deposited in a series of submarine fans. The mechanism of sedimentation was likely turbidity flow at a moderate to high rate of deposition.

Tectonic Setting

The conclusions of this study concerning the tectonic setting of the Pinal Schist in southeastern Arizona can be summarized in order of decreasing confidence as follows:

1) The rocks of the Pinal Schist in southeastern Arizona

evolved in a magmatic arc environment.

2) This arc formed on the margin of the North American continent, rather than in a strictly oceanic setting.

3) The Pinal Schist accumulated in a marginal basin behind a continental arc located perhaps to the south or southeast.

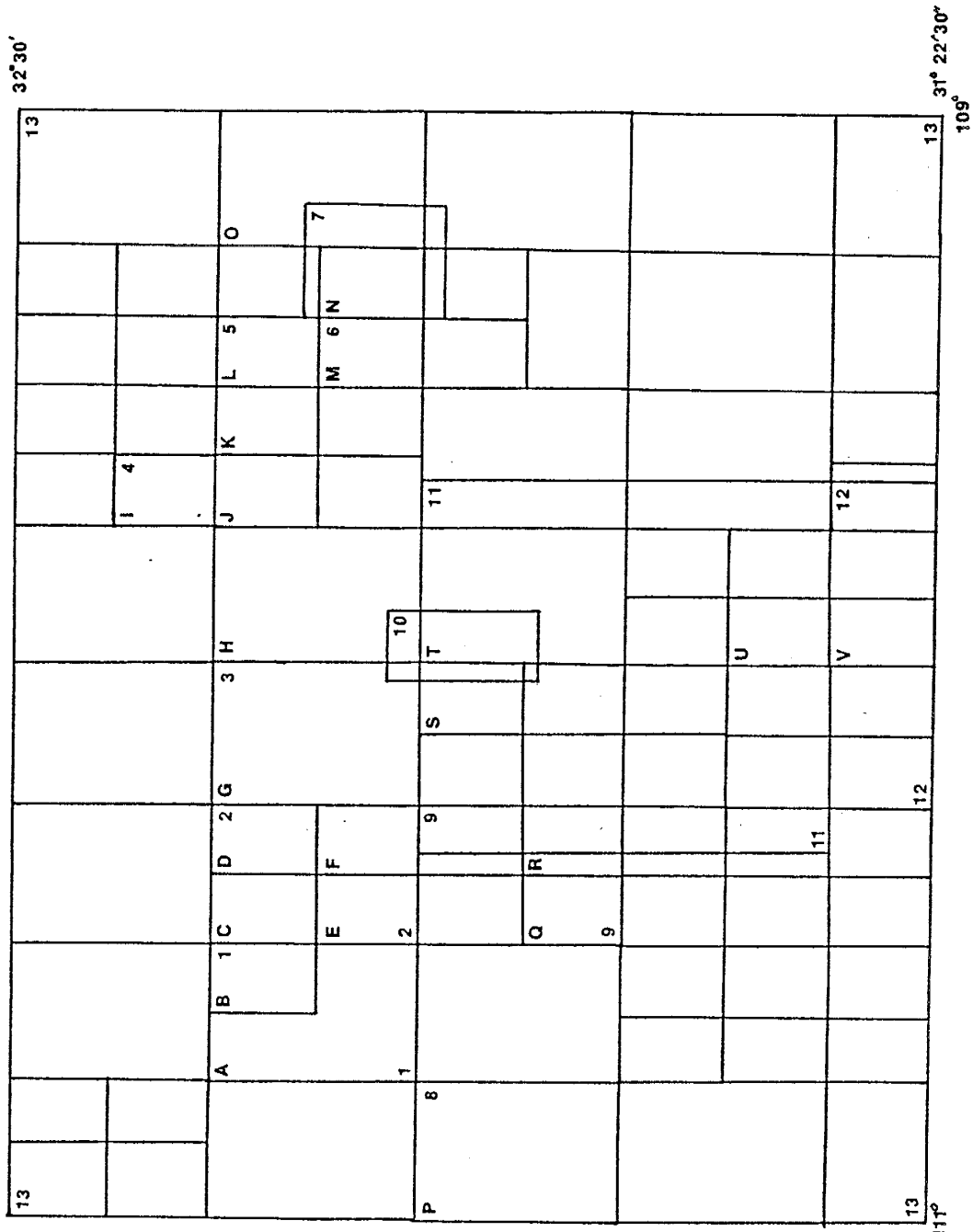

Figure A-1. Index map of topographic and geologic maps covering the study area. Explanation on next page.

[illegible] Table

[illegible]

[illegible] Valley	[illegible]
[illegible] Mountain	[illegible]
[illegible] Valley	[illegible]
[illegible] [illegible]	[illegible]
[illegible] [illegible]	[illegible]
[illegible] [illegible]	[illegible]
[illegible]	[illegible]
[illegible]	[illegible]
[illegible] [illegible]	[illegible]
[illegible]	[illegible]
[illegible] [illegible]	[illegible]
[illegible] [illegible]	[illegible]
[illegible]	[illegible]
[illegible]	[illegible]
[illegible]	[illegible]
[illegible]	[illegible]
[illegible]	[illegible]
[illegible]	[illegible]
[illegible]	[illegible]
[illegible]	[illegible]

[illegible]

1. [illegible], [illegible]
2. [illegible], [illegible]
3. [illegible] [illegible] [illegible], [illegible]
4. [illegible] [illegible] [illegible], [illegible]
5. [illegible], [illegible]
6. [illegible], [illegible]
7. [illegible], [illegible]
8. [illegible], [illegible]
9. [illegible], [illegible]
10. [illegible] [illegible] [illegible], [illegible]
11. [illegible], [illegible]
12. [illegible] [illegible] [illegible], [illegible]
13. [illegible], [illegible]

Figure A-2. Cooper and Silver (1964), southern Johnny Lyon Hills.

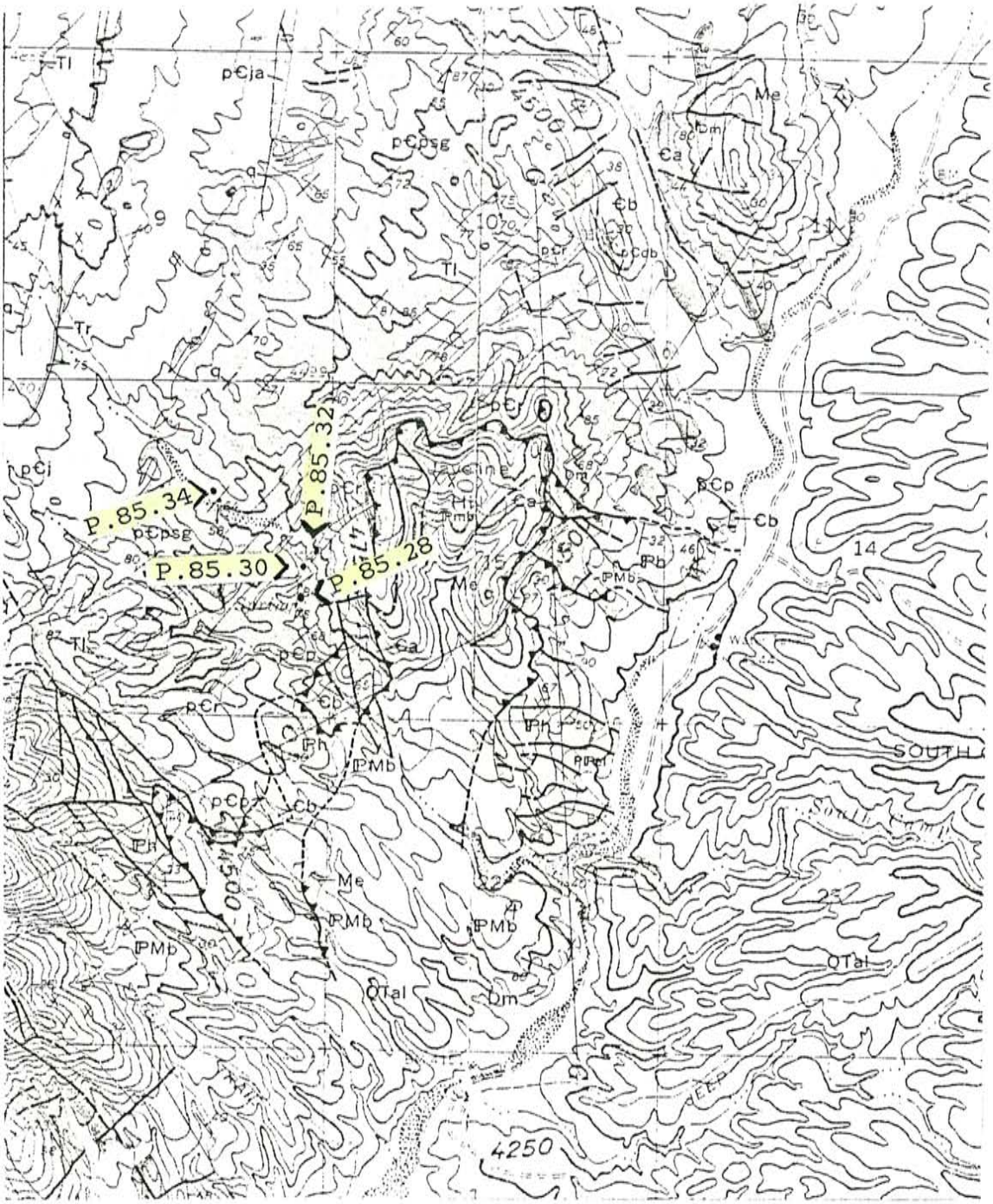

Figure A-3. Cooper and Silver (1964), northern Johnny Lyon Hills.

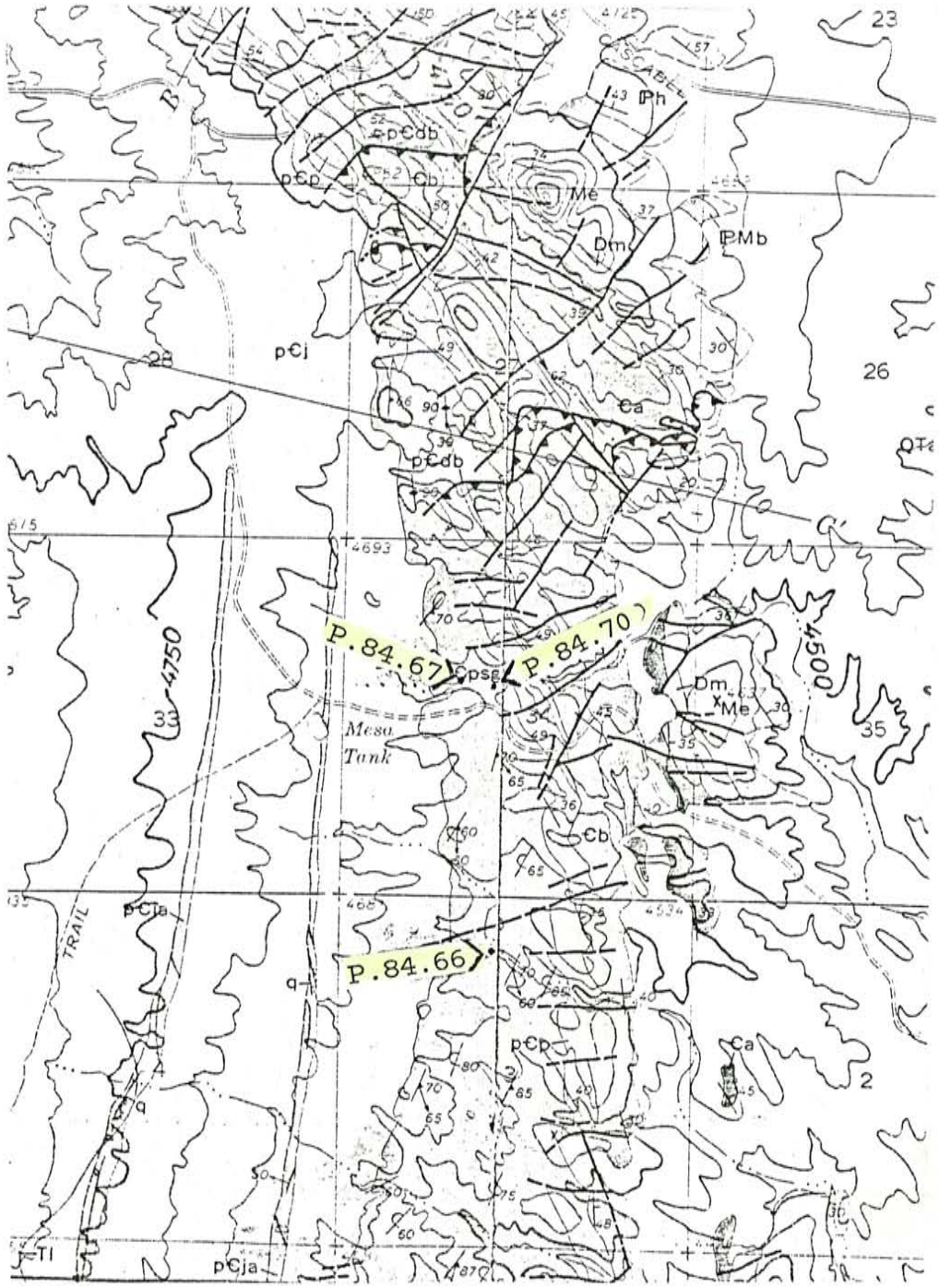

Figure A-4. Cooper and Silver (1964), northern Little Dragoon Mountains.

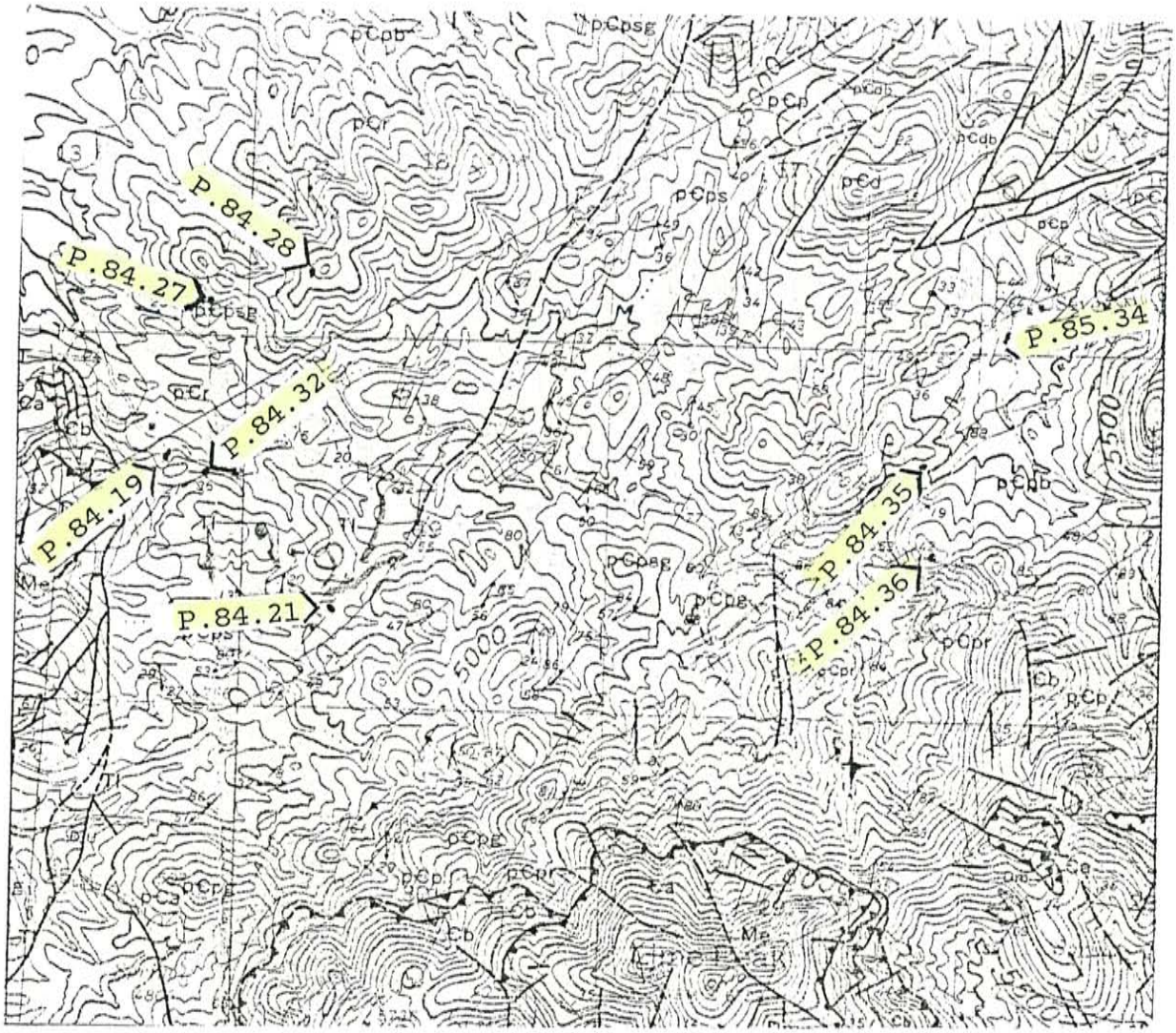

Figure A-5. Drewes (1981), northern Dragoon Mountains.

Figure A-6. Drewes and Meyer (1983), north central Dragoon Mountains.

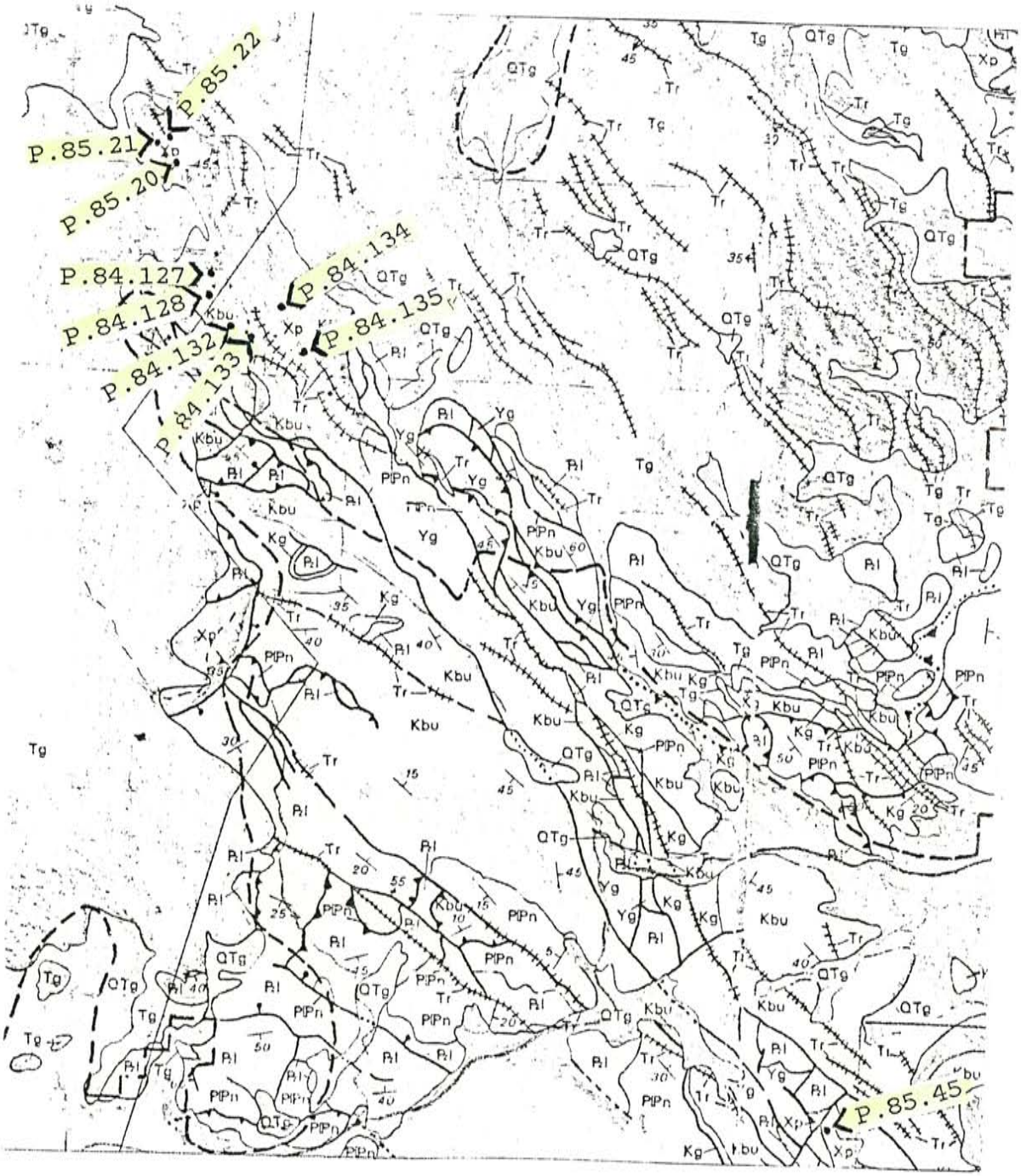

Figure A-7. Pearce 15 minute topographic, central Dragoon Mountains.

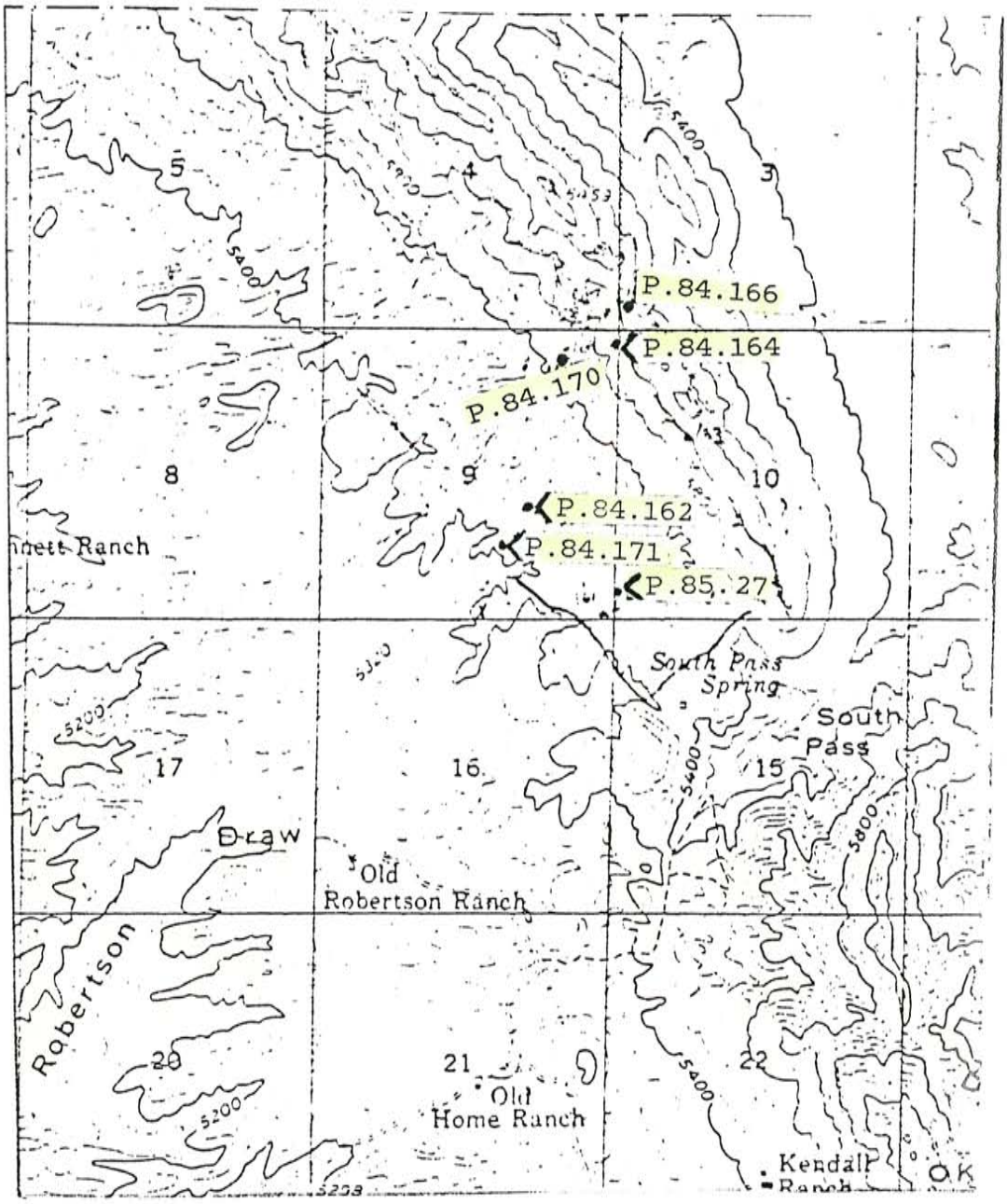

Figure A-8. Creasy (1967), Whetstone Mountains.

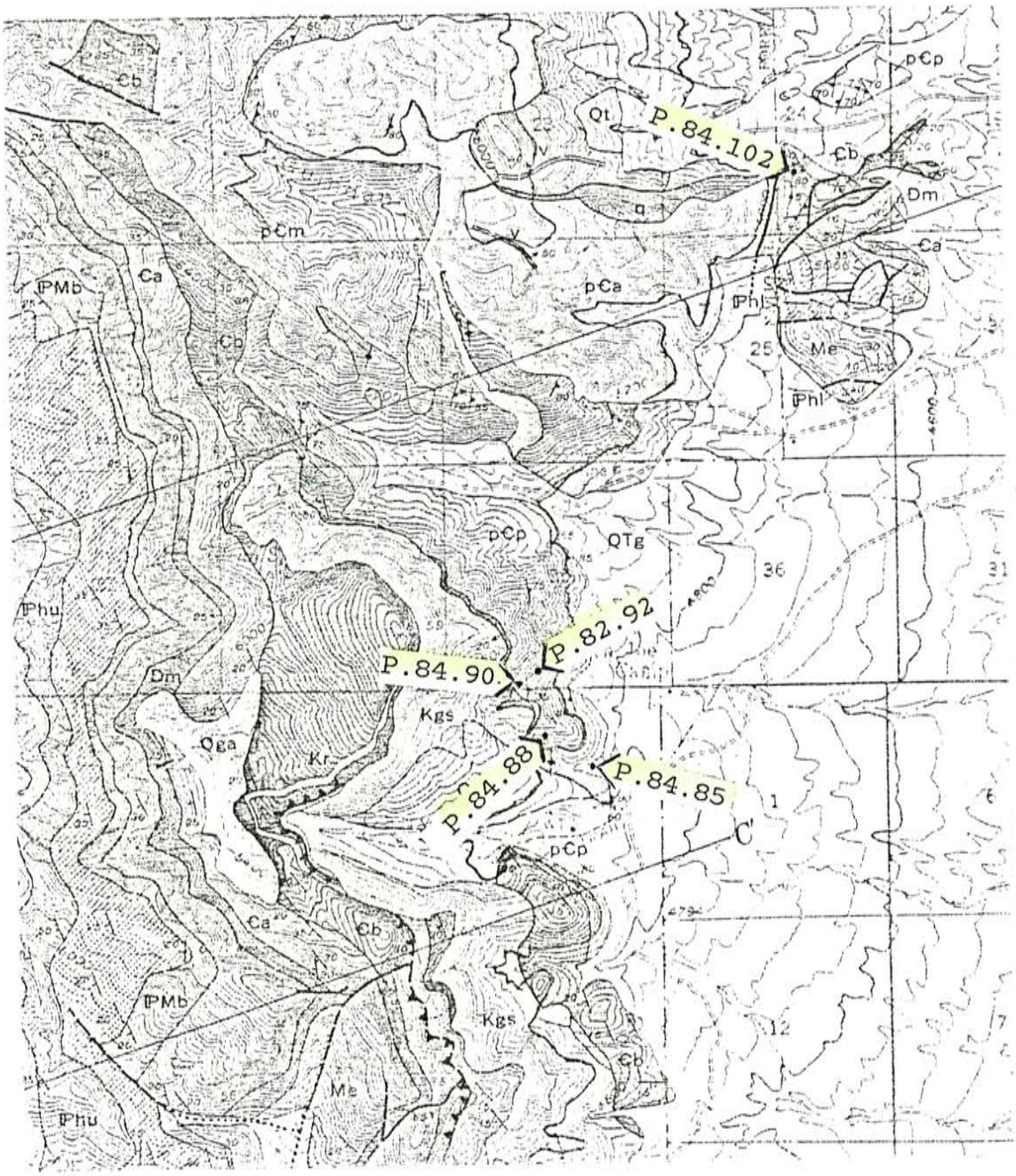

Figure A-9. Drewes (1984), Chiricahua Mountains.

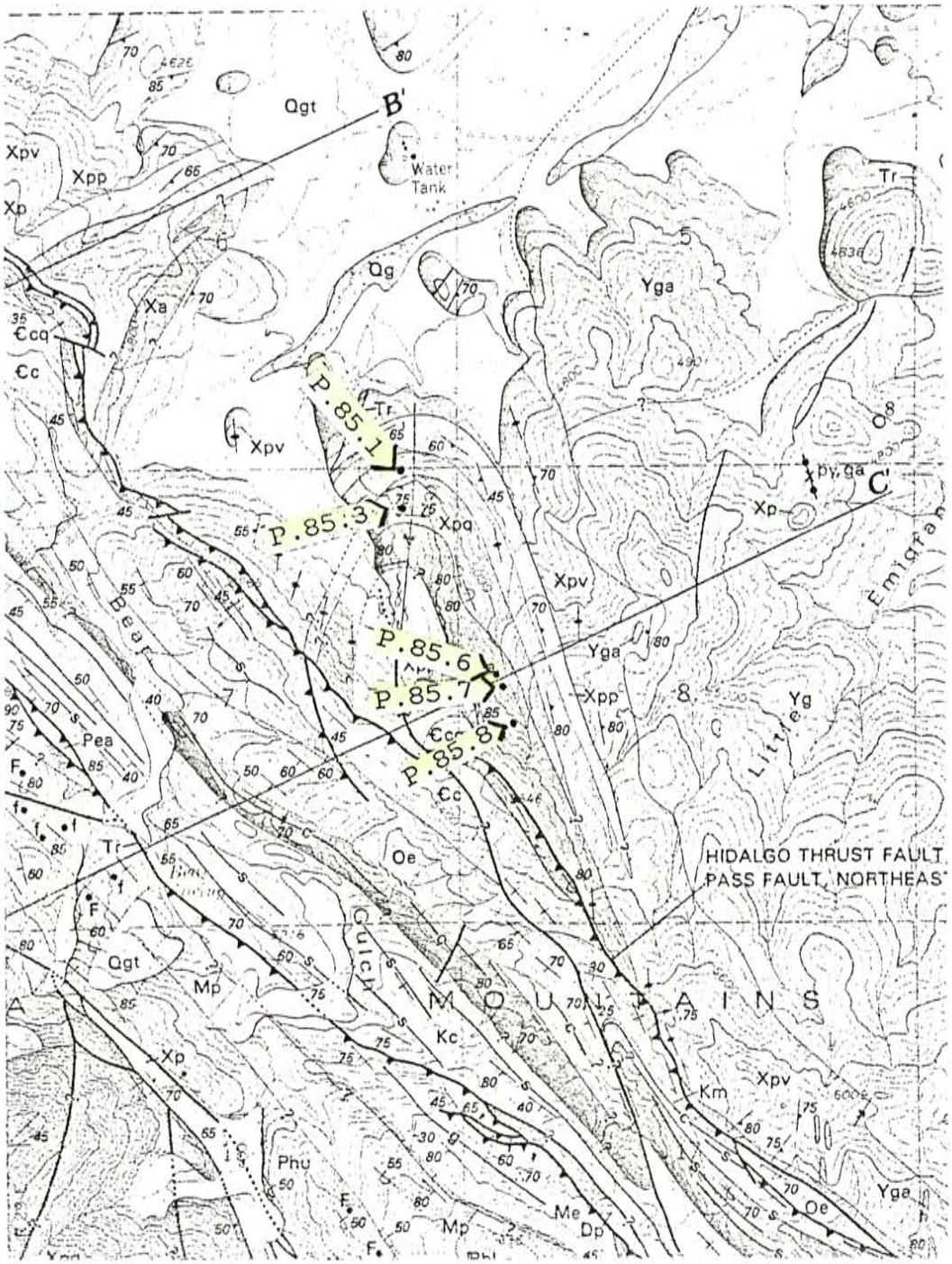

Figure A-10. Drewes (1977), Rincon Mountains.

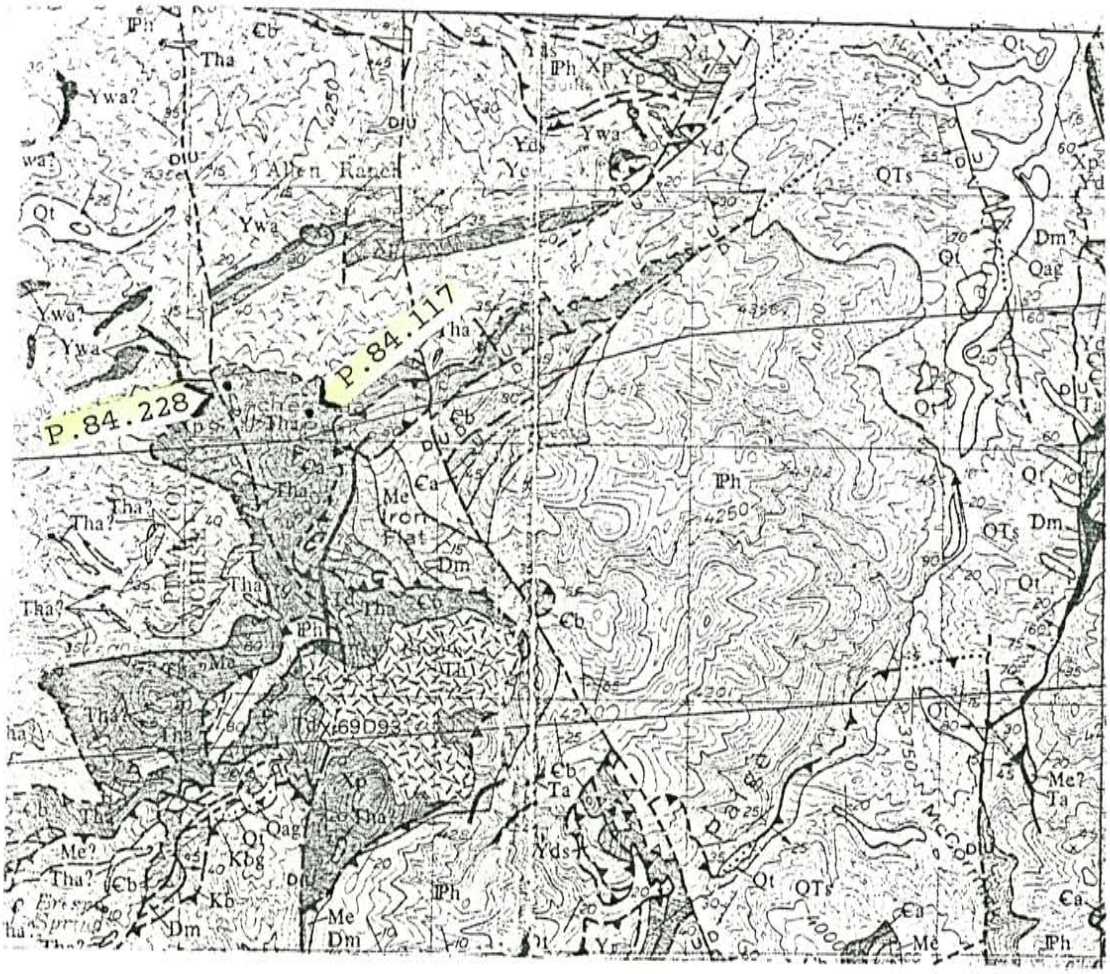

Figure A-11. Drewes (1977), Rincon Mountains.

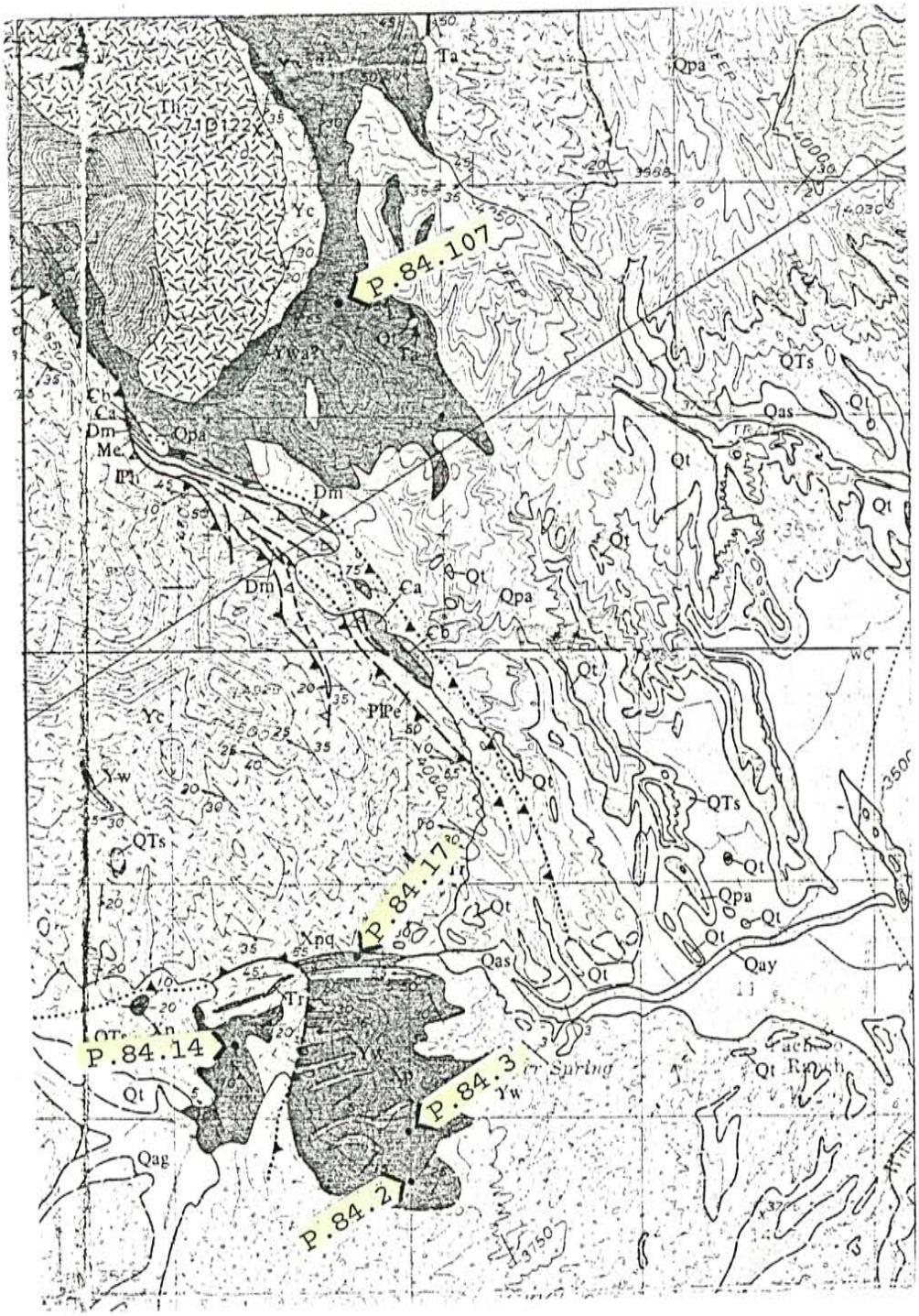

Figure A-12. Dos Cabezas 7.5 minute topographic, Dos Cabezas Mountains.

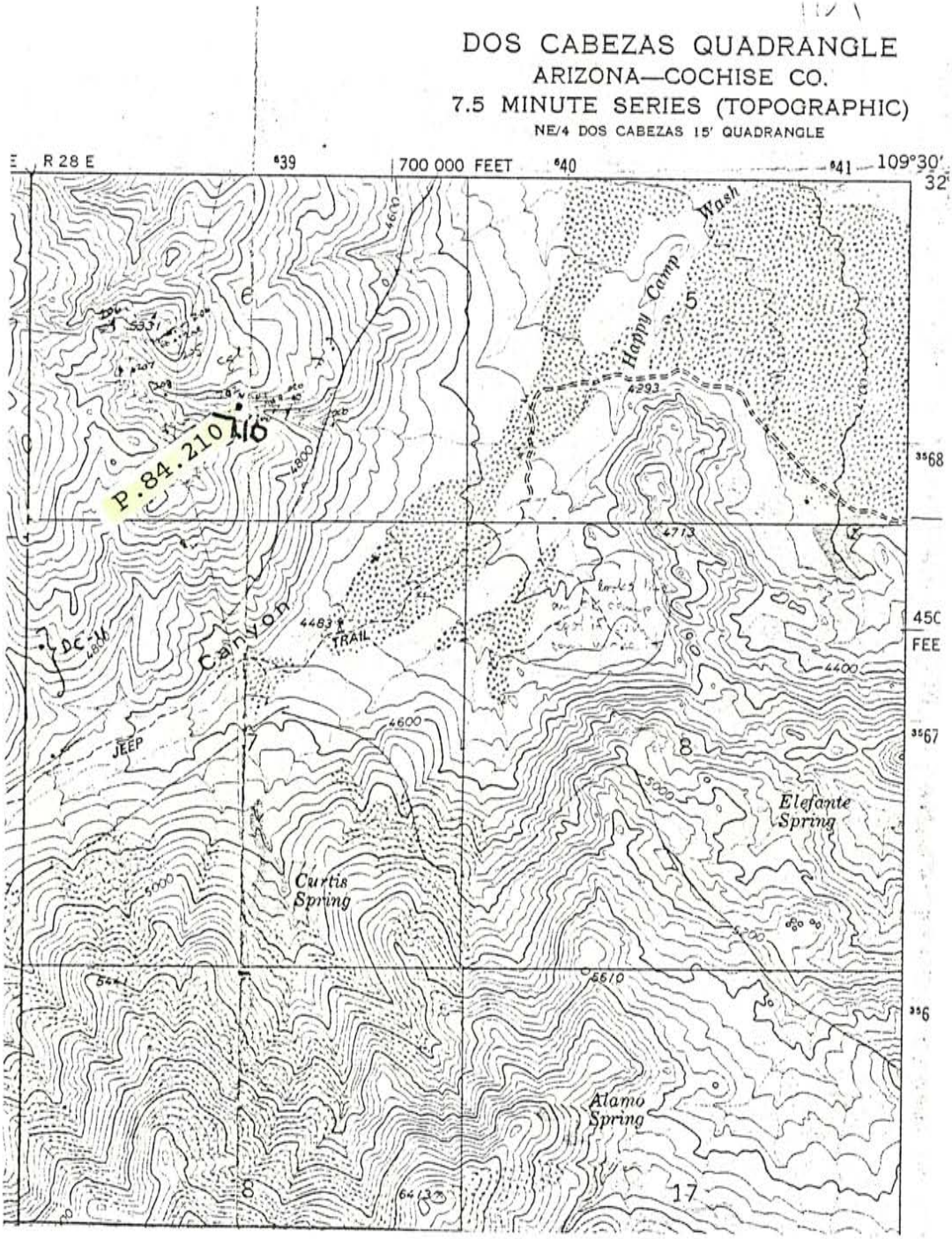

Figure A-13. Drewews (1971), Santa Rita Mountains.

Figure A-14. Drewes (1974), Rincon Mountains

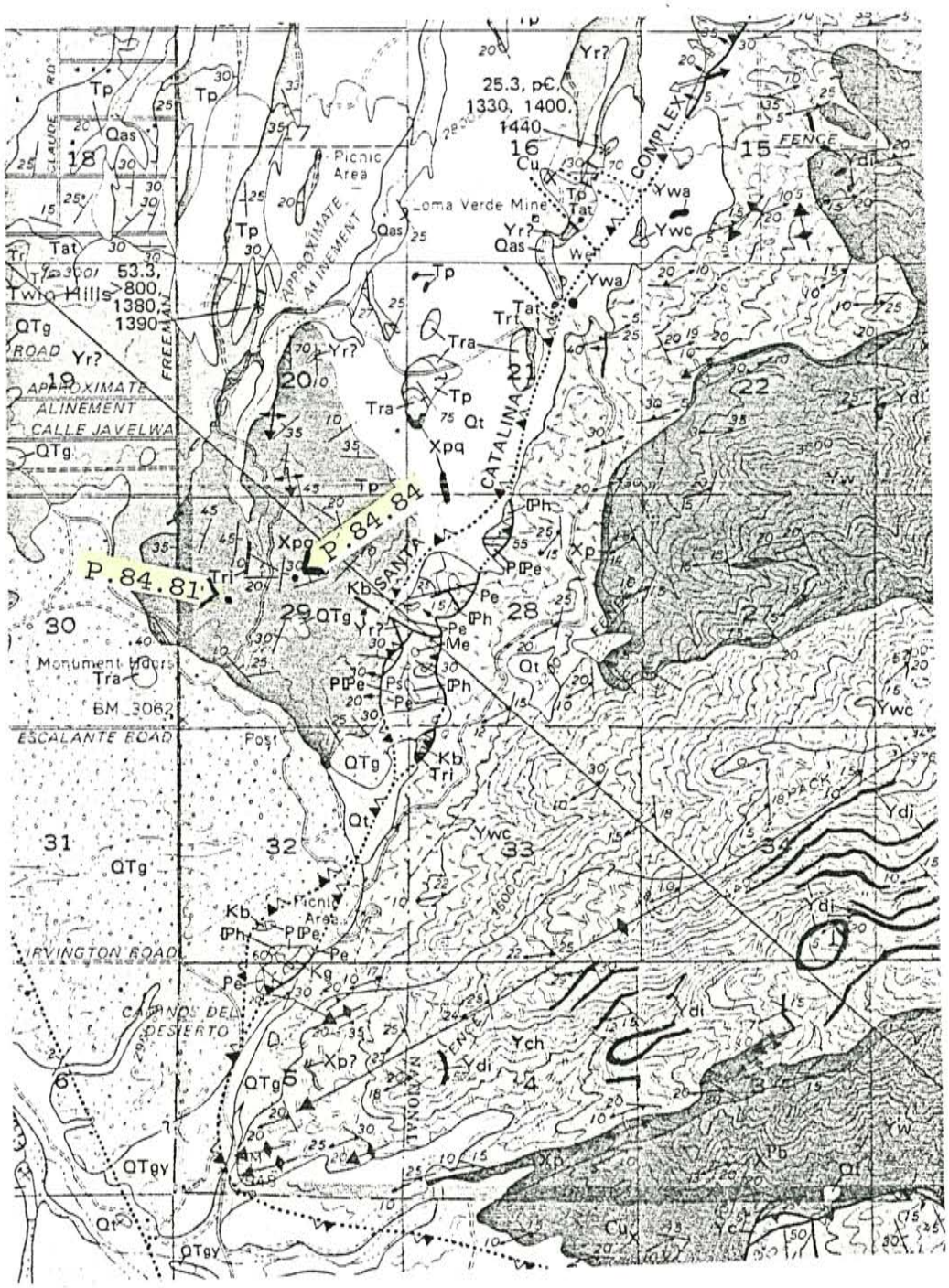

Figure A-15. Drewews (1974), Rincon Mountains.

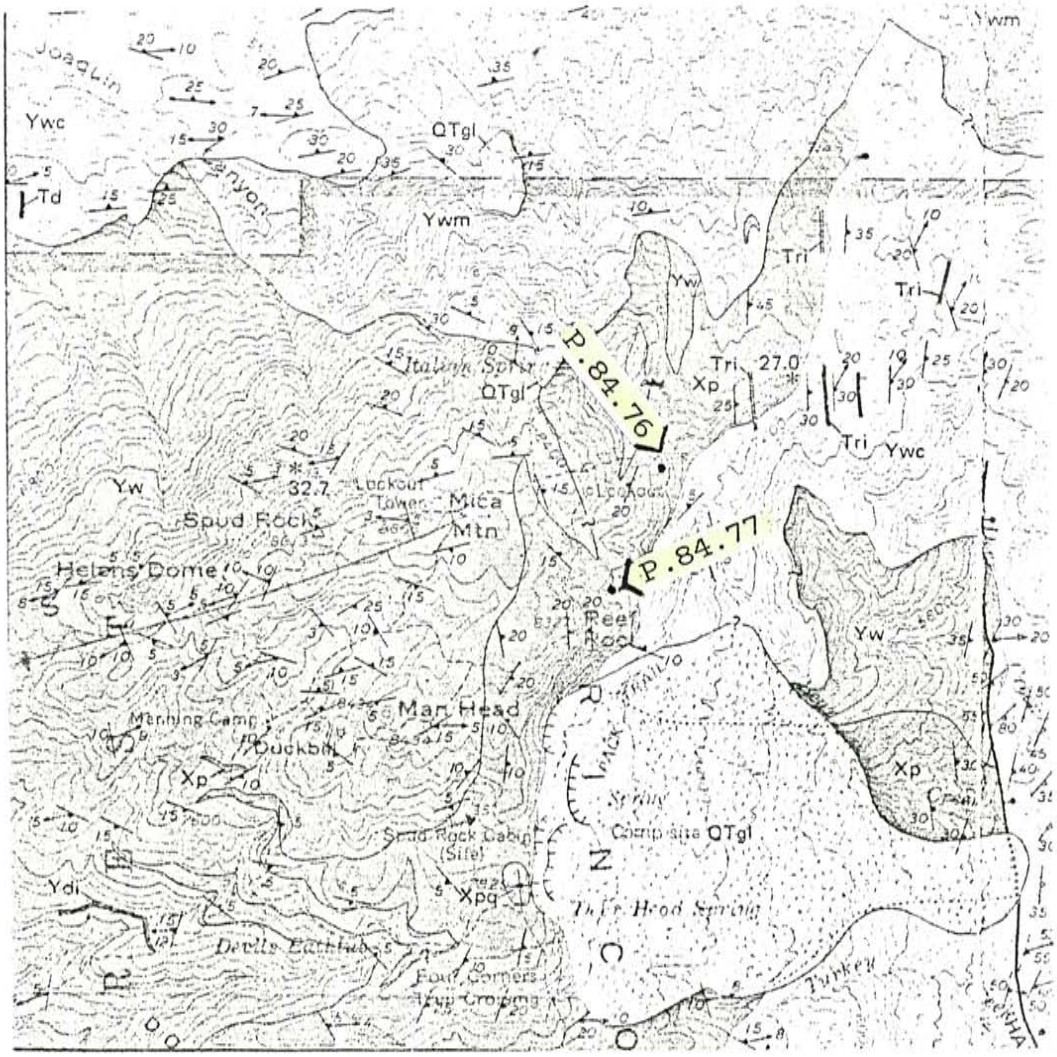

Figure A-16. Bisbee 7.5 minute topographic, Mule Mountains.

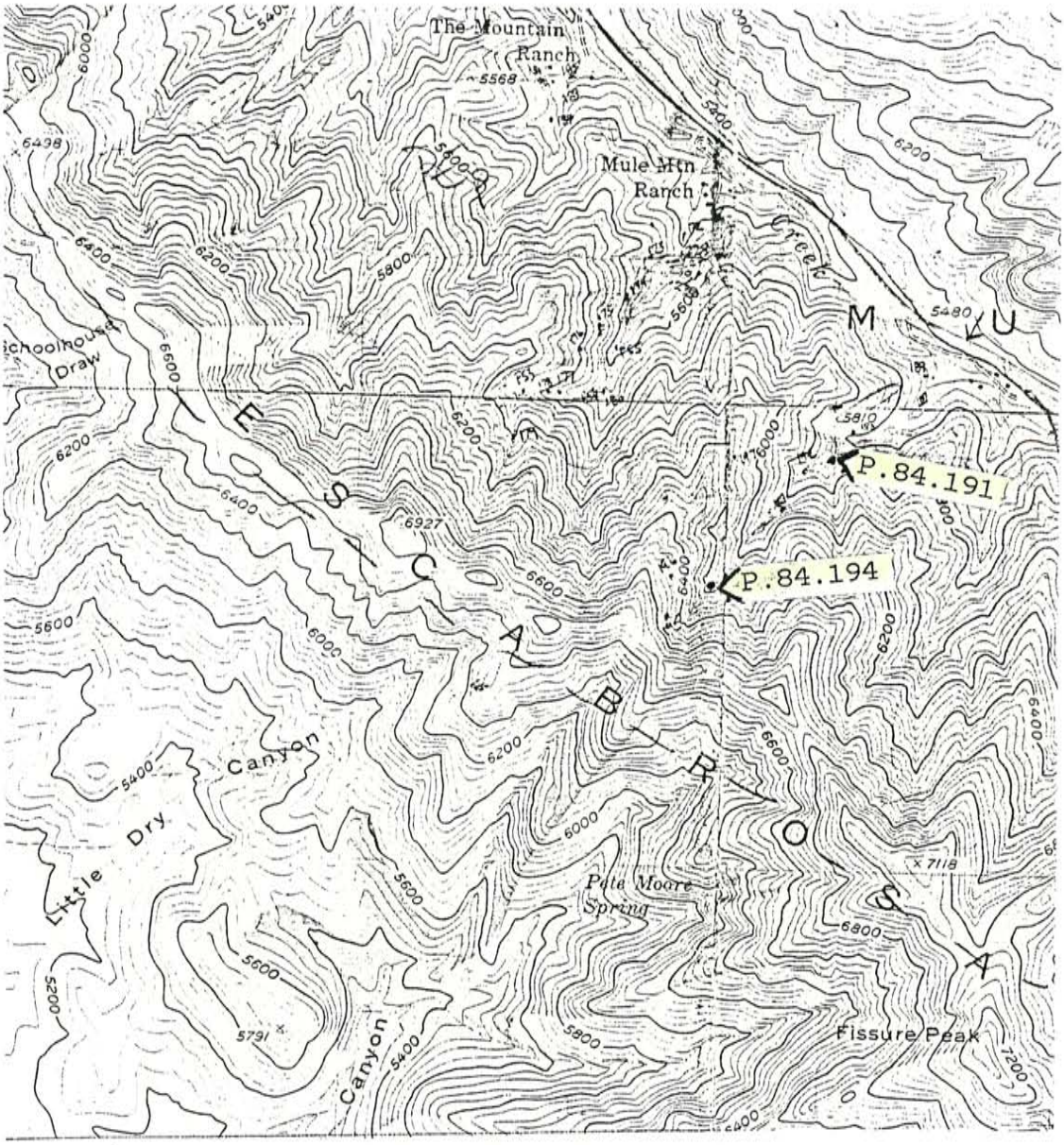

APPENDIX C: Accuracy and precision of geochemical data

The quality of the chemical data obtained in this study varies greatly. Accuracy and precision were detetermined by analyzing international and in-house rock standards. Table C-1 lists the standards analyzed and the number of replicate analyses preformed for each element. Root mean square percent error was calculated by the equation:

$$RMS_{error} = \sqrt{\frac{\sum_{i=1}^{n}\left(\frac{r_i - m_i}{m_i}\right)^2}{n}} \times 100$$

where r is the recommended value, m is the measured value, and n is the number of analyses considered for that element. Recommended values are taken from Abbey (1981). Table C-2 lists the elements analyzed for, the associated rms % error, and the average of 1 sigma deviations expressed as a percentage of the mean, for which three or more replicate analyses were made. This is used as a measure of precision, with lower values indicating high degrees of precision.

In general elements with large associated rms errors are strongly influenced by analyses of standards with concentrations near the detectability level. This is particularily true for MgO, P2O5, and Nb. Elements in this data set which are analytically most reliable are SiO2, Sr, Fe2O3, Eu, Zr, Sc, and La.

Appendix E: Geochemical Modeling

Batch melting and fractional crystallization relationships were used in modeling the geochemistry of some of the rocks of the Pinal Schist. Equations and partition coefficients used are listed in tables E-1 and E-2 respectively.

In modeling these rocks the first step was to use the computer program MIXFRAC written by M. Knoper. This program computes by least-squares approximation mineral proportions needed to produce a given major element composition from a hypothetical parent composition by fractional crystallization. The second step in modeling was to test the mineral proportions given by MIXFRAC using trace elements. Using these mineral proportions calculated daughter trace element concentrations were determined. These calculated values were then compared to the observed concentrations in the proposed daughter. This comparison was done by graphing log (C_l / C_o) vs. log D for each element for both the observed and calculated daughter. The goodness of fit was determined in a qualitative sense by visual examination.

Table E-3 lists the minerals and their compositions used in modeling the basalts in the northeastern Little Dragoon Mountains to the rhyodacite porphry in the

Table E-1. Equations used in geochemical modeling.

Fractional Crystallization

$$C_o / C_l = F^{(D-1)}$$

Batch Melting

$$C_o / C_l = D+F(1-P)$$

$$D = m_i K_{di}$$

$$P = p_i K_{di}$$

where

C_o = initial concentration of an element

C_l = instantaneous concentration of an element

F = fraction of melt

D = bulk distribution coefficient

P = bulk distribution coefficient for melting

K_d = distribution coefficient for an element (solid/liquid)

m_i = mass fraction of a mineral in a rock

p_i = mass fraction of a mineral entering melt

Table E-2. Kd's used in geochemical modeling

mafic systems

	AMPH	OPX	OL	MAG	CPX	PLAG
Rb	0.20	0.02	0.01	0.0	0.02	0.13
Ba	0.70	0.013	0.01	0.0	0.005	0.25
K	0.96	0.014	0.007	0.0	0.011	0.17
Sr	0.60	0.02	0.015	0.0	0.10	2.00
Th	0.05	0.13	0.02	0.0	0.02	0.05
U	0.00	0.007	0.04	0.0	0.05	0.06
La	0.20	0.007	0.01	0.0	0.07	0.15
Ce	0.26	0.008	0.007	0.0	0.10	0.12
Sm	0.70	0.02	0.007	0.0	0.40	0.067
Eu	0.80	0.02	0.01	0.0	0.40	0.35
Tb	0.80	0.05	0.03	0.0	0.50	0.06
Yb	0.60	0.15	0.02	0.0	0.60	0.07
Lu	0.50	0.18	0.016	0.0	0.50	0.06
Y	1.00	0.20	0.01	0.2	0.50	0.03
Sc	1.50	1.00	0.30	2.0	2.00	0.04
Hf	0.40	0.04	0.04	0.4	0.30	0.01
Ta	0.40	0.00	0.03	0.5	0.06	0.04
Ti	1.50	0.10	0.02	7.5	0.30	0.04
Zr	1.50	0.03	0.01	0.1	0.10	0.01
Nb	0.80	0.15	0.01	0.4	0.10	0.01
Ni	7.00	5.00	14.0	30.0	2.60	0.00
Co	2.00	3.00	3.80	10.0	1.20	0.00
Cr	15.0	10.0	2.10	150	8.40	0.00

felsic systems

	OPX	KF	MAG	PLAG	ZIR
Rb	0.003	0.35	0	0.04	0
Ba	0.003	6.0	0	0.3	0
K	0.002	1.5	0	0.1	0
Nb	0.8	0.05	2.5	0.06	50
La	0.1	0.05	0	0.08	2
Ce	0.15	0.04	0	0.25	2.5
Sm	0.25	0.02	0	0.13	3.1
Eu	0.17	1.1	0	1.5	3.5
Tb	0.65	0.006	0.1	0.6	100
Yb	0.85	0.01	0.1	0.05	200
Lu	0.9	0.006	0.1	0.05	200
Y	1	0.1	2	0.1	60
Sc	7	0.02	8	0.04	60
Hf	0.1	0.1	0.5	0.04	500
Ta	0.15	0.05	5	0.05	50
Th	0.15	0.01	0.4	0.05	100
Zr	0.2	0.1	0.8	0.1	1000
U	0.006	0.005	0.1	0.006	0

Table E-3. Modeling of P.84.19 to P.84.34 by FXL

INPUT DATA:

	4-19	PLAG	CPX	OL	MAG	AP	4-34
SiO2	71.82	51.94	48.82	40.79	0.10	0.00	47.37
TiO2	0.64	0.01	0.55	0.05	22.71	0.00	2.02
Al2O3	13.74	30.01	0.77	0.56	1.37	0.00	14.14
Fe2O3	4.29	0.84	22.90	4.68	73.18	0.03	15.57
MgO	0.68	0.00	15.91	53.69	2.25	0.02	8.29
CaO	1.69	13.53	9.72	0.00	0.06	57.06	10.03
Na2O	3.56	3.58	0.64	0.00	0.00	0.00	1.97
K2O	3.37	0.09	0.10	0.00	0.00	0.00	0.14
MnO	0.08	0.00	0.58	0.23	0.32	0.01	0.26
P2O5	0.13	0.00	0.00	0.00	0.00	42.88	0.20

OUTPUT DATA:

	Y.OBS	Y.EST.	residuals	component	proportion
SiO2	47.37	47.37	0.009	4-19	0.0570
TiO2	2.02	2.01	0.012	PLAG	0.4307
Al2O3	14.14	14.14	-0.001	CPX	0.4016
Fe2O3	15.57	15.57	-0.003	OL	0.0316
MgO	8.29	8.30	-0.006	MAG	0.0769
CaO	10.03	10.05	-0.021	AP	0.0038
Na2O	1.97	2.00	-0.032		
K2O	0.14	0.27	-0.131		
MnO	0.26	0.27	-0.010		
P2O5	0.20	0.17	0.028		
TOTAL	100.00	100.16	squared residuals = 0.0198		

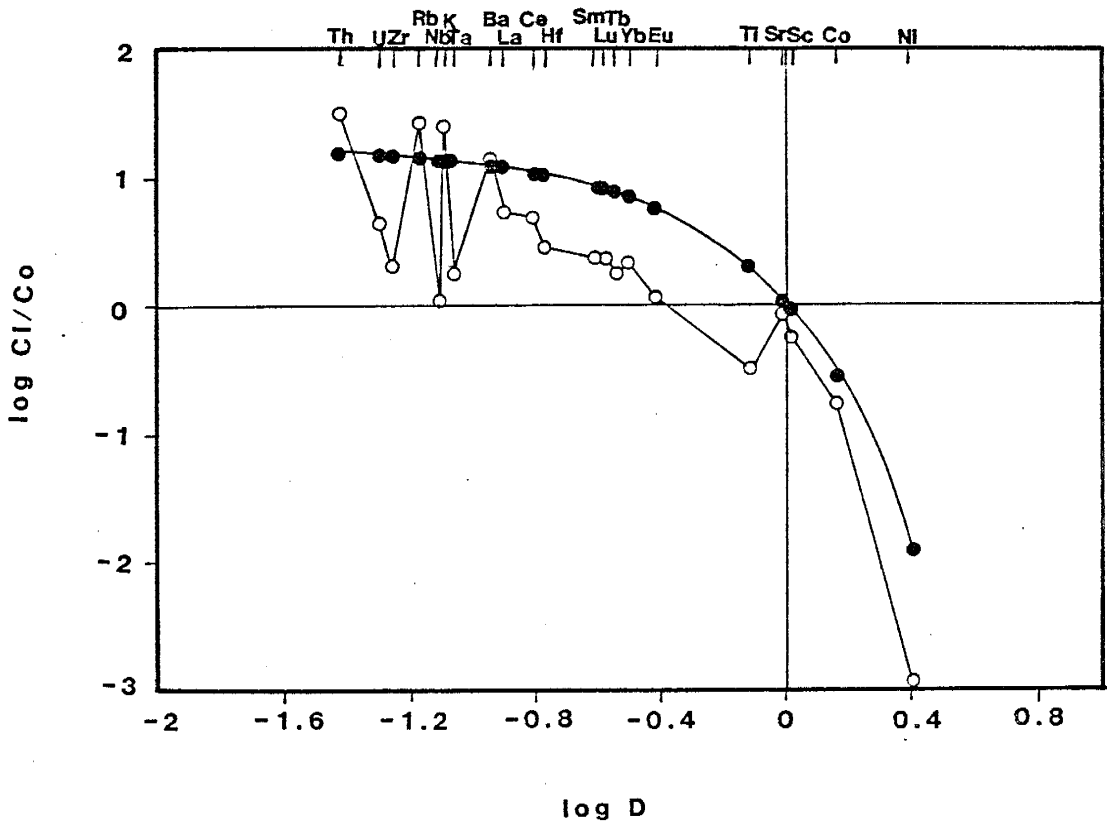

Figure E-1. Plot of log C_l / C_o vs. log D for observed and calculated trace elements for results of modeling rhyodacite porphry and basalt in northern Little Dragoon Mountains. Filled circles, calculated; open circles, observed.

northwestern Little Dragoons by fractional crystallization. These two samples (P.84.34 and P.84.19) were chosen because they seem to be the least altered of their respective groups. The fit between these two hypothetical end-members and the chosen minerals is quite good. However, the Mg content of olivine in this model is quite high, and probably unrealistic for these rock types. Figure E-1 shows the relationships between the calculated and observed trace element concentrations in the hypothetical daughter and P.84.19. The observed fit between these two sets of data is considered unsatisfactory and this model is rejected. A second model for the production of the rhyodacite porphry in the northwestern Little Dragoon Mountains was partial melting of a felsic granulite. To do this P.84.19 was considered to be the daughter liquid and was calculated using the mineral proportions and degree of melting listed in table E-3. Table E-4 compares the calculated rhyodacite source with average felsic granulite from India and Scotland. The similarity between the calculated source and the values of observed felsic granulites suggests this model to be a possible mechanism of production of the Little Dragoon rhyodacites. This is the same conclusion Condie and others (1985) came to for the production of the felsic rocks of the Pinal Schist in the Dos Cabezas Mountains.

Table E-4. Modeling of Little Dragoon rhyodacite porphry as partial melt of felsic granulite.

	mode	melt
OPX	0.1595	0
KF	0.12	0.37
MAG	0.01	0.01
PLAG	0.36	0.32
ZIR	0.0005	0
QTZ	0.35	0.3

F = 0.25

	calculated rhyodacite source	Madras	S. India	Lewisian
Nb	6.1	9	7	5
Yb	2.8	2.5	1	1.2
Rb	35	100	35	11
Y	25	23	12	9
Ti	2811	2200	2400	3240
La	13	36	25	22
Ce	34	67	45	44
Eu	1.3	1.5	1.6	1.2
Zr	195	277	175	202
Th	5.4	19	2	0.4
Ba	335	879	650	757
Sr	289	166	400	569

references: Madras, Weaver (1980)
S. India, Condie and Allen (1984)
Lewisian, Weaver and Tarney (1981)

The most evolved (P.85.20) and the most primitive (P.84.128) samples from the basalts near Cochise Stronghold in the Dragoon Mountains were chosen as end-members in a fractional crystallization modeling scheme. Table E-4 shows the results of the MIXFRAC program. The squared residuals are 0.77. This is rather high but 94% of this value comes from Na2O, P2O5 and MnO. There are no minerals which contain MnO or P2O5 in this list. The trace elements show a good but not excellent match between the observed and calculated daughter composition (figure E-2). Small amounts of contaminant, which are not considered here, could possibly perturb this system to the degree seen on figure E-2. The smooth variation of these rocks on plots of Mg number vs. Ni and Cr (figure 6) suggest that fractional crystallization is a possible mechanism for production of these basalts.

Table E-4. Modeling of P.84.128 to P.85.20 by FXL

INPUT DATA:

	5-20	OL	CPX	PLAG	MAG	4-128
SiO2	54.41	37.12	50.39	49.80	0.35	48.26
TiO2	1.52	0.00	0.67	0.02	20.22	0.98
Al2O3	13.96	0.00	2.99	31.40	2.08	11.67
Fe2O3	14.85	24.82	8.58	0.96	74.16	12.55
MgO	3.48	37.40	15.08	0.10	2.42	12.52
CaO	6.96	0.24	21.88	16.25	0.23	12.77
Na2O	4.00	0.00	0.21	1.30	0.00	0.49
K2O	0.44	0.00	0.00	0.17	0.00	0.19
MnO	0.25	0.41	0.20	0.00	0.54	0.37
P2O5	0.13	0.00	0.00	0.00	0.00	0.19

OUTPUT DATA:

	Y.OBS	Y.EST	residuals	component	proportion
SiO2	48.26	48.17	0.092	5-20	0.2364
TiO2	0.98	1.00	-0.025	OL	0.1769
Al2O3	11.67	11.71	-0.042	CPX	0.3387
Fe2O3	12.55	12.54	0.001	PLAG	0.2342
MgO	12.52	12.62	-0.098	MAG	0.0204
CaO	12.77	12.91	-0.134		
Na2O	0.49	1.32	-0.828		
K2O	0.19	0.14	0.048		
MnO	0.37	0.21	0.163		
P2O5	0.19	0.03	0.161		
TOTAL	100.00	100.65	squared residuals = 0.7788		

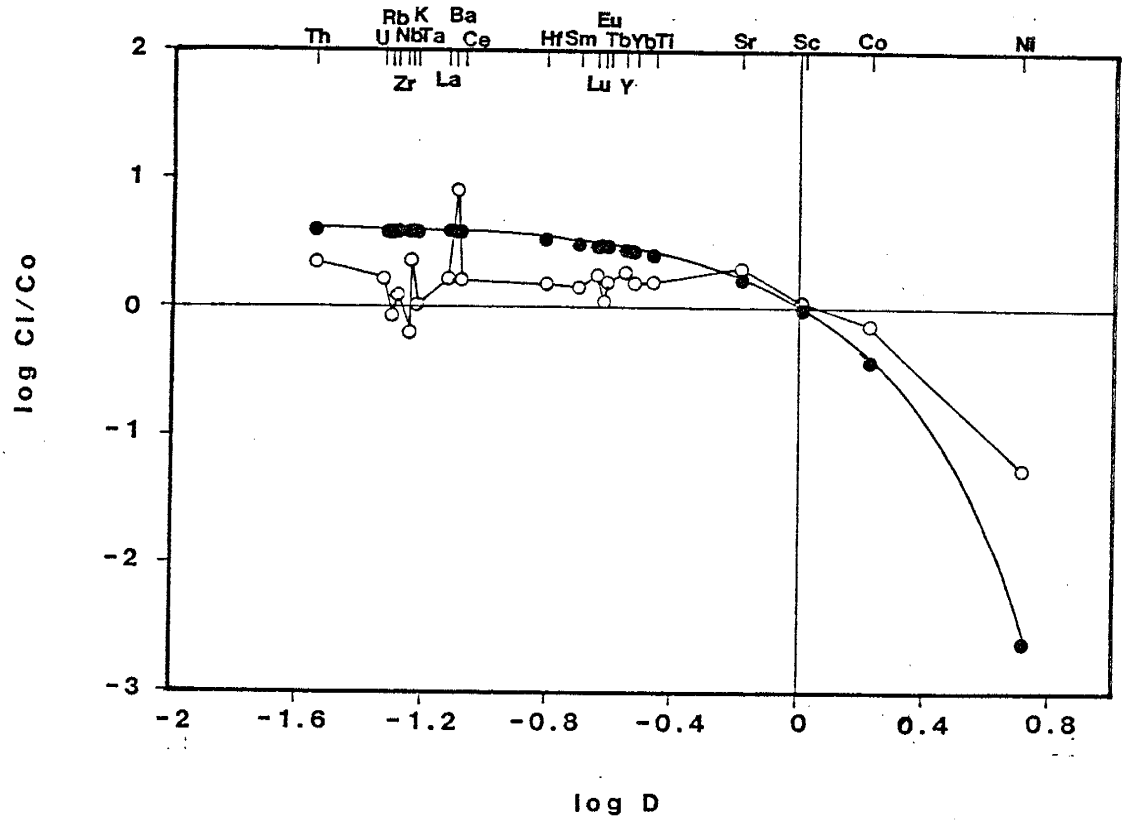

Figure E-2. Plot of log C_l / C_o vs. log D for observed and calculated trace elements for results of modeling Pinal basalts in the central Dragoon Mountains. Filled circles calculated; open circles, observed.

[illegible]

	[illegible]	[illegible]	[illegible]
[illegible]	[illegible]	[illegible]	[illegible]
[illegible]	[illegible]	[illegible]	[illegible]
[illegible]	[illegible]	[illegible]	[illegible]
[illegible]	[illegible]	[illegible]	[illegible]
[illegible]	[illegible]	[illegible]	[illegible]
[illegible]	[illegible]	[illegible]	[illegible]
[illegible]	[illegible]	[illegible]	[illegible]
[illegible]	[illegible]	[illegible]	[illegible]
[illegible]	[illegible]	[illegible]	[illegible]
[illegible]	[illegible]	[illegible]	[illegible]
[illegible]	[illegible]	[illegible]	[illegible]
[illegible]	[illegible]	[illegible]	[illegible]
[illegible]	[illegible]	[illegible]	[illegible]
[illegible]	[illegible]	[illegible]	[illegible]
[illegible]	[illegible]	[illegible]	[illegible]
[illegible]	[illegible]	[illegible]	[illegible]

	[illegible]	[illegible]	[illegible]
[illegible]	[illegible]	[illegible]	[illegible]
[illegible]	[illegible]	[illegible]	[illegible]
[illegible]	[illegible]	3.7	[illegible]
[illegible]	[illegible]	[illegible]	[illegible]
[illegible]	[illegible]	[illegible]	[illegible]
[illegible]	[illegible]	[illegible]	[illegible]
[illegible]	[illegible]	3.0	[illegible]
[illegible]	[illegible]	45	[illegible]
[illegible]	[illegible]	[illegible]	[illegible]
[illegible]	[illegible]	[illegible]	[illegible]
[illegible]	11	177	[illegible]
[illegible]	[illegible]	[illegible]	[illegible]
[illegible]	[illegible]	[illegible]	[illegible]
[illegible]	[illegible]	[illegible]	[illegible]
[illegible]	[illegible]	[illegible]	[illegible]
[illegible]	[illegible]	[illegible]	[illegible]

[illegible]
[illegible]
all values in ppm

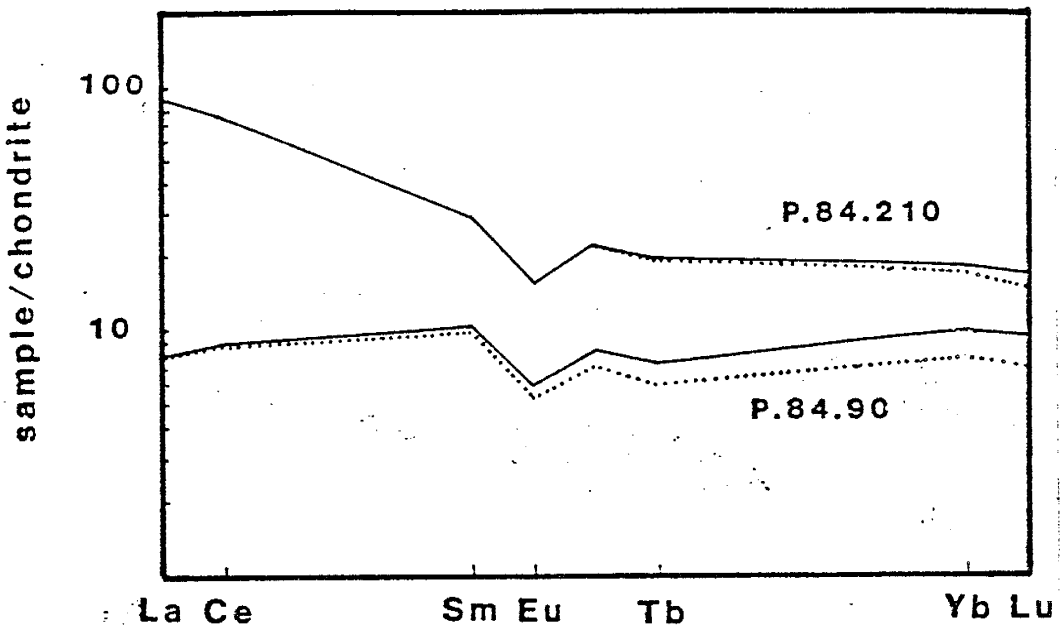

Figure F-1. REE distributions of P.84.90 and P.84.210 and their respective REE concentrations after the calculated contribution of zircon is subtracted. Solid line is whole rock, dotted line is whole rock minus contribution of zircon.

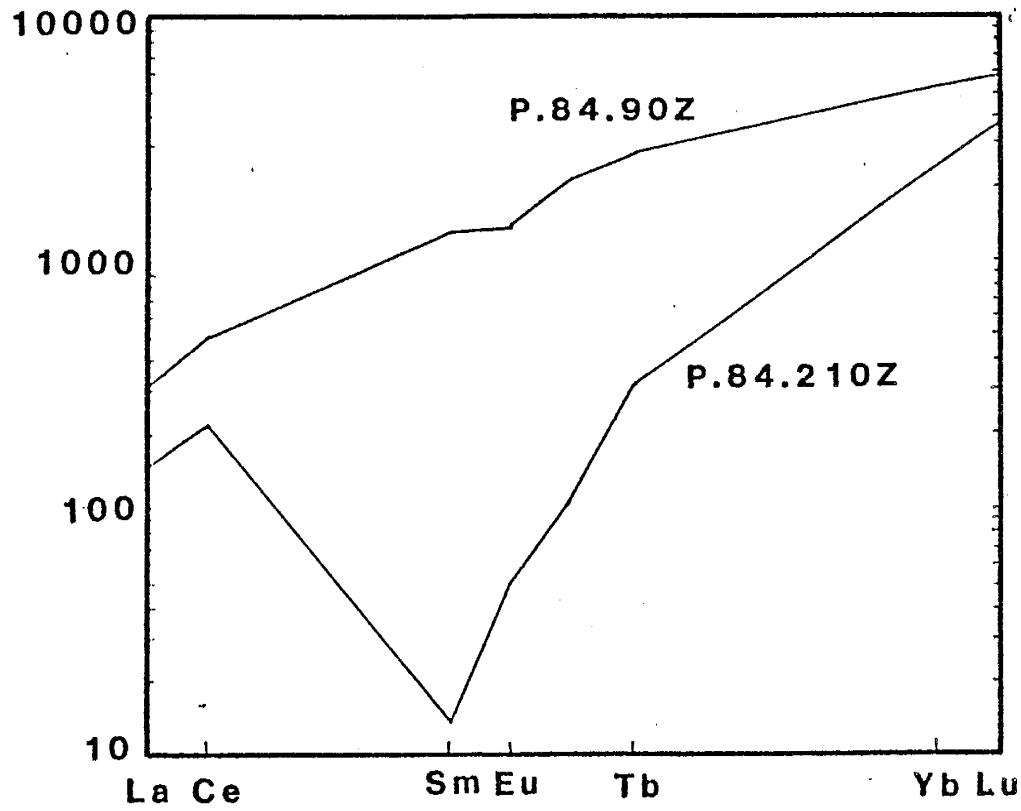

Figure F-2. REE distributions of zircon concentrates from samples P.84.90 and P.84.210.

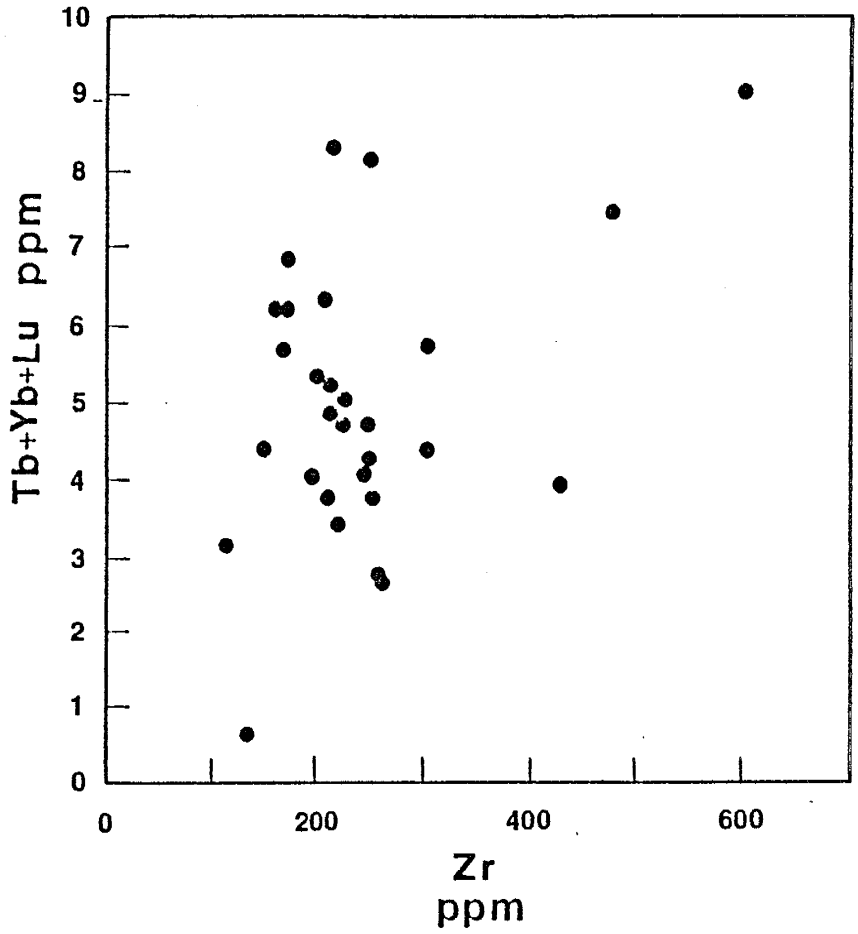

Figure F-3. Zr vs. Tb+Yb+Lu for Pinal metasediments.

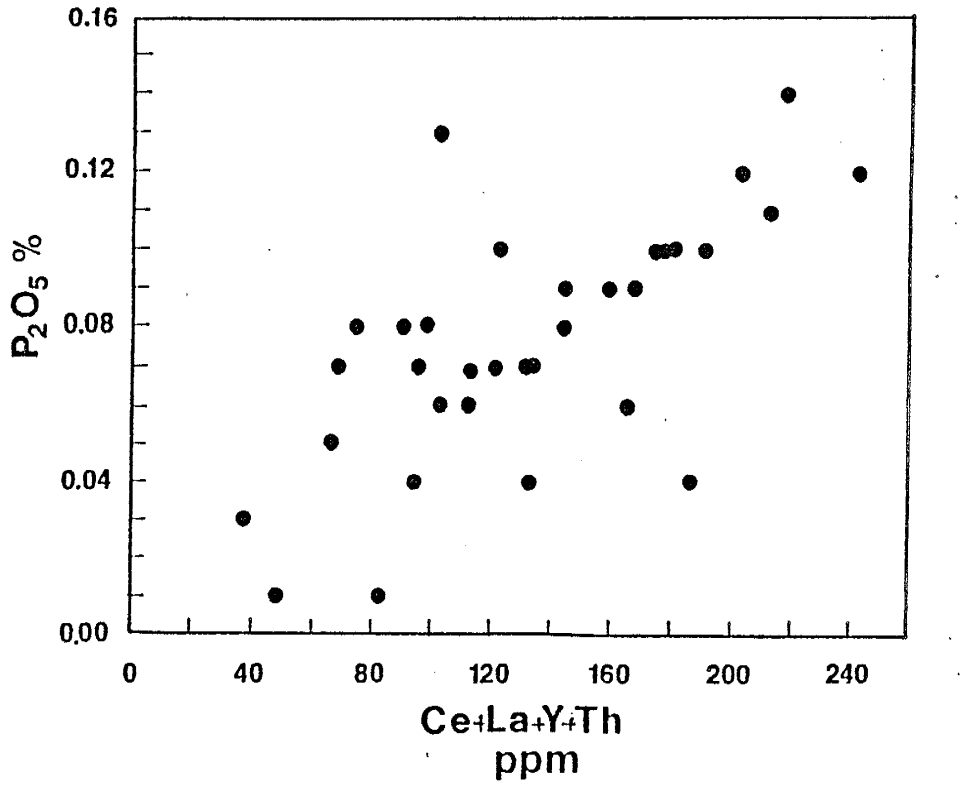

Figure F-4. Ce+La+Y+Th vs. P2O5 for Pinal metasediments.

REFERENCES

Abbey, S., 1983, Studies in "standard samples" of silicate rocks and minerals: Canadian Geol. Surv. Paper 83-15.

Atherton, M.P., Warden, V., and Sanderson, L.M., 1985, The Mesozoic marginal basin of central Peru: a geochemical study of within-plate-edge volcanism: in Pitcher, W.S., and Atherton, M.P., eds., Magmatism at a plate edge, the Peruvian Andes, John Wiley and Sons, p. 58-47.

Bhatia, M.R., 1983, Plate tectonics and geochemical composition of sandstones: J. Geol., v. 91, p. 611-627.

Blatt, H., Middleton, G., and Murray, R., 1980, Origin of sedimentary rocks. Prentice Hall, 728p.

Bonatti, E., 1985, Punctiform initiation of seafloor spreading in the Red Sea during transition from a continental to an oceanic rift: Nature, v. 316, p. 33-37.

Bowling, G.P., in prep, Geology and geochemistry of Proterozoic supracrustal rocks from the western Dos Cabezas Mountains, Cochise County, Arizona, unpub MS thesis, New Mexico Inst. Mining and Tech., Socorro.

Busby-Spera, C.J., 1984, The Lower Mesozoic continental

margin and marine intra-arc sedimentation at Mineral King, California: in Crouch, J.K., and Bachman, S.B., eds., Tectonics and sedimentation along the California margin, Pacific Section, SEPM, v. 38, p. 135-156.

Busby-Spera, C.J., 1985, A sand-rich submarine fan in the Lower Mesozoic Mineral King Caldera Complex, Sierra Nevada, California: J. Sed. Petrol., v. 55, p. 376-391.

Condie, K.C., 1982, Plate tectonic model for Proterozoic continental accretion in the southwestern United States: Geology, v.10, p. 37-42.

Condie, K.C., and Allen, P., 1984, Origin of Archean charnokites from southern India: in, Kroner, A., and others, eds., Archean Geochemistry, Springer-Verlag, p.183-203.

Condie, K.C., Bowling, G.P., and Vance, R.K., 1985, Geochemistry and origin of Early Proterozoic supracrustal rocks, Dos Cabezas Mountains, southeastern Arizona: Geol. Soc. Am. Bull., v. 96, p. 655-622.

Condie, K.C., and De Melas, J.P., 1985, The Pinal Schist: An Early Proterozoic quartz wacke association in southeastern Arizona: Precamb. Res., v. 27, p. 337-356.

Cooper, J.R., and Silver, L.T., 1964, Geology and ore deposits of the Dragoon quadrangle, Cochise County,

Arizona: USGS Prof. Paper 416, 196p.

Conway C.M., 1976, Petrology, structure, and evolution of a Precambrian volcanic and plutonic complex, Tonto Basin, Gila County, Arizona: unpub. Ph. D. dissertation, California Inst. Technology, Pasedena, 460p.

Conway, C.M., and Silver, L.T., in press, 1700-1610 Ma Proterozoic rocks in central to southeastern Arizona: Arizona Geological Soc. Digest.

Crook, K.A., 1974, Lithologies and geotectonics: the significance of compositional variations in flysh arenites (graywackes): in Dott, R.H., and Shaver, R.H., eds., Modern and Ancient Geosynclinal Sedimentation, Soc. Econ. Paleontologists and Mineralogists Spec. Pub. 19, p.304-310.

Creasy, S.C., 1967, Geologic map of the Benson quadrangle, Cochise and Pima Counties, Arizona: U.S. Geol. Surv. Misc. Geol. Inv. Map I-470.

De Melas, J.P., 1983, The geology, petrology and provenance of the Pinal Schist: unpub. M.S. thesis, New Mexico Inst. Mining and Tech., Socorro, 128 p.

Dickinson, W.R., Beard, L.S., Brakenridge, G.R., Erjavec, J.L., Ferguson, R.C., Inman, K.F., Knepp,R.A., Lindberg, F.A., and Ryberg, P.T., 1983, Provenance of North American Phanerozoic sandstones

in relation to tectonic setting: Geol. Soc. Am. Bull., v.94, p. 222-235.

Dott, R.H., Winn, R.D., and Smith, C.H.L., 1982, Relationship of Late Mesozoic and Early Cenozoic sedimentation to the tectonic evolution of the southernmost Andes and Scotia Arc: in Craddock, C., ed., Antarctic Geoscience, Univ of Wisconsin Press, p. 193-202.

Drewes, H., 1971, Geologic map of the Sahuarita quadrangle, southeast of Tucson,Pima County, Arizona: U.S. Geol. Surv. Misc. Geol. Inv. Map I-613.

Drewes, H., 1977, Geologic map of the Rincon Valley quadrangle, Pima and Cochise Counties, Arizona: U.S. Geol. Surv. Misc. Geol. Inv. Map I-997.

Drewes, H., 1980, Tectonic map of southeast Arizona: U.S. Geol. Surv. Misc. Geol. Inv. Map I-1109.

Drewes, H., 1981 Tectonics of southeastern Arizona: U.S. Geol Surv. Prof. Paper 1144, 96p.

Drewes, H., 1982, Geologic map and sections of Cochise Head quadrangle and adjacent areas, Cochise County, Arizona: U.S. Geol. Surv. Misc. Geol. Inv. Map I-1312.

Drewes, H., 1983, Geologic map and structure sections of Bowie Mountain South quadrangle, Cochise County,

Arizona: U.S. Geol. Surv. Misc. Geol. Inv. Map I-1363.

Drewes, 1984, Geologic map and sections of the Bowie Mountain North quadrangle, Cochise County, Arizona: U.S. Geol. Surv. Misc. Geol. Inv. map I-1492.

Drewes, H., and Meyer, G.A., 1983, Geologic map of the Dragoon Mountains roadless area, Cochise County, Arizona: U. S. Geol. Surv. Misc. Field Studies Map MF-1521-A.

Ehlers, E.G., and Blatt, H., 1982, Petrology: igneous sedimentary and metamorphic, W.H. Freeman and Co., 732p.

Erickson, R.C., 1969, Petrology and geochemistry of the Dos Cabezas Mountains, Cochise County, Arizona, unpub. Ph D. dissertation, Univ. of Arizona, Tucson, 441p.

Erickson, R.C., and Drewes, H., 1984, Geologic map of the Railroad Pass quadrangle, Cochise County, Arizona, U.S. Geol. Surv. Misc. Field Studies Map MF-1688.

Ewart, A., 1979, A review of the mineralogy, and chemistry of Tertiary-Recent dacitic, latitic, rhyolitic, and related salic [sic] volcanic rocks: in Barker, F., ed., Trondhjemites, Dacites, and Related Rocks, Elsevier, p. 13-121.

Gibson, I.L., and Jagam, P., 1980, Instrumental neutron

activation analysis of rocks and minerals: in, Muecke, G.K., ed., Short course in neutron activation analysis in the geosciences, Mineralogical Association of Canada, p. 109-131.

Gill, J.B., 1976, Composition and age of Lau Basin and Ridge volcanic rocks: implications for evolution of an interarc basin and remnant arc: Geol. Soc. Am. Bull., v. 87, p. 1384-1395.

Gilluly, J., 1956, General geology of central Cochise County, Arizona: U.S. Geol. Surv. Prof. Paper 281.

Gordon, G.E., Randle, K., Goles, G., Corliss, J., Beeson, M., and Oxley, S., 1968, Instrumental neutron activation analysis of standard rocks with high resolution gamma-ray detectors: Geochem. Cosmochem. Acta, v. 32, p. 369-396.

Gromet, L.P., Dymek, R.F., Haskin, L.A., and Kootev, L., 1984, The "North American shale composite": Its compilation, major and trace element characteristics: Geochem. Cosmochem. Acta, v. 48, p. 2469-2482.

Hildebrand, R.S., and Bowring, S.A., 1984, Continental intra-arc depressions: A nonextentional model for their origin, with a Proterozoic example from Wopmay orogen: Geology, v. 12, p. 73-82.

Hoffman, P.H., and Bowring, S.A., 1984, Short-lived 1.9 Ga continental margin and its destruction, Wopmay

Orogen, northwest Canada: Geology, v. 12, p. 68-72.

Huckenholz, H.G., 1963, Mineral composition and texture in graywackes from the Harz Mountains (Germany) and in arkoses from the Auvergne (France): J. Sed. Petrol., v.33, p. 914-918.

Ingersoll, R.V., 1978, Petrofacies and petrologic evolution of the Late Cretaceous fore-arc basin, northern and central California: J. Geol., v. 86, p. 335-352.

Irvine, T.N., and Baragar, W.R.A., 1971, A guide to the chemical classification of the common volcanic rocks: Can. J. Earth Sci., v. 8, p. 523-548.

Jensen, L.S., 1976, A new cation plot for classifying subalkaline volcanic rocks. Ontario Division of Mines Misc. Paper 66, 22p.

Karlstrom, K.E., and Houston, R.S., 1984, The Cheyenne Belt: Analysis of a Proterozoic suture in southern Wyoming: Precamb. Res., v. 25, p. 415-446.

Karlstrom, K.E., and Puls, D.D., 1984, Geometry of structures in a Proterozoic thrust belt, Mazatzal Mountains, central Arizona: Geol. Soc. Am. Abst. Prog., v. 16, p.554.

Krieger, M.H., 1968, Geologic map of the Holy Joe Peak quadrangle, Pinal County, Arizona: U.S. Geol. Surv. Map GQ-699.

Krieger, M.H., 1974a, Geologic map of the Winkelman

quadrangle, Pinal and Gila Counties, Arizona: U.S. Geol. Surv. Map GQ-1106.

Krieger, M.H., 1974b, Geologic map of the Putnam Wash quadrangle, Pinal County, Arizona: U.S. Geol. Surv. Map GQ-1109.

Leeman, W.P., and Vitaliano, C.J., 1976, Petrology of McKinney Basalt, Snake River Plain, Idaho: Geol. Soc. Am. Bull., v. 87, p. 1777-1792.

Levi, B., and Aguirre, L., 1981, Ensialic spreading-subsidence in the Mesozoic and Paleogene Andes of Central Chile: J. Geol. Soc. Lond., v. 138, p.75-81.

Livingston, D.E., 1969, Geochronology of older Precambrain rocks in Gila County, Arizona: unpub. Ph. D. dissertation, Univ. of Arizona, Tucson, 224p.

Ludwig, K.R., 1974, Precambrain geology of the central Mazatzal Mountains, Arizona: unpub. Ph. D. dissertation, California Inst. Technology, Pasedena, 218 p.

Mack, G.H., 1984, Exceptions to the relationship between plate tectonics and sandstone composition: J. Sed. Petrol., v. 54, p. 212-220.

Maynard, J.B., Valloni, R., and Yu, H., 1982, Composition of modern deep-sea sands from arc related basins: Geol. Soc. Lond. Spec. Paper number 10, p. 551-561.

Marsh, N.G., Saunders, A.D., Tarney, J., and Dick, H.J.B., 1980, Geochemistry of basalts from the Shikoku and Daito Basins: Deep Sea Drilling Reports, Project Leg 58, p. 805-842.

Maynard, J.B., 1984, Composition of plagioclase feldspar in modern deep-sea sands: relationship to tectonic setting: Sedimentology, v. 31, p. 493-501.

McLennann, S.M., 1984, Petrologic characteristics of Archean graywackes: J. Sed. Petrol., v. 54, p. 889-898.

Mercier, J.L., 1981, Extentional-compressional tectonics associated with the Aegean arc: comparison with the Andean Cordillera of south Peru-north Bolivia: Phil. Trans. R. Soc. Lond., v. A300, p. 337-355.

Mullen, E.D., 1983, $MnO/TiO_2/P_2O_5$: a minor element discrimination for basaltic rocks of oceanic environments and its implications for petrogenesis: Earth Plan. Sci Lett., v. 62, p. 53-62.

Nesbitt, H.W., and Young, G.M., 1982, Early Proterozoic climates and plate motions inferred from major element chemistry of lutites: Nature v. 299, p. 715-717.

Norrish, K., and Chappel, B.W., 1977, X-ray fluorescence; in Zussman, J., ed., Physical methods in determitive mineralogy, Academic Press, p. 235-

262.

Norrish, K., and Hutton, J.T., 1969, An accurate x-ray spectrographic method for the analysis of a wide range of geological samples: Geochem. Cosmochem. Acta, v.33, p. 431-435.

Pearce, J.A, 1983, Role of sub-continental lithosphere in magma genesis at active continental margins: in Hawkesworth, C.J., and Norry, M.J., eds., Continental basalts and mantle xenoliths, Shiva Press, p. 230-249.

Pearce, J.A., and Cann, J.R., 1973, Tectonic setting of basic volcanic rocks determined using trace element analysis: Earth Plan. Sci. Lett., v. 19, p. 290-300.

Pearce, J.A., Lippard, S.J., and Roberts, S., 1984, Characteristics and tectonic significance of supra-subduction ophiolites: in Kokelaar, B.P., and Howells, M.F., eds., Marginal Basin Geology, Geol. Soc. Lond. Spec. Pub. 16, p. 77-94.

Pettijohn, F.J., 1963, Chemical composition of sandstones excluding carbonate and volcanic sands: Data of Geochemistry, Chapter S, U.S. Geol. Surv. Prof. Paper 440.

Pharaoh, T.C., and Pearce, J.A., 1984, Geochemical evidence for the geotectonic setting of Early Proterozoic metavolcanic sequences in Lapland: Precamb. Res., v. 25, p. 283-308.

Poldervaart, A., 1955, Zircons in rocks, 1. Sedimentary rocks: Am. J. Sci., v. 253, p. 433-461.

Potter, P.E., 1984, South American modern beach sand and plate tectonics: Nature, v. 311, p.645-648.

Ransome, F.L., 1903, Geology of the Globe copper district, Arizona: U.S. Geol. Surv. Prof. Paper 12, 168 p.

Ransome, F.L., 1904, The geology and ore deposits of the Bisbee quadrangle, Arizona: U.S. Geol. Surv. Prof. Paper 21, 168p.

Saunders, A.D., and Tarney, J., 1984, Geochemical characteristics of basaltic volcanism within back-arc basins: in Kokelaar, B.P., and Howells, M.F., eds., Marginal basin geology, Geol. Soc. Lond. Spec. Pub. 16, p. 59-76.

Saunders, A.D., Tarney, J., Stern, C.R., and Dalziel, I.W.D., 1979, Geochemistry of Mesozoic marginal basin floor igneous rocks from southern Chile: Geol. Soc. Am. Bull., v. 90, p.237-258.

Silver, L.T., 1963, The use of cogenetic uranium- lead isotope systems in zircon geochronology: Radioactive dating, International Atomic Energy Agency, Vienna, p.279-285.

Silver, L.T., 1978, Precambrain formations and Precambrain history in Cochise County, southeastern Arizona: New Mexico Geological Soc. Guidebook, 29th Field Conference, Land of Cochise, p. 157-

163.

Silver, L.T., and Deutch, S., 1961, Uranium-lead method on zircons: in Geochronology of rock samples, Anal. N.Y. Acad. Sci., v. 91, p. 279-283.

Simons, F.S., 1974, Geologic map and sections of the Nogales and Lochiel quadrangles, Santa Cruz County, Arizona: U.S. Geol. Surv. Map I-762.

Stern C.R., 1980, Geochemistry of Chilean ophiolites: evidence for the compositional evolution of the mantle source of back arc basalts. J. Geophys. Res., v. 85 p. 955-966.

Tanner, P.W.G., 1982, Geologic evolution of South Georgia:in Craddock, C., ed., Antarctic Geoscience, Univ. of Wisconsin Press, p. 167-176.

Taylor, S.R., and McLennan, S.M., 1985, The continental crust: Its composition and evolution, Blackwell Scientific Publications, 312p.

Valloni, R., 1985, Reading provenance from modern marine sands: in Zuffa, G.G., ed., Provenance of Arenites, D. Reidel Pub. Co., p. 309-332.

Valloni, R., and Mezzadri, 1984, Compositional suites of terrigenous deep-sea sands of the present continental margins: Sedimentology, v. 31, p. 353-364.

Vance, R.K., 1983, Investigations in the Precambrian rocks of the Dos Cabezas Mountains, southeast Arizona: unpub. manuscript.

Velbel, M.A., 1985, Mineralogically mature sandstones in accretionary prisms: J. Sed. Petrol., v. 55, p.685-690.

Walker, R.G., 1965, The origin and significance of the internal sedimentary structures of turbidites: Proc. Yorkshire Geol. Soc., v. 33, p. 1-29.

Walker, R.G., 1978, Deep-water sandstone facies and ancient submarine fans: Models for exploration for stratigraphic traps: Am. Assoc. Petrol. Geol. Bull., v. 62, p. 932-966.

Weaver, B.L., 1980, Rare-earth geochemistry of Madras granulites: Contr. Min. Petrol., v. 71, p. 271-279.

Weaver, B.L., and Tarney, J., 1981, Lewisian gneiss geochemistry and Archean crustal development models: Earth Plan. Sci. Lett., v. 55, p. 171-180.

Weaver, S.D., Saunders, A.D., Pankurst, R.J., and Tarney, J., 1979, A geochemical study of magmatism associated with the initial stages of back-arc spreading: Cont. Min. Petrol., v. 68, p. 151-169.

Wilson, E.D., Moore, R.T., and Cooper, J.R., 1969, Geologic map of Arizona: U.S. Geol. Surv. and Arizona Bureau of Mines.

Wilson, E.D., Moore, R.T., and Cooper, J.R., 1969, Geologic map of Arizona: U.S. Geol. Surv. and

Arizona Bureau of Mines.

Winchester, J.A., and Floyd, P.A., 1976, Geochemical magma type discrimination of different magma series and their differentiation products using immobile elements: Chem. Geol., v. 20, p. 325-343.

Wood, D.A., 1980, The application of a Th-Hf-Ta diagram to problems of tectonomagmatic classification and to establishing the nature of basaltic lavas of the British Tertiary Volcanic Province: Earth Plan. Sci. Lett., v. 50, p.11-30.

This thesis is accepted on behalf of the faculty of the Institute by the following committee:

Advisor

Andrew Campbell

David B. Johns

1/23/96
Date